COSMIC-RAY SCINTILLATIONS

Thesis by

Aaron James Owens

In Partial Fulfillment of the Requirements

for the Degree of

Doctor of Philosophy

California Institute of Technology
Pasadena, California

1973

(Submitted May 21, 1973)

ACKNOWLEDGMENT

First, I would like to thank J. R. Jokipii - my advisor, teacher, and friend - for his help. He suggested the topic of investigation, gave me encouragement and guidance through the early stages of work, and provided constructive criticism and helpful suggestions as the research progressed. His contribution to many of the ideas and physical concepts presented in this Thesis has been great, both through informal discussion and direct collaboration.

I am indebted to E. C. Stone for his thorough reading of several manuscripts covering parts of the research presented here, and for his incisive comments and thoughtful suggestions. Several useful discussions with Jon Mathews, Joseph V. Hollweg and R. Vogt are gratefully acknowledged. T. Garrard was extremely cooperative in providing data in a readily-accessible form. Eileen Gribben cheerfully and expertly executed the arduous task of typing this manuscript.

Finally, I wish to thank Janet - my closest companion and best friend - for her kindness, understanding, encouragement, and support, and for being such a warm and wonderful person.

Part of my graduate study has been supported by the National Science Foundation through its Graduate Fellowship and Graduate Trainee programs. This research was also supported, in part, by the National Aeronautics and Space Administration through grant NGR-05-002-160.

ABSTRACT

This Thesis reports the observation and theoretical interpretation of a new physical phenomenon. Cosmic-ray "scintillations" are temporal fluctuations in the counting rate of a detector pointing in a fixed direction in space. Power-spectral analyses of energetic-particle counting rate data are used to demonstrate that scintillations are a statistically significant, persistent, and interesting feature of the cosmic-ray flux observed near earth for a wide range of frequencies (10^{-7} Hz to 10^{-4} Hz) and energies (~1 MeV to 10 GeV protons, 3 to 12 MeV electrons). The observed power spectra of cosmic-ray scintillations are approximately power laws in frequency with exponents of -1.5 to -2.0, and for protons the relative scintillations are a rapidly-decreasing function of energy.

Quantitative theoretical models, based on generalized quasi-linear solutions of the collisionless Liouville equation with a stochastic magnetic field, are presented for the production of cosmic-ray scintillations by random magnetic fields in the magnetosheath and in interplanetary space. It is shown that the ~1-10 MeV proton scintillations observed during quiet times inside the magnetosphere are probably caused by fluctuations in the magnetic field of the magnetosheath. Scintillations of high-energy particles ($\gtrsim$1 GeV/nucleon) are probably generated by the stochastic interplanetary magnetic field. The detailed theoretical prediction for the power spectrum of the flux from neutron monitors, including the effect of the earth's rotation on the interplanetary scintillations model, is calculated and shown to be in

excellent agreement with observations from the Alert and Deep River Neutron Monitors. The shape and amplitude of the observed spectra, and in particular a broad enhancement in the Deep River spectrum near one cycle per day, are explained by the theory.

This investigation gives relations for the power spectrum $P^j(f)$ of the cosmic-ray flux of the form

$$\frac{P^j(f)}{j_0^2} = A(f) \frac{P^B(f)}{B_0^2} \delta^2,$$

where j_0 is the average flux, $P^B(f)$ is the power spectrum of a component of the magnetic field, B_0 is the average magnetic field strength, and δ is the cosmic-ray anisotropy. The factor A(f) is a frequency-dependent function which exhibits enhancements near frequencies corresponding to cyclotron resonances (and near 1 cycle per day for neutron monitors) but which is essentially constant for 1 MeV - 10 GeV proton scintillations at frequencies $\lesssim 10^{-4}$ Hz. The cosmic-ray scintillations thus can provide information about magnetic fluctuations, and neutron-monitor power spectra can give information about the interplanetary magnetic field from ground-based measurements. The shape of the theoretical spectrum near cyclotron resonances depends strongly on non-linear terms in the generalized quasi-linear equations, so scintillations may provide a useful test of non-linear plasma theories. The agreement of the theory of scintillations with observation supports the standard theory of cosmic-ray diffusion near earth and the relation between the diffusion coefficient and magnetic-field fluctuations. Thus the previously-ignored "noise" in the cosmic-ray intensity may contain much useful information.

TABLE OF CONTENTS

LIST OF FIGURES

LIST OF TABLES

I. INTRODUCTION AND SUMMARY OF RESULTS

A. Introduction

Cosmic rays are energetic particles of extraterrestrial origin. Their existence was first reported by Hess in 1912 and confirmed during the 1920's by an ingenious series of experiments by Millikan, who gave the name "cosmic rays" to the observed extraterrestrial radiation. (For a history of cosmic-ray research through 1964, see Rossi, 1964.) It has only been in the last few decades, since the advent of satellite and balloon observations, however, that intensive investigation of the properties of the primary cosmic rays has been possible. Since cosmic rays are the only samples of extraterrestrial matter that we have, apart from meteorites and moon rocks, they have proven extremely valuable in inferring properties of astrophysical objects.

For the purposes of this Thesis, I will limit the discussion to charged particles. The charged particles observed near earth are predominantly protons (~95%), although heavier nuclei and electrons are also present. Local observations indicate that the primary cosmic rays are isotropic, and studies of electron synchrotron emission using radio telescopes show that the cosmic-ray flux is reasonably constant throughout the galaxy. Studies using measurements of induced radioactivity in meteorites conclude that the local flux is fairly constant over time scales of the order of a million years. The observed cosmic radiation is therefore constant over long periods of time in our galaxy. Abundances of certain rare nuclei (Li, Be, B) indicate that the age of a typical cosmic-ray particle in the galaxy is about one million years,

much longer than the rectilinear transit time for unscattered particles. Energy considerations and the lack of observed gamma radiation from the scattering of hypothetical extragalactic cosmic rays off of the cosmic $3^{o}K$ blackbody continuum indicate that the source of the major portion of the cosmic rays lies inside our galaxy. Although the details of the mechanism for cosmic-ray acceleration are not understood, it is widely believed that cosmic-ray production is in some way connected with supernova explosions and the remnants which they leave behind. (For a continuing review of these points, see Ginzberg and Syrovatskii, 1964, Ginzberg, 1969, Ginzberg, 1970, and Syrovatskii, 1971.)

Since supernova events are rare (~1 per 50 years in our galaxy) and the typical cosmic ray spends many rectilinear transit times in the galaxy, there must be considerable scattering of the cosmic rays in their propagation from the sources to the point of observation near earth. The mechanism for this scattering process most likely involves "collisions" with irregularities in astrophysical electromagnetic fields, since ion-ion and ion-neutral collisions are rare and the gravitational force on individual particles is negligible. Since scales of interest in astrophysical discussions of cosmic rays are much larger than the Debye length, and since the velocity of cosmic rays is much larger than the Alfvén speed or the speed of magnetohydrodynamic waves, the major influence on the propagation of cosmic rays in interplanetary and interstellar space is the magnetic field. Therefore, the scattering of high-energy particles by irregular magnetic fields is an interesting phenomenon which has important astrophysical applications.

Although little quantitative data are available concerning magnetic fields and cosmic rays in interstellar space, much data exist for particles and fields in interplanetary space near earth. For this reason, I will subsequently consider the scattering of cosmic rays by magnetic fields in interplanetary space, although the same kind of mechanism presumably applies also in the interstellar medium. A schematic picture of interplanetary space in the vicinity of the solar equatorial plane is indicated in Fig. I-1, taken from Jokipii (1971). The "solar wind" is an outflow of plasma from the sun. It is composed primarily of protons ($\sim 5\ cm^{-3}$ near earth) and electrons flowing radially away from the sun with velocity $V_w \approx 350$ km/sec. The interplanetary magnetic field is, on the average, an Archimedes spiral (Parker, 1963), with large fluctuations. Cosmic rays incident from interstellar space are scattered by the magnetic irregularities and become nearly isotropic in the rest frame of the outflowing plasma. The sun is occasionally an important source of particles with kinetic energy $T \gtrsim 10$ MeV/nucleon, during solar flare events, and it may be a continuous source of particles with energies $T \lesssim 10$ MeV/nucleon. A quantitative theory has been developed to relate the average cosmic-ray distribution function to properties of the interplanetary medium, and the resulting diffusion equation has been useful in analyzing such phenomena as the 11-year variation in the cosmic-ray intensity, cosmic-ray anisotropies and gradients, and the time history of the cosmic-ray flux during impulsive solar flare events. (See the thorough review of these topics in Jokipii, 1971.) The long-term, time-averaged properties (i.e., time scales of months or years) of the cosmic-ray flux near earth seem to be

Figure I-1: Schematic view of the interplanetary magnetic field projected into the solar equatorial plane. Rotation of the sun at angular speed Ω_Θ results in indicated spiral average field. $\psi = \tan^{-1} (\Omega_\Theta r/V_w)$ is the angle between the average field and the radius vector from the sun. Note that magnetic lines of force do not actually cross, but are braided and intertwined in three dimensions.

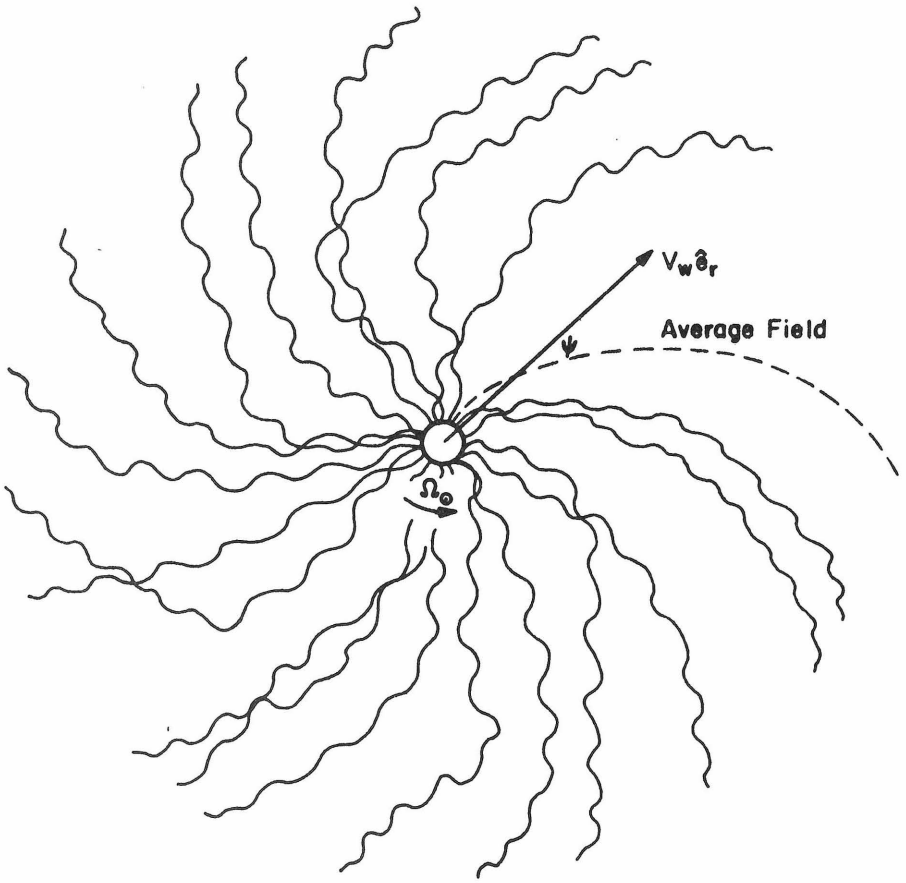

Figure I-1

well understood in terms of this model. On the shorter time scale, on the order of hours or days, however, the cosmic-ray flux is also observed to vary, even during "quiet" times in interplanetary space.

It is the purpose of this Thesis to inquire about the characteristics and the origin of broad-band cosmic-ray fluctuations and to see if these short-term fluctuations can be analyzed in a manner which can provide useful information about the cosmic rays and the plasmas through which they propagate. This type of investigation has not previously been pursued systematically. Generally, the "noise" in the cosmic-ray counting rate has been ignored or explored in an ad hoc manner. Here I review the use of power spectra as a systematic scheme for analyzing the data and then present the first quantitative models of physical processes by which the broad-band cosmic-ray fluctuations may be produced. This Thesis has basically two major parts. The first is an analysis of several different types of cosmic-ray data to show that the fluctuations are an interesting and persistent feature of the cosmic-ray flux for a wide range of energies and frequencies. The second part is the construction of quantitative models for the production of cosmic-ray "scintillations" by interplanetary and magnetospheric magnetic-field fluctuations and the demonstration that the observed scintillations are in good agreement with the results of the theoretical models.

B. Cosmic-Ray Scintillations: Results

By scintillations, I mean the fluctuations in intensity which a cosmic-ray detector sees as a function of time while pointed in a given direction in space. The use of the term "scintillations" to describe this type of fluctuation will be clarified in Chapter III, where the similarity between cosmic-ray "scintillations" and interplanetary scintillations of radio waves will be discussed. The physical picture is that cosmic rays are guided along magnetic field lines. The cosmic-ray intensity varies as a function of time, because as the direction of the field varies different particle intensities are brought into the detector's viewing cone if there is a field-aligned anisotropy. Thus the magnetic-field fluctuations and a cosmic-ray anisotropy cause cosmic-ray scintillations.

The quantitative description of this phenomenon begins with Liouville's equation for the conservation of particle density in phase space,

$$\left[\frac{\partial}{\partial t} + \underset{\sim}{w}\cdot\frac{\partial}{\partial \underset{\sim}{x}} + \frac{d\underset{\sim}{p}}{dt}\cdot\frac{\partial}{\partial \underset{\sim}{p}}\right] f(\underset{\sim}{x},\underset{\sim}{p},t) = 0. \qquad (1)$$

Here the coordinates are position, ($\underset{\sim}{x}$), momentum ($\underset{\sim}{p}$), and time (t); $\underset{\sim}{w}$ is the particle velocity, $f(\underset{\sim}{x},\underset{\sim}{p},t)$ is the distribution function of particles in phase space, and $\frac{d\underset{\sim}{p}}{dt}$ is the force. As discussed above, short-range particle-particle collisions are ignorable, so there is no collision operator in equation (1). The dominant force is magnetic, and both the magnetic force and the particle distribution function f have a slowly-varying (average) part and a rapidly-varying (fluctuating) part. Equation (1) is linearized and solved for various cases of

interest in interplanetary space in Chapters III - V below.

Chapter II is a discussion of the observation of cosmic-ray scintillations. It begins with a discussion of the theory of stationary random functions and the calculation of power spectra. Using this framework, I then present power spectra of cosmic-ray counting rates from several types of detectors. Power spectra are presented for low-energy (1-40 MeV) protons inside the earth's magnetosphere, low-energy (1-10 MeV) protons in interplanetary space during a solar flare, the Alert and Deep River Neutron Monitors, interplanetary >50 MeV protons together with >4 MeV electrons, and interplanetary electrons (3-12 MeV). All these types of data exhibit scintillations that are significantly above the noise level, and it is found that relative scintillations (i.e., fluctuations divided by average flux) are dependent on particle species and energy but are generally independent of time for a given species and energy during undisturbed periods in interplanetary space. For protons, scintillations are a rapidly decreasing function of energy, and the contribution to the scintillations from processes near the earth (inside the earth's bow shock) seems to be important for low energies (~1-10 MeV).

The theory of magnetic-field-induced cosmic-ray scintillations is discussed in Chapters III - V and the Appendices. Chapters III and IV give the simplified theories of magnetospheric and interplanetary scintillations, respectively, while the more general theory of interplanetary scintillations is presented in Chapter V and the Appendices.

Chapter III is a discussion of the theory of magnetosheath-induced cosmic-ray scintillations. It takes as a model of the earth's

magnetosheath a thin, turbulent plasma between the two relatively unperturbed regions of interplanetary space and the magnetosphere. The model is appropriate for cosmic rays with cyclotron radius and mean-free-path large compared to the thickness of the slab, or for protons with $T \gtrsim 1$ MeV. The model leads to an equation for the cosmic-ray fluctuations in terms of average cosmic-ray gradients and the magnetic-field fluctuations, and its result is so similar to the equations for the interplanetary scintillations of radio waves that the term scintillations is borrowed to describe cosmic-ray fluctuations. It is shown that the observed scintillations of the 1-40 MeV flux inside the magnetosphere can be reasonably understood in terms of the thin-slab model of the magnetosheath. The magnetosheath fluctuations cannot be the source of the observed neutron-monitor scintillations because they decrease too rapidly with energy.

Chapter IV gives the theory of the interplanetary scintillations of cosmic rays in the low-frequency limit: $\omega, \underset{\sim}{k}\cdot\underset{\sim}{w} \ll \omega_0$. The model assumes that cosmic rays spend many scattering times in the interplanetary medium before being detected, and it leads to a relation between the cosmic-ray flux power spectrum, the power spectrum of the interplanetary magnetic field, and the average cosmic-ray anisotropy in the rest frame of the solar wind. After deriving the general equation, I consider the effect that the earth's rotation has on the predicted power spectrum observed by neutron monitors. For detectors with asymptotic viewing directions near 90° terrestrial lattitude, the predicted neutron-monitor scintillations are proportional to the interplanetary magnetic-field fluctuations at the same frequency. For

detectors with equatorial asymptotic viewing cones, however, there is a predicted enhancement in the power spectrum near a frequency of 1/day and a cutoff for lower frequencies. Taking these effects into account, I show that all the major features of the power spectra of the Alert and Deep River Neutron Monitor fluxes are explained by the interplanetary scintillations model, including a prominent feature for Deep River near f = 1/day. The model of interplanetary scintillations is in excellent agreement with the observations for frequencies $5 \times 10^{-7}\text{Hz} \lesssim f \lesssim 10^{-4}\text{Hz}$.

A mathematically more detailed consideration of the theory of interplanetary cosmic-ray scintillations is given in Chapter V, where the simplifying assumptions of Chapter IV are generalized and the scintillation equations are considered in their general form for arbitrary $\underset{\sim}{k}$ and ω. It is shown that the usual quasi-linear approach is inadequate due to the strong resonant interaction between cosmic rays and the magnetic-field fluctuations near the cyclotron-resonant wave-number. A generalization of the quasi-linear equations, incorporating the effects of the non-linear interactions explicitly, is developed. The choice of an appropriate coordinate system reduces the problem to a simple differential equation in one variable, and the solution is obtained. It is shown that the interplanetary scintillations seen by an omnidirectional detector will be quite different from those seen by a unidirectional detector. For conditions typical for 1 GeV protons near earth, in the limit $k_\perp = 0$ (i.e., the fluctuations propagate only along the average magnetic field), the more detailed consideration of the resonant interactions in Chapter V differs only slightly from the low-frequency limit of Chapter IV for all frequencies up to $\sim 10^{-4}\text{Hz}$.

Although the general scintillation equations are presented in Chapter V, and the solution to the problem involves the use of techniques of non-linear plasma theory, the simpler theoretical framework of Chapter IV adequately describes the physical processes involved.

Further details of topics related to those covered in the text of the Thesis are given in three Appendices. Appendix A contains a derivation of the most general allowed form of the magnetic-field power spectrum, using symmetry properties and assuming that the fluctuations are axially symmetric. Appendix B gives a new derivation of the diffusion equation for the average cosmic-ray distribution function using the techniques of Chapter V. The general form of the diffusion coefficients is derived, allowing arbitrary axially-symmetric magnetic-field fluctuations, and the result agrees with those of Hall (1967) and Hasselmann and Wibberenz (1968). In Appendix C, a quantitative method for including the non-linear terms in the scintillation equations of Chapter V is discussed. Following Rudakov and Tsytovich (1971), I introduce an effective scattering operator into the equations and then iterate to obtain an expression for the lowest-order non-vanishing contribution of the non-linear terms. The result is a resonance width which depends on frequency but which is of the same approximate size as the widths obtained by dimensional analysis in Chapter V. The conclusion that the low-frequency limit of Chapter IV applies for frequencies up to 10^{-4}Hz for 1 GeV protons in interplanetary space is strengthened by this analysis.

C. Implications

The purpose of this Thesis is to investigate, for the first time, cosmic-ray scintillations in an attempt to discover their origin and to consider their possible uses as probes of astrophysical electromagnetic fields. The theory of cosmic-ray scintillations in the magnetosphere and in interplanetary space was developed, and it was shown that the theory is in good agreement with power spectra calculated from several types of cosmic-ray data. The validity of the models used seems to have been reasonably established, so that it is safe to conclude that the origin of cosmic-ray scintillations under most circumstances is in random interplanetary magnetic fields and their scattering and focusing of cosmic-ray trajectories.

If this interpretation is valid, several important points can be made concerning the utility of cosmic-ray scintillations as a probe of astrophysical plasmas. First, as shown in Chapter III, low-energy (~1-10 MeV) proton scintillations inside the magnetosphere are related to the cosmic-ray anisotropy and to the magnetosheath magnetic-field fluctuations. Since most space probes spend little time passing through the magnetosheath, low-energy cosmic-ray scintillations may be a useful tool in obtaining information about the magnetic-field configuration and its variation in the magnetosheath.

Similarly, as shown in Chapters IV and V, scintillations for cosmic rays of neutron-monitor energies (~1 GeV) are related to the cosmic-ray anisotropy and interplanetary magnetic-field fluctuations. Neutron monitors, with their high counting rates, are ideal detectors of

cosmic-ray scintillations, and perhaps data from them could be used to obtain information about the interplanetary magnetic field when direct observation is not possible. In particular, neutron-monitor data are available for time periods during the 1950's and the 1960's when little interplanetary magnetic field data are available. High-counting-rate neutron monitors can be used to extend the investigation of scintillations to frequencies larger than 10^{-4}Hz, and in many cases the data are already suitable for analysis and thus provide an inexpensive source of possibly interesting information.

An immediate consequence of the excellent agreement between the theory and observation of interplanetary scintillations is the validation of the basic theoretical structure underlying the model. Thus, the standard picture of cosmic-ray propagation and diffusion in interplanetary space (Jokipii, 1971) has passed a rather stringent test. As indicated in Appendix B, the Fokker-Planck diffusion equation is based on the same set of assumptions as the scintillation equations. Whereas some other observational tests of the diffusion theory - such as radial gradient measurements, for example - are difficult to perform, the "scintillations test" described here simply involves comparing cosmic-ray and interplanetary magnetic-field power spectra.

Finally, as shown in Chapter V and Appendix C, cosmic-ray scintillations may be an ideal testing-ground for non-linear plasma theories. In the cyclotron-resonant regime, the contribution of the non-linear terms is quite large. Although neutron monitors have too large an energy response (and hence too broad a cyclotron resonance) to distinguish between theories for the non-linear terms, the basic

agreement between theory and observation for frequencies up to $\sim 10^{-4}$ Hz indicates that the method of including the non-resonant terms in the resonance width as presented in Chapter V and Appendix C is approximately correct. It is possible that other detectors could provide a meaningful test of non-linear plasma theory, since the average distribution function is well understood and the non-linear effects are very important near the cyclotron resonance.

Thus, there are many valuable avenues of research to which the study of cosmic-ray scintillations may contribute.

II. OBSERVATIONS OF COSMIC-RAY SCINTILLATIONS

An inspection of the cosmic-ray flux measured by a given detector as a function of time reveals fluctuations even during "quiet" times in interplanetary space. In this chapter, I introduce the subject of power spectral analysis as a means of quantitatively describing the nature of the fluctuations. I then present analyses of several different types of cosmic-ray data and show that in each case the scintillations are larger than can be explained on the basis of Poisson fluctuations alone.

A. The Theory of Stationary Random Functions

In order to develop a statistical framework to evaluate random fluctuations, imagine an ensemble of independent systems which are identical in all respects except that the random fluctuations in each member may be different. Each member of the ensemble is called a realization, and a typical realization may be as shown in Fig. II-1. The random function at each instant of time t_n can be averaged over the entire ensemble of realizations to yield the average value $x_0(t_n)$, and the fluctuating part of x is given by

$$x_1(t) = x(t) - x_0(t), \tag{1a}$$

with

$$x_0(t) = \langle x(t) \rangle \tag{1b}$$

and $\langle a \rangle$ represents the ensemble average of any random function a. A random function is one which can be visualized as being composed of many independent realizations as described here, and the function is defined

Figure II-1: Stationary random function. An illustration of a stationary random function, x(t). The mean is x_o and the fluctuating part of x(t) is x_1. The correlation time τ_c is the time after which the function at $t + \tau_c$ is no longer correlated with the function at t.

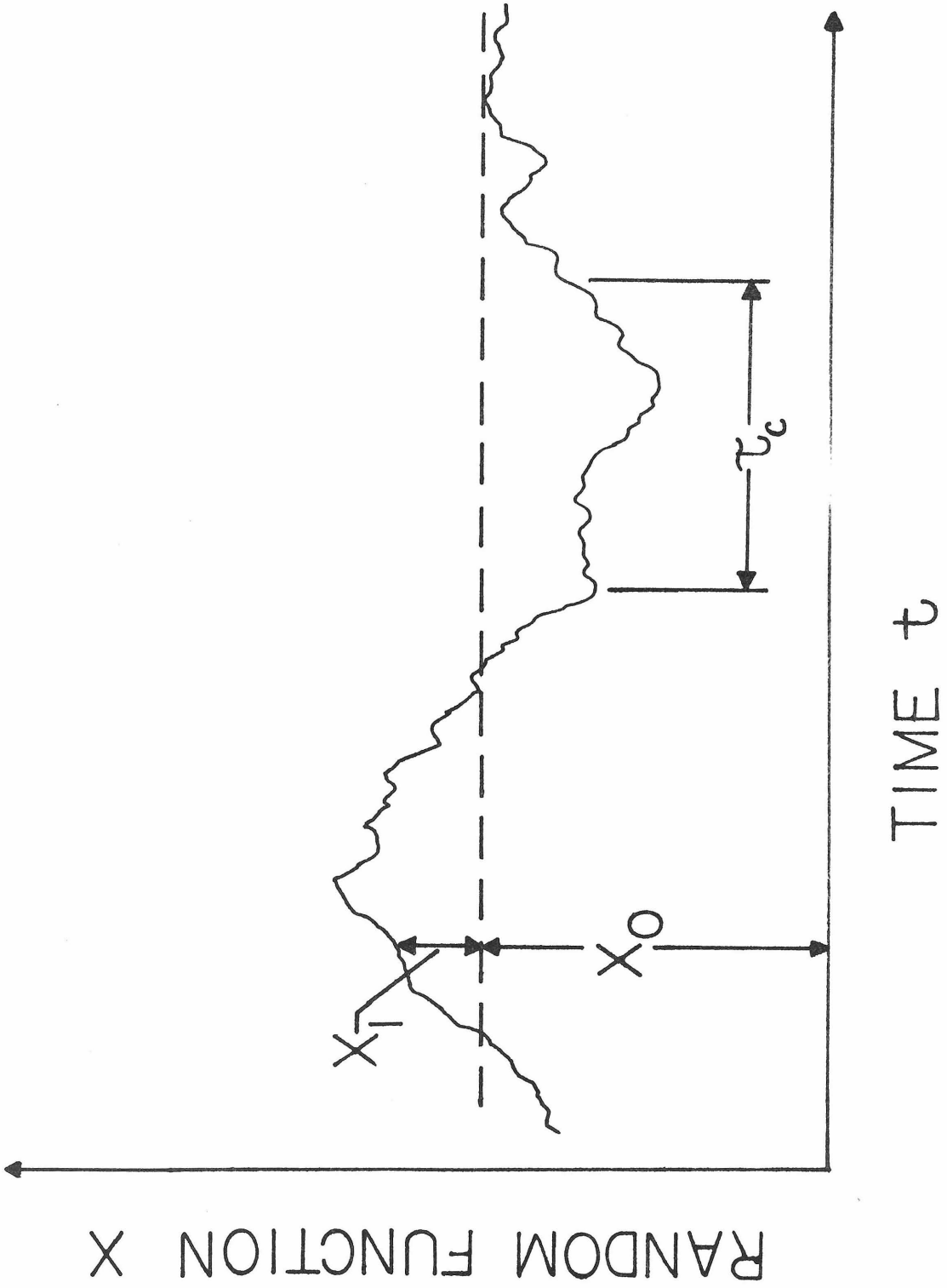
RANDOM FUNCTION X
TIME t
τ_c
X_0
X_{-1}

as stationary if all of the moments $\langle x(t)^j \rangle$, j=1,2,3.... are independent of time. In practice, weakly stationary (or quasi-stationary) random functions - random functions whose ensemble average varies, but on a time scale much longer than the correlation time of the fluctuations - are often encountered and have the same basic properties as perfectly stationary random functions.

In most cases of physical importance only one realization is obtained over a period of time. In order to utilize this data, it is necessary to append the ergodic hypothesis to the definition of the random functions. The ergodic hypothesis simply states than an ensemble average is equivalent to a temporal average over any one realization if the temporal average is taken over a long enough period of time. That is, for arbitrary a(t), the ergodic hypothesis is equivalent to the equation

$$\langle a(t) \rangle = \lim_{T \to \infty} \frac{1}{2T} \int_{-T}^{T} a(t + t')\, dt' \quad \text{(ergodic hypothesis).} \tag{2}$$

Under the ergodic hypothesis, x_0 for a stationary random function is simply the temporal average of the function.

The autocorrelation function, or simply the correlation function, is defined as

$$R^x(\tau) = \langle x_1(t)\, x_1(t + \tau) \rangle \, . \tag{3}$$

Since $x_1(t)$ is stationary, the correlation function is a symmetric function of τ. It follows from the nature of the random functions that $R^x(\tau) \leq R^x(\tau = 0)$, or the correlation function reaches its maximum value at "zero lag" ($\tau = 0$). If x(t) is a continuous function, the

derivative of $R^x(\tau)$ with respect to τ is zero at $\tau = 0$, so the correlation function is flat near $\tau = 0$. The time τ_c beyond which the correlation function falls off rapidly is called the correlation time, and it is shown schematically in Fig. II-1.

The Fourier transform of the correlation function is called the power spectrum, $P^x(\omega)$:

$$P^x(\omega) = \int_{-\infty}^{\infty} e^{i\omega\tau} R^x(\tau)\, d\tau \tag{4}$$

and the inverse transform gives

$$R^x(\tau) = \int_{-\infty}^{\infty} \frac{d\omega}{2\pi} e^{-i\omega\tau} P^x(\omega). \tag{5}$$

The power spectrum is an even, positive-definite function of frequency, ω. From the theory of Fourier transforms, it follows that the "spread" in frequency space over which the power spectrum is near its maximum value is given by

$$\omega_c \sim 1/\tau_c.$$

For a rigorous discussion of the topics in this sections, see Yaglom (1962). The power spectrum is a quantitative measure of the frequency distribution of the fluctuations being considered.

A natural generalization of the concept of random functions to more than one independent variable is possible. In four-dimensional space-time, a homogeneous, stationary random function has properties similar to those of a one-dimensional stationary random function for each of its four dimensions. For example, the ergodic hypothesis in

equation (2) is replaced by an expression in which the right side involves integrals over x', y', and z' as well as t'. In equation (3), the correlation function becomes a function of the four separations $\underset{\sim}{\xi}$ and τ, and the right-hand side becomes $\langle x_1(\underset{\sim}{r},t)\ x_1(\underset{\sim}{r} + \underset{\sim}{\xi},\ t + \tau)\rangle$. The power spectrum then becomes a function of the four arguments k_x, k_y, k_z and ω. These generalizations are straightforward and will not be discussed further.

B. The Calculation of Power Spectra

Most cosmic-ray data are composed of a set of discrete, equally-spaced, counting rates. For simplicity, only this type of data will be discussed here. Since information is available only once every T time units, it is evident that such data can contain no information for frequencies larger than 1/T. Actually, since $P^X(\omega)$ is an even function of frequency, half of the information content in the data is redundant and consequently only information about frequencies

$$f \leq f^* \equiv 1/2T \tag{6}$$

is available. The frequency f^* is called the aliasing frequency. Let $\underline{T}$ be the total length of the data record, so that there are $n = \underline{T}/T$ equally-spaced data points in the record to be analyzed.

As is conventional, the observed power spectrum will be considered a function of frequency in the range $0 \leq f < \infty$, which together with equation (4) and the even nature of $P^X(f)$ yield

$$P^X(f) = 4 \int_0^\infty R(\tau) \cos(2\pi f \tau)\, d\tau. \tag{7}$$

Since the correlation function at zero lag, $R^X(\tau = 0)$, is simply the variance σ^2, it is easy to show from equation (5) that the variance of x(t) and the power spectrum are related via

$$\sigma^2 = \int_0^\infty P^X(f)\, df. \tag{8}$$

Although the measured power spectrum contains no information about frequencies $f > f^*$ as discussed above, the actual physical process may have significant power for frequencies larger than the aliasing

frequency. In essence, the collection of data at times separated by T results in the folding of the entire frequency range $0 \leq f < \infty$ onto the smaller range $0 \leq f \leq f^*$ in an accordian-like manner. The calculated power spectrum $P^x(f)_{calculated}$ will be related to the true power spectrum $P^x(f)$ by

$$P^x(f)_{calculated} = P^x(f) + \sum_{\substack{j=2 \\ even}}^{\infty} P^x(jf^*-f)+P^x(jf^*+f) \quad . \qquad (9)$$

This "aliasing" of the spectrum is a result of gathering data at discrete points and is independent of the method used to estimate the power spectrum. For a power spectrum falling off as f^{-p} for $f \gtrsim f^*$, where $p \gtrsim 1.5$, it can be shown that the effects of aliasing are less than 30% over the entire frequency range and less than 10% for $f < \frac{1}{2}f^*$. It will be shown below that the spectra of cosmic-ray scintillations generally fall off rapidly enough that aliasing is unimportant.

Given an equally-spaced (in time) series of data points, there are three commonly-used methods of calculating power spectral estimates. The first is the "fast Fourier transform" method. Given a function x(t) from time t = 0 to t = T, one first takes the full Fourier transform of x(t) to obtain $\tilde{x}(\omega)$. Use is then made of the Wiener-Khinchin theorem,

$$2\pi P^x(\omega)\ \delta(\omega - \omega') = \langle \tilde{x}(\omega)\ \tilde{x}(\omega')^* \rangle, \qquad (10)$$

where the star signifies complex conjugation, to obtain the power spectrum. This method yields one power-spectral estimate for each data point, and the estimates are equally spaced in frequency space. Each estimate has only one degree of freedom, so in practice a smoothing routine is used

to average over several estimates, thus giving a smaller number of independent estimates, each with better statistical accuracy.

The second method used to calculate power spectra is the "correlation-function" method, discussed in detail by Blackman and Tukey (1958). For an asympotitically large number of data points, the Blackman-Tukey algorithm produces the same results as the fast Fourier transform method and has the same statistical properties. The method is based on equations (3) and (4); first the correlation function $R_i^x(\tau)$ is calculated for m values of τ, and then $R_i^x(\tau)$ is Fourier-transformed as in equation (4) to obtain m estimates of the power spectrum. The estimates are then smoothed to produce new estimates with slightly better statistical properties. (In the applications discussed below, smoothing in the frequency domain is done using the "hanning" algorithm.) It can be shown that the number of degrees of freedom that each of the m power spectral estimates has is 2n/m, and the errors in the estimates have a chi-squared distribution with 2n/m degrees of freedom. In practice, estimates are usually made with at least 10 degrees of freedom so that the errors are not too large. If too few degrees of freedom are allowed in the calculation, the algorithm can produce such spurious results as power spectra which are negative over some range of frequencies.

A third method of calculating power spectra is the nested-variance method, called the pilot method by Blackman and Tukey. Its first step is to calculate the variance $\langle \sigma_1^2 \rangle$ obtained from consecutive intervals of duration T. Next one calculates the variance $\langle \sigma_2^2 \rangle$ obtained from consecutive intervals with twice the duration. That is, one calculates

$$\langle \sigma_1^2 \rangle = \langle \left(\frac{1}{T} \int_t^{t+T} x(t')\, dt'\right)^2 \rangle \qquad (11a)$$

and

$$\langle \sigma_2^2 \rangle = \langle \left(\frac{1}{2T} \int_t^{t+2T} x(t')\, dt'\right)^2 \rangle. \qquad (11b)$$

Then it can be shown (Siscoe and Jokipii, 1966) that

$$\int_0^\infty df \left[\frac{1}{2\pi} \left(\frac{\sin^2 \pi f T}{\pi f T}\right)^2\right] P^x(f) = \langle \sigma_1^2 \rangle - \langle \sigma_2^2 \rangle. \qquad (12)$$

The function in brackets is a rather sharply-peaked function of frequency with maximum located at $f \sim 0.7f^*$, where $f^* = 1/2T$ as above. If the power spectrum is a smoothly-varying function of frequency, it can be pulled out of the integral in equation (12) and the integral can be evaluated to yield

$$P^x(f \sim 0.7f^*) \approx (4\pi/f^*) \left[\langle \sigma_1^2 \rangle - \langle \sigma_2^2 \rangle\right]. \qquad (13)$$

Thus the calculation of two variances gives an estimate of the power spectrum for frequencies between $f^*/2$ and f^*. If one next calculates the variance $\langle \sigma_4^2 \rangle$ from consecutive intervals of duration 4T, one can use equation (12) with the substitutions $\langle \sigma_1^2 \rangle \rightarrow \langle \sigma_2^2 \rangle$, $\langle \sigma_2^2 \rangle \rightarrow \langle \sigma_4^2 \rangle$, and $T \rightarrow 2T$. An estimate of the power spectrum for frequencies between $f^*/4$ and $f^*/2$ is then obtained. The procedure can be continued to give p-1 estimates of the power spectrum at p-1 frequency intervals going down by factors of two from f^* if there are 2^p data points in the data record.

An analysis of the error involved in the estimation of power spectra by the nested-variance technique is straightforward. For Gaussian statistics, or for <u>any</u> statistics if the number of data points n is large, it can be shown that the variance $\langle \sigma_1^2 \rangle$ is distributed according to the chi-squared distribution with n degrees of freedom. Similarly, $\langle \sigma_2^2 \rangle$ has a chi-squared distribution with n/2 degrees of freedom since only half as many data points are available. Since the difference $\chi_s^2 - \chi_t^2$ between two chi-squared distributions with s and t degrees of freedom respectively is again chi-squared with the number of degrees of freedom given by (s-t) (e.g., Section 2.6 of Theil, 1971), it follows immediately from equation (13) that the power-spectral estimate indicated has a chi-squared distribution with n/2 degrees of freedom. The next estimate, based on $\langle \sigma_2^2 \rangle - \langle \sigma_4^2 \rangle$, has a distribution of $\chi_{\frac{n}{4}}^2$, and so forth. The j^{th} estimate has a chi-squared distribution with $n/2^j$ degrees of freedom.

It is instructive to compare the types of estimates of the power spectrum obtained by the correlation-function and the nested-variance methods. For a data record with n points, the correlation-function method with 20 degrees of freedom yields approximately m = n/10 estimates of the power spectrum, equally spaced by intervals of $10f^*/n$ in frequency space. The nested-variance method yields p estimates of the power spectrum, where $n = 2^p$, and the estimates are equally spaced in log f since they correspond to frequencies differing by factors of two. Therefore, if the power spectrum is to be plotted on a log-log scale or is expected to be a power law in frequency, the nested-variance

method of finding estimates is more appropriate. In both cases the observed power spectrum is obtained from a convolution of the true power spectrum with a "filtering" factor in frequency space. The correlation-function method's hanning filter is described in Blackman and Tukey (1958), and the nested-variance filter is the term in brackets in equation (12),

$$Q(f) \propto \left[\frac{\sin^2 \frac{\pi}{2} f/f^*}{(\frac{\pi}{2} f/f^*)} \right]^2, \qquad (14)$$

where f^* is the aliasing frequency, 1/2T. A comparison of the frequency filters of the two methods is shown in Fig. II-2, where two decades of frequency are shown and it is assumed that m = 10 (ten lags used) for the correlation-function method. Notice that, on the logarithmic scale used, the nested-variance method's filter has the same shape for all frequency bins, whereas the correlation-method's filter shape gets narrower for larger frequencies. In both cases, however, the filter has decreased to about 80% of its maximum value at the ends of the nominal width of the frequency band and has a value of less than 20% of its maximum in the second frequency band away from the central one. Both filters fall off approximately as f^{-2} far from the central frequency, indicating that these methods are inaccurate if the power spectrum falls off more rapidly than f^{-2} over a large range of frequencies.

Figure II-2. Frequency filters for power spectral analysis. A comparison of the frequency filters for the correlation-function method (solid curve) and the nested-variance method (dashed curve) of calculating power spectra. Ten estimates are used in the correlation-function method, and a logarithmic frequency scale is used. The vertical scale is linear. The two divided lines at the top of the figure give the nominal widths of the frequency filters for the two methods.

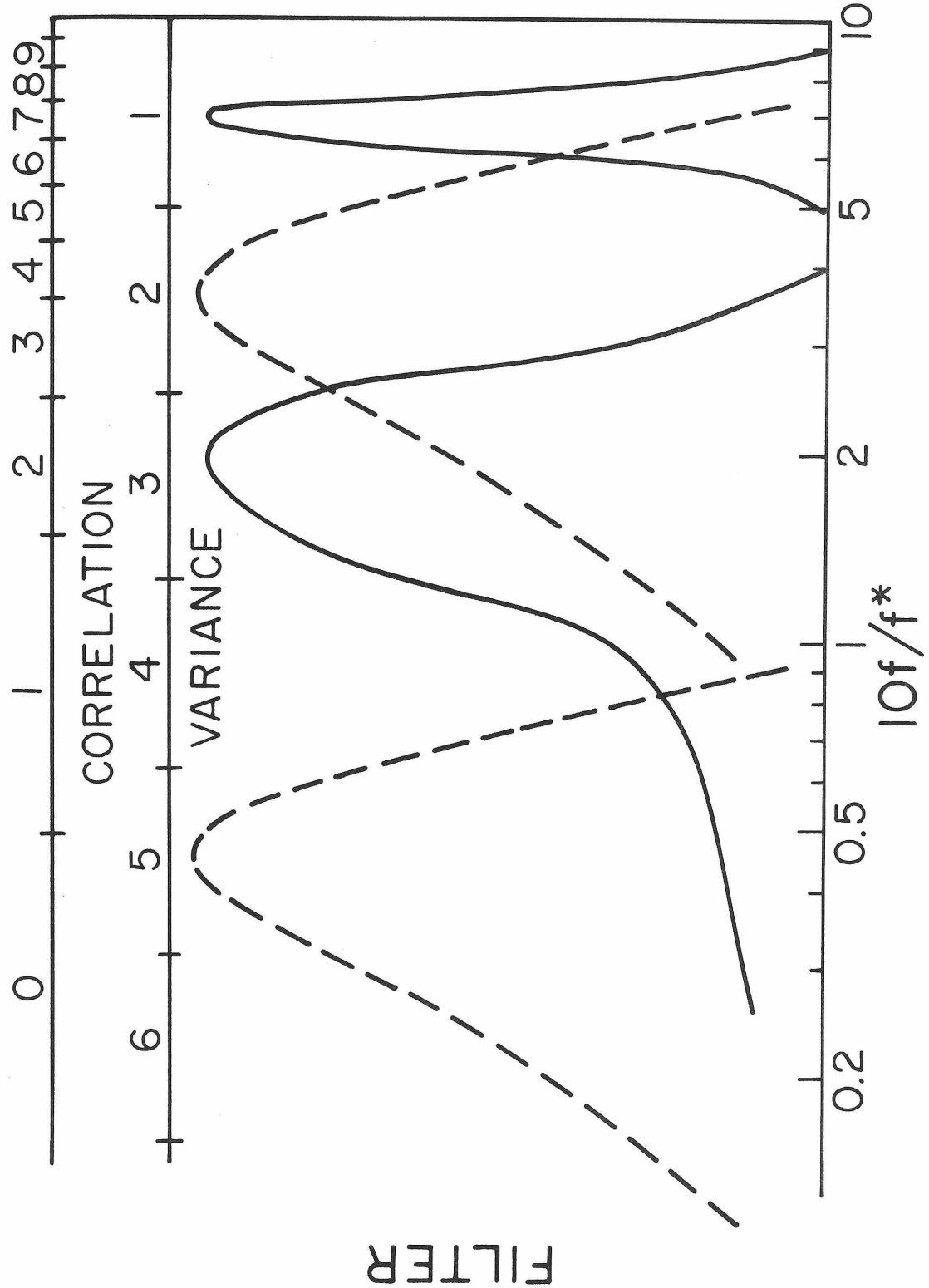
CORRELATION
VARIANCE
FILTER
10f/f*
0
1
2
3
4
5
6
7
8
9
10
5
2
1
0.5
0.2

C. The Power Spectrum of Poisson Noise

Consider a detector which samples an average counting rate of n particles/sec for t sec. For Poisson statistics, the expected relative mean-square error of the total number of particles counted will be

$$\frac{\langle \delta N^2 \rangle}{N^2} = \frac{N}{N^2} = \frac{1}{N} = \frac{1}{nt} \quad . \tag{15}$$

An important property of Poisson statistics is that each observation is completely independent of the previous time-history of the system, so the frequency spectrum must be flat. As discussed above, the power spectrum is defined for frequencies $0 \leq f \leq f^*$ where $f^* = 1/2T$. Another property of the power spectrum, as shown in equation (8) above, is that the variance is the integral of the power spectrum over all frequencies. From these properties of Poisson statistics and of power spectra, it is straightforward to show that the power spectrum of the relative fluctuations $\delta N/N$ is given by (Owens and Jokipii, 1972)

$$P(f)_p = 2/Dn, \quad 0 \leq f \leq f^*. \tag{16}$$

Here $D = t/T$ is the "duty cycle", or the fraction of the data-gathering cycle during which data are collected by the detector.

For a detector, such as any cosmic-ray detector, which samples particles subject to Poission counting statistics, the Poission power indicated by equation (16) is the minimum or noise level. Any other mechanism which causes fluctuations will cause frequency-dependent increases in the power spectrum over the level indicated by equation (16). A spectrum which demonstrates this effect strikingly is Fig. II-11, which

will be discussed below. Power spectra which exceed Poisson power over some range of frequencies therefore exhibit statistically significant fluctuations. In order to facilitate comparison both with the Poisson noise level and with the results of the theory presented in the later sections, I present power spectra of the relative fluctuations (i.e., x_1/x_0 in the notation of Section II.A above) of the cosmic-ray counting rate. Data for which power spectra may be calculated must satisfy several general requirements. The process must be approximately stationary; that is, the average value of the cosmic-ray counting rate must be constant or vary slowly over the time scale to be investigated. Data must be available at fixed intervals, with few data gaps. Finally, for the spectra to be physically interesting, the counting rate must be high enough so that fluctuations merely due to Poisson counting statistics are insignificant. These three restrictions limit the types of cosmic-ray data which are suitable for power-spectral analysis.

D. Scintillations of Low-Energy Protons (1 MeV < T < 40 MeV)

Counting rates of low-energy protons from polar passes of a low-altitude polar orbiting satellite (OGO VI) were graciously provided by the Caltech group under the direction of E. C. Stone and R. Vogt. A solid-state detector with an effective threshold of about 1 MeV/nucleon and an upper cutoff of about 40 MeV for protons (150 MeV/nucleon for alpha particles) was used to sample the counting rate at terrestrial latitude greater than 74 degrees on each polar pass. The rigidity cut-off for 1 MeV protons in the magnetosphere during quiet times occurs at less than 72 degrees latitude, so temporal variations are due to a variation in the flux of cosmic rays and not to varying geomagnetic cut-offs. The data-collecting time was about eight minutes over each pole, and the transit time between poles was about 50 minutes. The fraction of the counting rate due to alpha particles was less than 5% and there was essentially no electron contribution, so that essentially the entire flux measured is due to protons with kinetic energies 1 MeV $\lesssim$ T $\lesssim$ 40 MeV. The counting rate during quiet times was typically one count per second, or 500 protons per polar pass. The orbital parameters were such that a certain fraction of the orbits were too far from the poles for polar data to be gathered and analyzed. Therefore, it was necessary to average over several polar passes to obtain data points which were equally spaced in time.

Data were available for approximately six months in the latter part of 1969. Although many periods showed too much activity to be suitable for power spectral analysis, several good stretches of data with a reasonably stationary mean were found. A straight line was

fitted to the data and subtracted to remove the average and the linear time trend, and power spectral analyses were performed separately for three representative quiet times. The relevant parameters for the three periods selected are presented in Table II-1.

The power spectra for the three periods given in Table II-1 are given in Figures II-3, II-4 and II-5 as indicated. In Fig. II-3, I have presented power spectra calculated on the identical data from both the correlation-function method (circles) and the nested-variance method (histograms). It can be seen that the two methods of calculating the spectrum are in basic agreement, with a frequency spectrum going approximately as f^{-2}. The spectra in Figures II-4 and II-5 have about the same shape as the one in Fig. II-3 and amplitudes which are nearly the same, in spite of a factor of 10 variation in the average flux as shown in Table II-1. The power spectra for all three periods are superimposed in Fig. II-6. It is clear that the three spectra coincide quite well, indicating that the relative quiet-time low-energy cosmic-ray fluctuations are a persistent feature, changing little in amplitude (for frequencies $10^{-6}\text{Hz} \lesssim f \lesssim 10^{-4}\text{Hz}$) over the course of a period of about $\frac{1}{2}$ year. Furthermore, the insensitivity of the power spectrum to shifts in average flux of greater than a factor of 10 indicates that the root-mean-square fluctuation $\sqrt{\langle j_1^2 \rangle}$ in the cosmic-ray flux observed inside the magnetosphere at these energies is proportional to the average flux j_0. That is, the observations establish the criterion that

$$\langle j_1^2 \rangle \propto j_0^2. \tag{17}$$

This is an important constraint which any model of the scintillations

1-40 MeV Proton Data Used for Power Spectral Analysis

Data Label	Dates	Average Counting Rate (counts/sec)	Poisson Noise Level (Hz^{-1})	Figure
C1	Sept. 19-25, 1969	5.	3.	II-3
C2	Nov. 11-21, 1969	0.4	30	II-4
C3	June 22-July 15, 1969	1.	15	II-5

Table II-1

Figure II-3. Power spectrum of the 1-40 MeV proton flux, C1. Data taken during a quiet time aboard OGO VI, inside the magnetosphere, Sept. 19-25, 1969. Histogram spectrum calculated via the nested-variance method, with 90% confidence intervals shown. Open circles are the spectrum calculated by the correlation-function method, with 90% confidence intervals shown. The average counting rate was 5/sec and the Poisson noise level 3 Hz^{-1}.

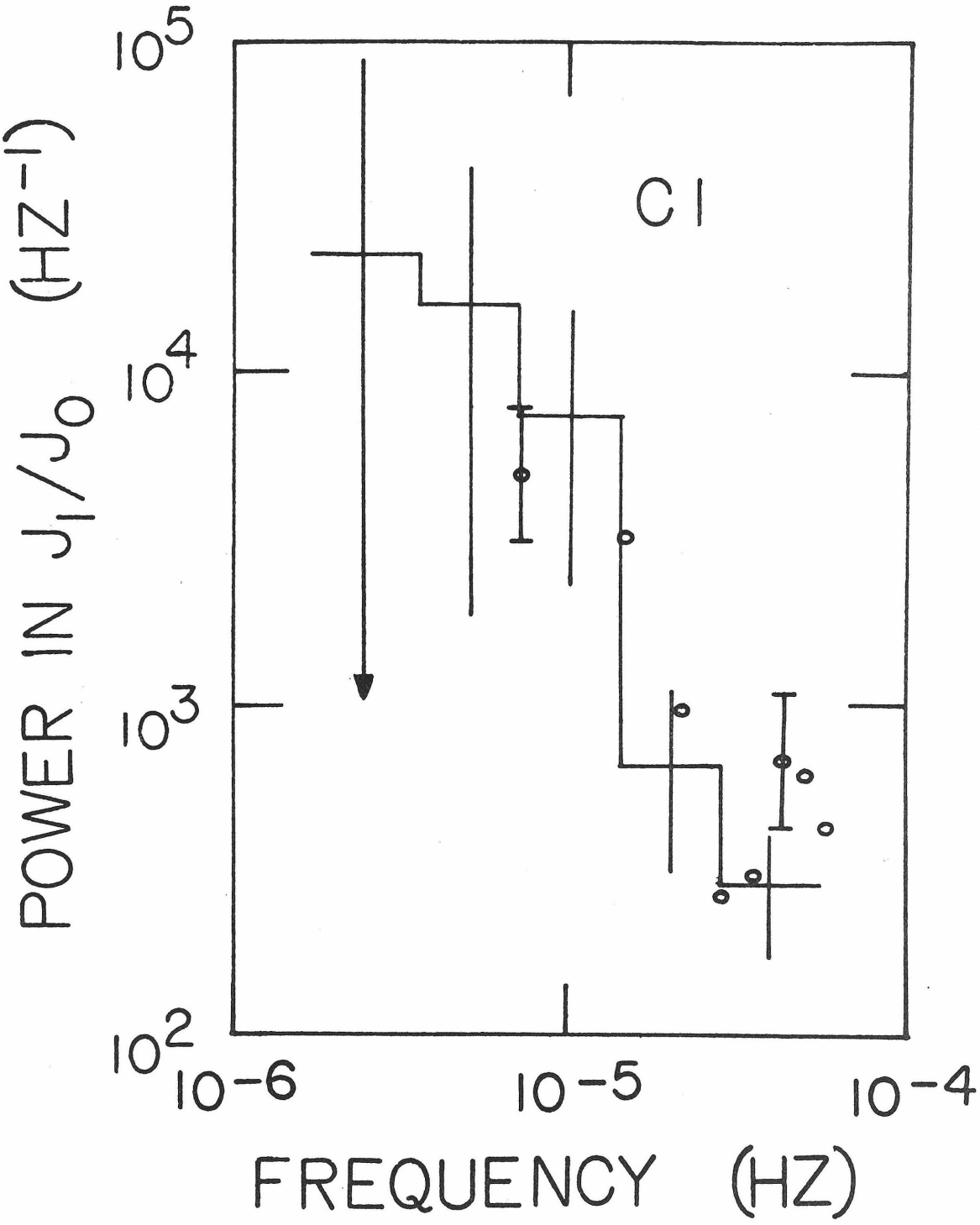
C1
POWER IN J_1/J_0 (HZ-1)
10^5
10^4
10^3
10^2
10^{-6}
10^{-5}
10^{-4}
FREQUENCY (HZ)

Figure II-4. Power spectrum of the 1-40 MeV proton flux, C2. Data taken during a quite time aboard OGO VI, inside the magnetosphere, Nov. 11-21, 1969. Spectrum calculated with the nested-variance method; 90% confidence intervals are shown. The average counting rate was 0.4/sec and the Poisson noise level 30 Hz^{-1}.

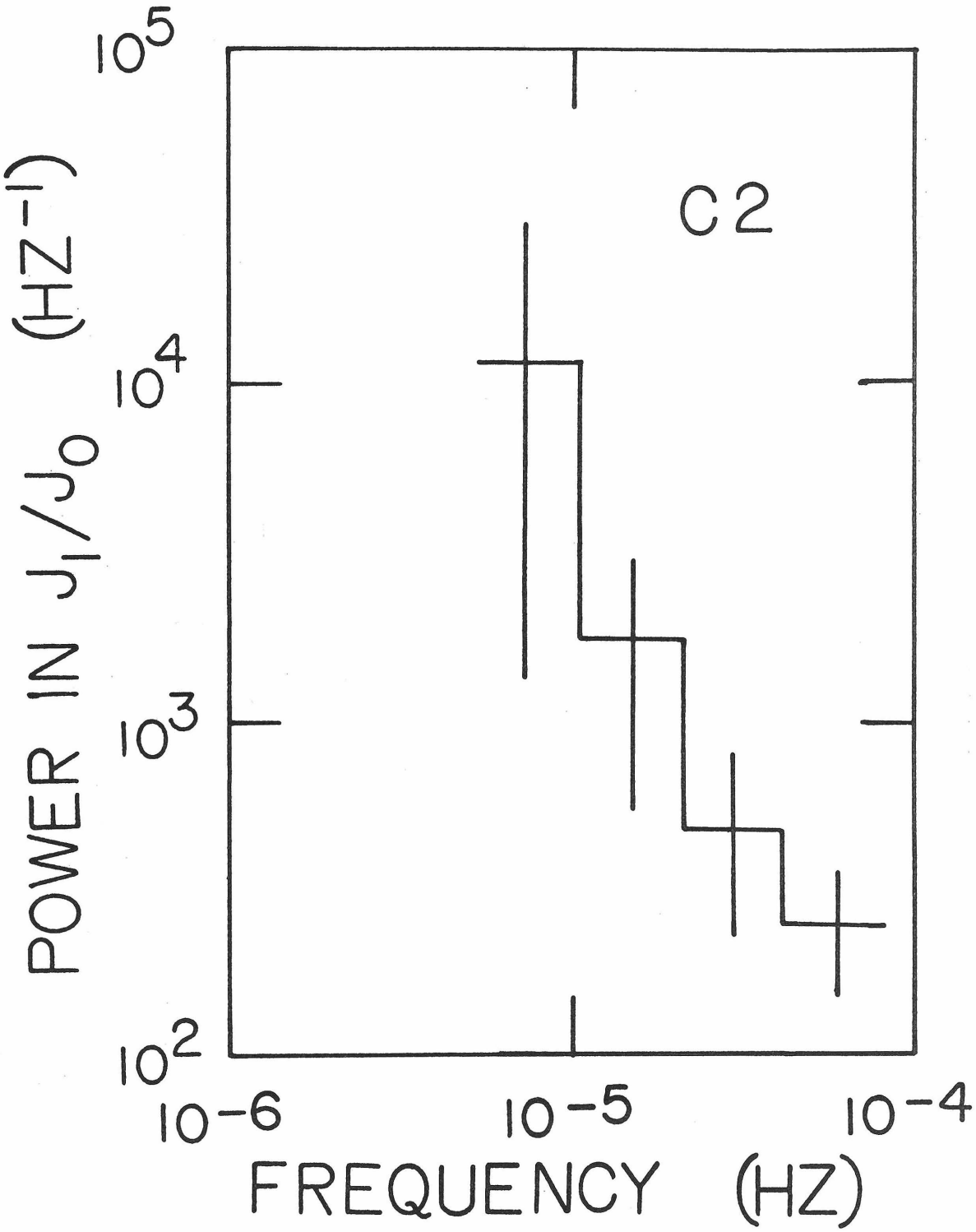
C2
POWER IN J_1/J_0 (HZ-1)
10^5
10^4
10^3
10^2
10^{-6}
10^{-5}
10^{-4}
FREQUENCY (HZ)

Figure II-5. Power spectrum of the 1-40 MeV proton flux, C3. Data taken during a quiet time aboard OGO VI, June 22 - July 15, 1969. The average counting rate was 1/sec and the Poisson noise level 15 Hz^{-1}.

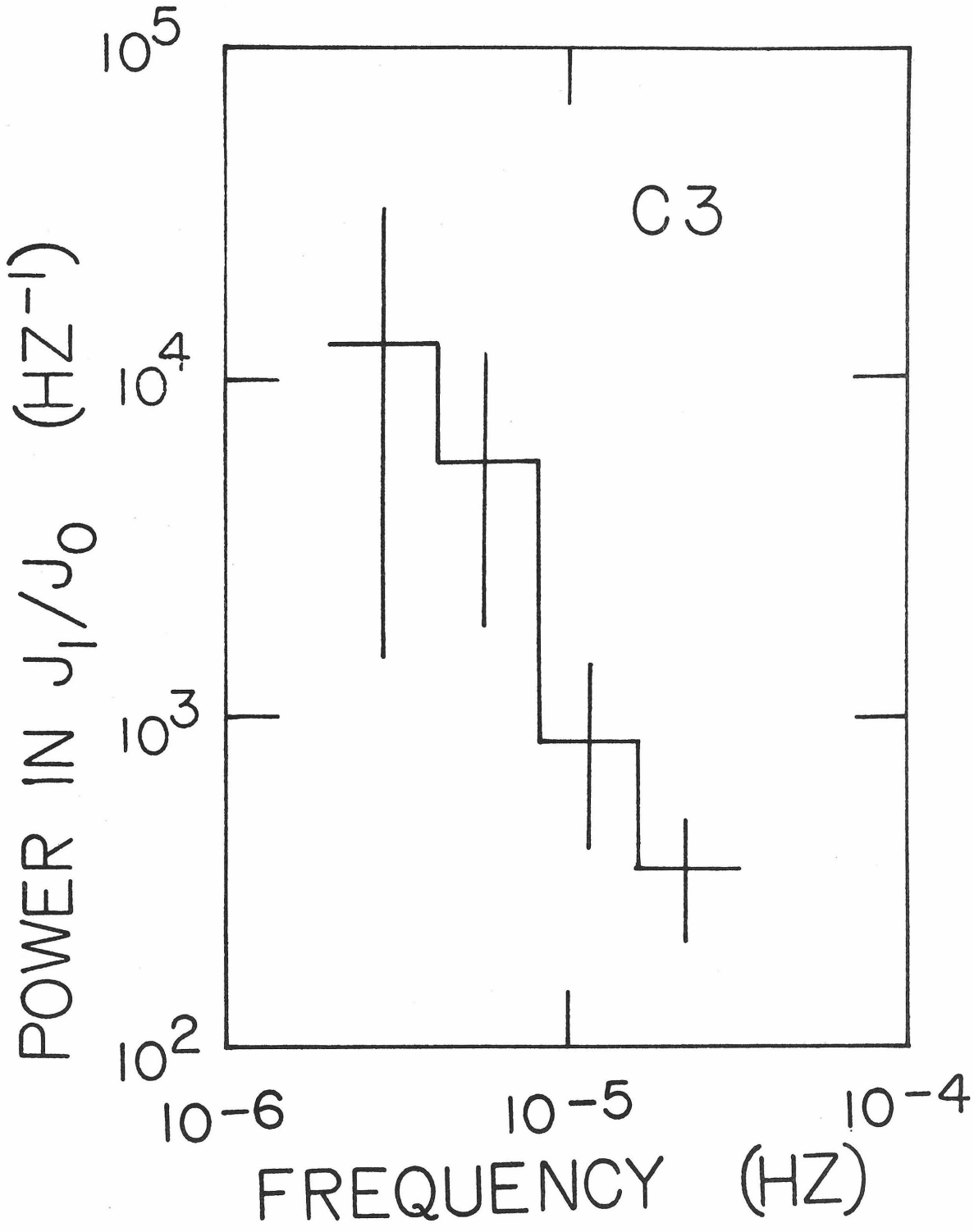
C3
POWER IN J_1/J_0 (HZ-1)
10^5
10^4
10^3
10^2
10^{-6}
10^{-5}
10^{-4}
FREQUENCY (HZ)

Figure II-6. Power spectra of the 1-40 MeV proton flux, C1, C2, and C3. Power spectra from the last three figures are superimposed on one graph, with coding indicated on the figure. The straight line is a visual best-fit to the data. Below 10^{-5} Hz, the dashed extension indicates that the spectrum may be turning away from the f^{-2} shape which best fits the higher-frequency data.

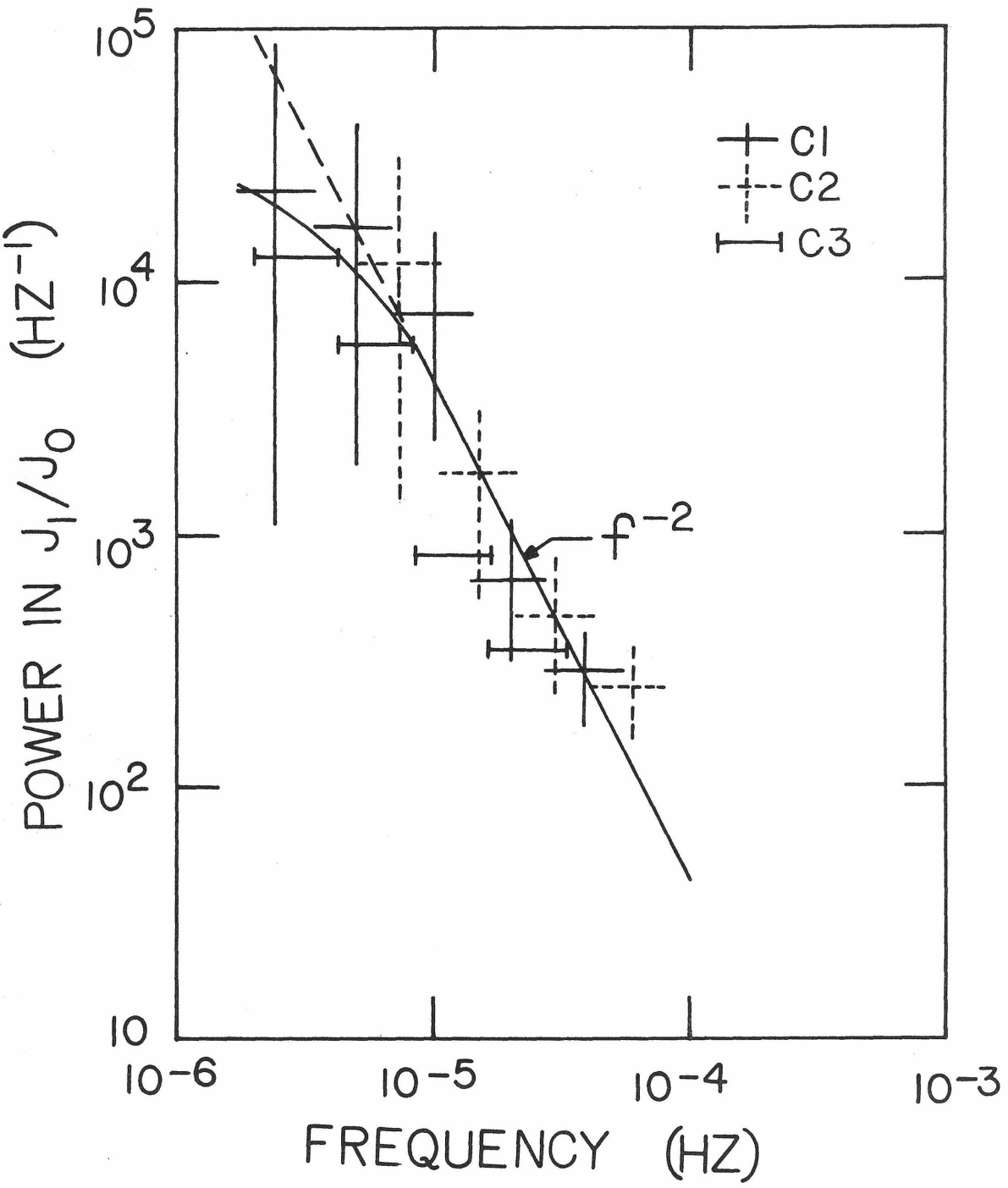
10^5
10^4
10^3
10^2
10
POWER IN J_1/J_0 (HZ^{-1})
C1
C2
C3
f^{-2}
10^{-6}
10^{-5}
10^{-4}
10^{-3}
FREQUENCY (HZ)

must satisfy.

The power spectra presented in Fig. II-6 indicate that the fluctuations are much larger than expected on the basis of Poisson counting statistics alone. The Poisson noise level for each spectrum, as calculated from expression (16), is indicated in Table II-1, and the observed power spectra are all a factor of 10 or more larger. The shape of the power spectrum of ~1-40 MeV proton scintillations inside the magnetosphere is approximately a power law in frequency with exponent of (-2) for $f \gtrsim 10^{-5}$Hz, perhaps leveling off somewhat for frequencies $f < 10^{-5}$Hz. The visual best-fit straight line is given by

$$P^{j}(f)/j_0^{\,2} \approx 45(f/10^{-4}\text{Hz})^{-2}\ \text{Hz}^{-1}, \qquad (18)$$

where $P^{j}(f)/j_0^{\,2}$ is the power spectrum of j_1/j_0 in the notation of Section II.A above.

Williams (1969) has obtained power spectra of 1-10 MeV protons in <u>interplanetary</u> space during solar flare events. A typical spectrum, for Nov. 15-16, 1967, is shown in Fig. II-7. Although this spectrum was taken during a non-quiet time in the interplanetary medium, so that the fluctuations might be expected to be larger than normal, a comparison with Fig. II-6 (for 1-40 MeV protons inside the magnetosphere) shows that the interplanetary spectrum (even though obtained during a disturbed period) is about an order of magnitude lower in amplitude than the spectrum observed near earth. This may be an indication that the major source of low-energy cosmic-ray scintillations near earth is the turbulent magnetosheath field. Unfortunately, Williams' detector has a small geometrical factor, so the counting rate during quiet times is low

Figure II-7. Power spectrum of the 1-10 MeV proton flux. Data taken during a solar flare in interplanetary space by a detector aboard Explorer 34, on Nov. 15-16, 1967. Power spectrum given by Williams and renormalized to give the power in j_1/j_o. The average counting rate was 100/sec. Power falls off below 5×10^{-5} Hz due to filtering of the data before analysis; this fall-off probably is not a feature of the cosmic-ray flux power spectrum.

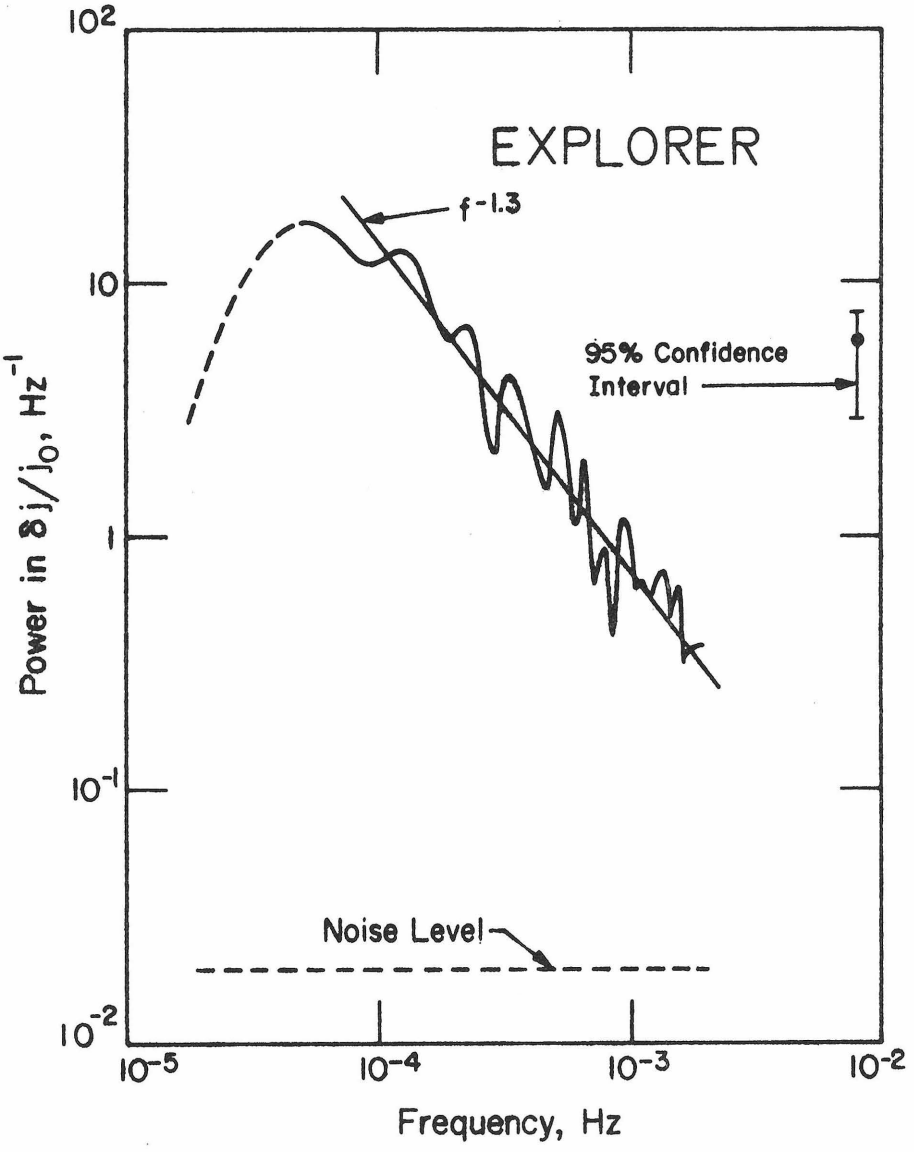
EXPLORER
f-1.3
95% Confidence Interval
Noise Level
Power in δj/j0, Hz-1
Frequency, Hz
10²
10
1
10-1
10-2
10-5
10-4
10-3
10-2

and real cosmic-ray scintillations during quiet time are masked by Poisson noise. Although further data, particulary simultaneous measurements at similar energies inside and outside the magnetosheath, are necessary before any definite conclusion can be drawn, it appears that the scintillations of cosmic rays of low energies (~1-40 MeV) may be much larger inside the magnetosphere than in interplanetary space during typical quiet times.

E. Scintillations of High-Energy Protons (T ~ 1 GeV) and Electrons (T ~ 5 MeV)

Neutron monitors are cosmic-ray detectors on earth which count neutrons produced as secondaries in the interaction of high-energy cosmic rays with the earth's atmosphere. Neutron monitors respond primarily to cosmic-ray protons with energies $T_0 \leq T \lesssim 50$ GeV incident at the top of the atmosphere, where the threshold value T_0 is called the geomagnetic cutoff energy and depends on the location of the neutron monitor in the earth's approximately dipole magnetic field. The calculation of the geomagnetic cutoff and of the detailed energy response of the monitors depends on the geomagnetic field and the cosmic-ray energy spectrum, and such calculations have been done previously (see, for example, Shea, Smart and McCracken, 1965). The relevant data for the two neutron monitors used in this study are given in Table II-2. It can be seen that the Alert Neutron Monitor responds primarily to particles with the same asymptotic direction in interplanetary space (corresponding to geographic latitude $\gtrsim 60^\circ$), while the Deep River Neutron Monitor samples different portions of interplanetary space as its asymptotic viewing cone is swept across the sky by the earth's rotation once each day.

In order to facilitate comparison with the low-energy data, I have analyzed the counting rates of the Alert and Deep River Neutron Monitors for the period Sept. 1-Nov. 30, 1969, a period which includes the data labeled C1 and C2 as discussed above. The data used were published pressure-corrected hourly averages of the two neutron monitor counting rates (Steljes, 1970). The power spectrum for the Alert Neutron

Parameters for the Alert and Deep River Neutron Monitors

Parameter	Alert	Deep River
Geographic Latitude[1]	82°30'N	46°06'N
Geographic Longitude[1]	62°20'W	77°30'W
Magnetic Inclination[1]	85.7°	76.0°
Altitude (meters)[1]	66	145
Cutoff Rigidity (GV)[1]	<0.05	1.02
L Value[1]	278.2	3.846
Asymptotic Latitude (2 GeV)[2]	84°	-21°
Asymptotic Longitude (2 GeV)[2]	-3°	-13°

Table II-2

[1]Booth (1970)

[2]Shea, Smart, and McCracken (1965). Uses internal field only. For extended geomagnetic tail, variation in asymptotic latitude for Alert for $T > 1$ GeV is $60^\circ < \lambda < 90^\circ$ (Shea, 1972).

Monitor is given in Fig. II-8. Of the two spectra in this figure, one was calculated after subtraction of a fitted straight line and the other after subtraction of only the average. The close correspondence between the two spectra indicates, as expected, a lack of dependence of the power spectrum on the method of removing long-term trends in the data. The shape and amplitude of the power spectrum are approximately given by

$$P^j(f)/j_0^2 \approx 3 \times 10^{-2} \, (f/10^{-4}\text{Hz})^{-1.5} \, \text{Hz}^{-1}. \qquad (19)$$

The power spectrum of the Deep River Neutron Monitor is given in Fig. II-9 for frequencies $f > 10^{-6}$ Hz. Power spectra were calculated using both the nested-variance method (histogram) and the correlation-function method (open circles). The overall shapes of the two spectra in this figure are the same, but there are differences in detail. Near $f \sim 1.5 \times 10^{-5}$ Hz, for example, the narrower-band analysis from the correlation-function method indicates a peak; this peak will be discussed in Chapter IV. The well-known diurnal anisotropy appears as a small, sharp spike in the power spectrum (Ables, 1967) which is unresolved in this analysis. Thus, the diurnal anisotropy is only a small perturbation to the power spectrum and not the dominant effect. Thus, it can be concluded that statistically-significant scintillations are exhibited by neutron monitors, indicating fluctuations in the cosmic-ray proton flux at ~2 GeV kinetic energy. Power spectra of neutron-monitor counting rates over more restricted frequency ranges have previously been presented by Dhanju and Sarabhai (1967) and by Jokipii (1969). Some of the data presented here were published previously in Owens and Jokipii (1972). Ables (1967)

Figure II-8. Power spectrum of the flux of the Alert Neutron Monitor. The solid points are obtained from the raw data after subtraction of a fitted straight line. The points marked X are the power spectrum obtained from the same raw data after subtraction of the mean only. The period is Sept. 1 - Nov. 30, 1969, and the average counting rate was about 180/sec. The noise level was $\sim 10^{-2}$ Hz^{-1}. 90% confidence intervals are shown for the first estimates.

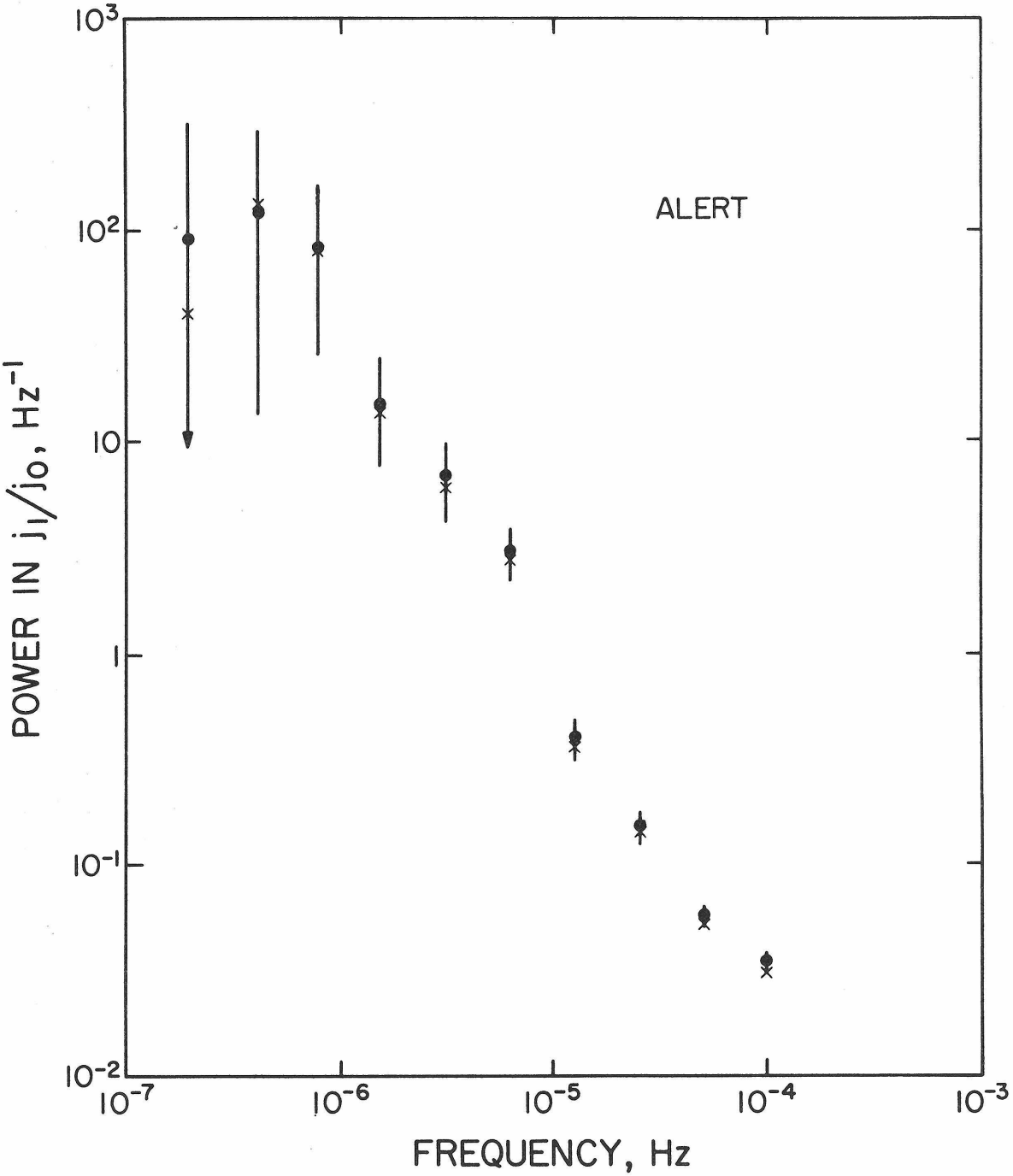
ALERT
POWER IN j_1/j_0, Hz^{-1}
FREQUENCY, Hz
10^3
10^2
10
1
10^{-1}
10^{-2}
10^{-7}
10^{-6}
10^{-5}
10^{-4}
10^{-3}

Figure II-9. Power spectrum of the flux of the Deep River Neutron Monitor. The solid histogram is the power spectrum obtained with the nested-variance method. The open circles are the power spectrum obtained with the correlation-function. The period is Sept. 1 - Nov. 30, 1969, and the average counting rate was about 510/sec. The noise level was $4 \times 10^{-3} Hz^{-1}$. Representative 90% confidence intervals are indicated on the histogram, and the 90% confidence intervals for the open circles are all of the size indicated.

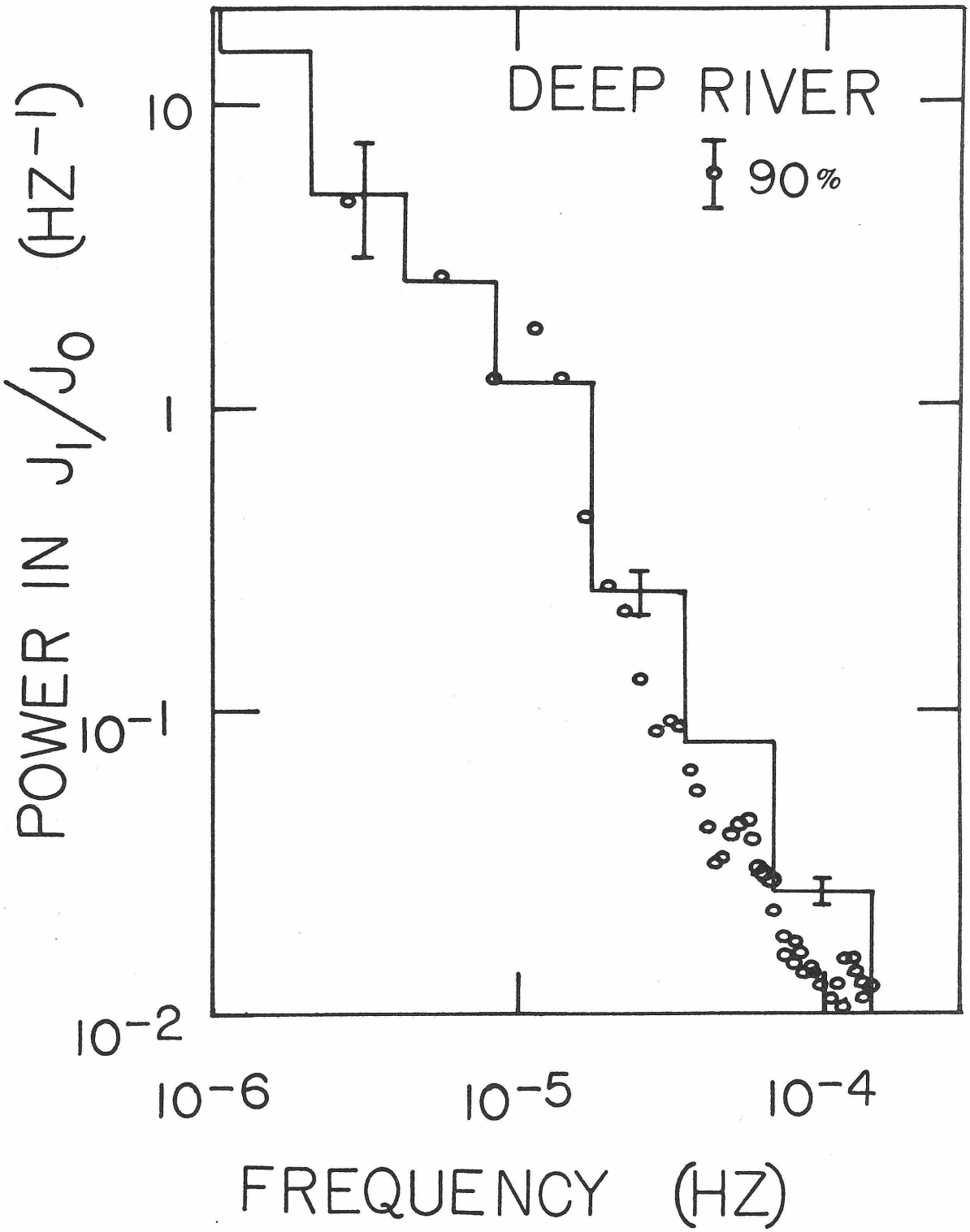
DEEP RIVER
90%
POWER IN J_1/J_0 (HZ-1)
10
1
10^{-1}
10^{-2}
10^{-6}
10^{-5}
10^{-4}
FREQUENCY (HZ)

has given the high-resolution spectrum for the Deep River Neutron Monitor flux for frequencies 1/11 years $\leq f \leq$ 1/hour. His spectrum agrees with those presented here, and the discussion in Chapter IV below will consider his high-resolution spectrum near f ~ 1/day in detail.

The power spectra of the Alert and Deep River Neutron Monitors are superimposed in Fig. II-10. It can be seen that the shapes and amplitudes are basically the same, with a few differences in detail. Near 10^{-5} Hz, the excess of the Deep River over the Alert power can be explained on the basis of the much larger diurnal anisotropy seen by the former and by effects of the earth's rotation (see Section IV.B). The coincidence of the spectra indicates a non-local origin of the scintillations, and the noise level of $\lesssim 1 \times 10^{-2}$ Hz^{-1} indicates that the scintillations are statistically very significant. The scintillations can be reasonably well approximated by equation (19) for frequencies 5×10^{-7} Hz $\leq f \leq 10^{-4}$ Hz. A comparison of equations (19) and (18) indicates that the scintillations are <u>much</u> larger for ~1 MeV protons than they are for ~1 GeV protons, by a factor of over 1000. Although the variation in j_0 was not large enough to establish that the relative fluctuations are constant (i.e., that equation (17) is satisfied) at relativistic energies as was established for low-energy protons, the high-energy data are consistent with $\sqrt{\langle j_1^2 \rangle} \propto j_0$.

An attempt was made to determine the scintillations of high-energy protons in interplanetary space from data provided by F. B. McDonald and V. K. Balasubrahmanyan. Their data come from four Geiger counters aboard a rotating spacecraft (IMP 3) in interplanetary space.

Figure II-10. Power spectra of the fluxes of the Alert and Deep River Neutron Monitors. Power spectra from the last two spectra are superimposed on one graph, with coding indicated on the figure. 90% confidence intervals for the Alert Neutron Monitor are indicated; those for Deep River are the same. The period is Sept. 1 - Nov. 30, 1969. The noise levels were $1 \times 10^{-2} Hz^{-1}$ and $4 \times 10^{-3} Hz^{-1}$ for Alert and Deep River, respectively.

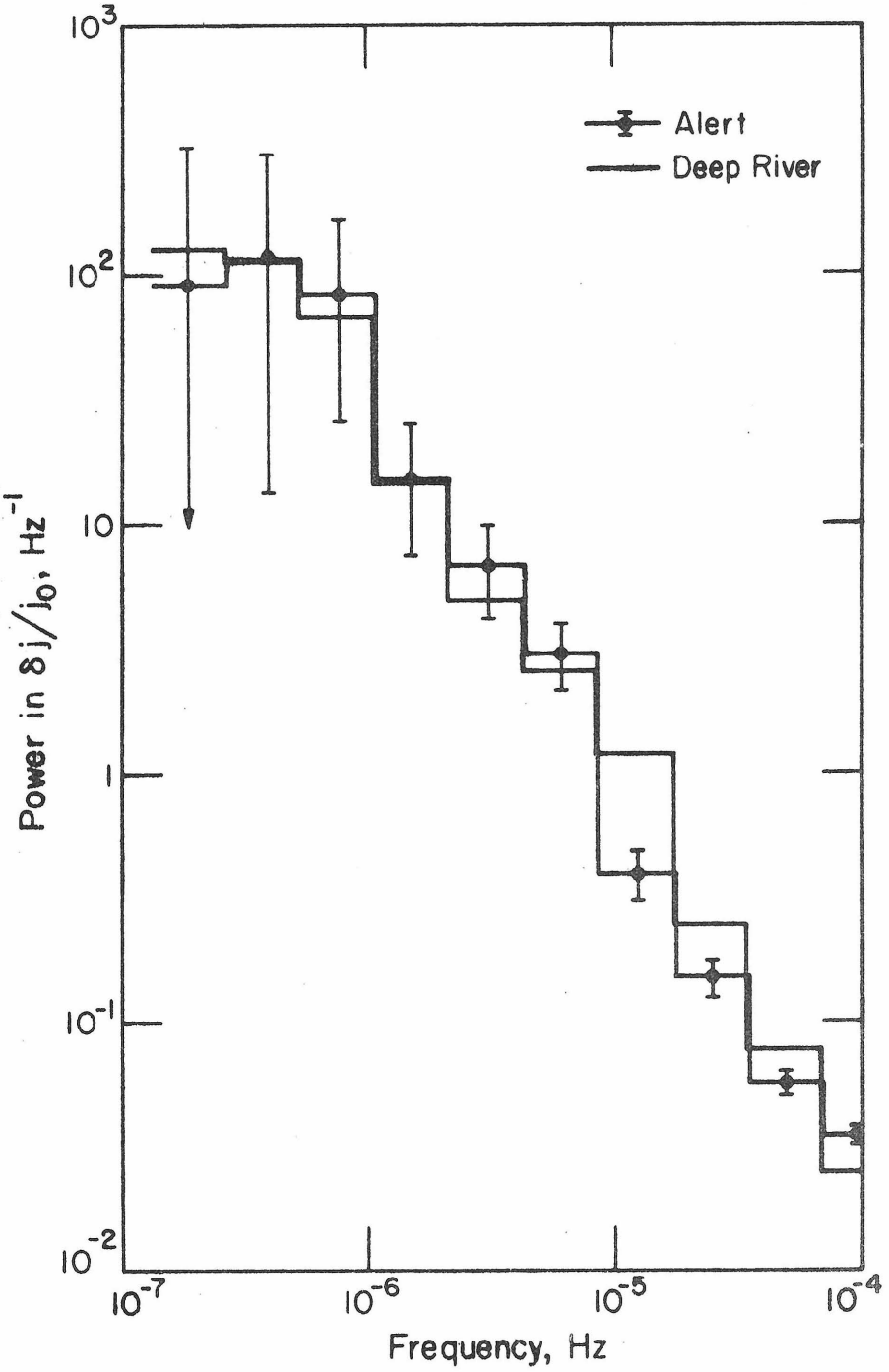
Alert
Deep River
Power in δj/j0, Hz-1
Frequency, Hz
10^3
10^2
10
1
10^-1
10^-2
10^-7
10^-6
10^-5
10^-4

The instrumentation has been previously described (Balasubrahmanyan et al., 1965). The detectors essentially sample the omnidirectional flux of cosmic-ray protons with energies above ~50 MeV and electrons with energies above ~4 MeV. The sampling time was approximately 5 minutes, and the average counting rate was 12 counts per second. The power spectrum of the counting rate for a typical 20-day quiet period in October, 1966 is given by the histogram in Fig. II-11. (Ignore the hexagons; these data will be discussed below.) The "noise" level marked in the figure is that calculated from equation (16). It is evident that Poisson noise dominates the spectrum (for this counting rate) for $f \gtrsim 10^{-4}$ Hz, in agreement with the relation (equation 16) derived in Section II.C. There are significant non-Poisson fluctuations in the frequency range $10^{-6} \lesssim f \lesssim 10^{-4}$ Hz.

One might at first assert that the power spectrum of Fig. II-11 corresponds to high-energy protons, since the electron contribution to the flux is about 5% and the heavier-nucleon componant of the flux is less than 5% for the detector used. However, simultaneous but independent measurements of the electron flux (McDonald et al., 1972) indicate that the electron componant varies by factors of order unity from day to day, whereas the proton scintillations inferred from the neutron-monitor measurements are in the order of 1% over the same period of time. To evaluate the electron contribution to the power spectrum of the IMP 3 flux shown in Fig. II-11, I have calculated rough power spectra from the published electron counting rates (McDonald et al., 1972) for the same period of October, 1966. From daily averages of the electron counting rate, I obtained the power spectra given in Fig. II-12. Once again, the two

Figure II-11. Power spectrum of the flux of >50 MeV protons and >4 MeV electrons. Power spectrum of the IMP 3 Geiger counter array for the period Oct. 8 - 28, 1966 is given by the histogram; the average counting rate was 12/sec and the noise level is indicated. The contribution to the power spectrum due to the electron componant, given by the electron power spectrum (see Fig. II-12) scaled by the flux ratio, is given by the hexagonal points. The statistical 90% confidence intervals are indicated; for the electron contribution, an additional uncertainty in normalization of about 25% exists.

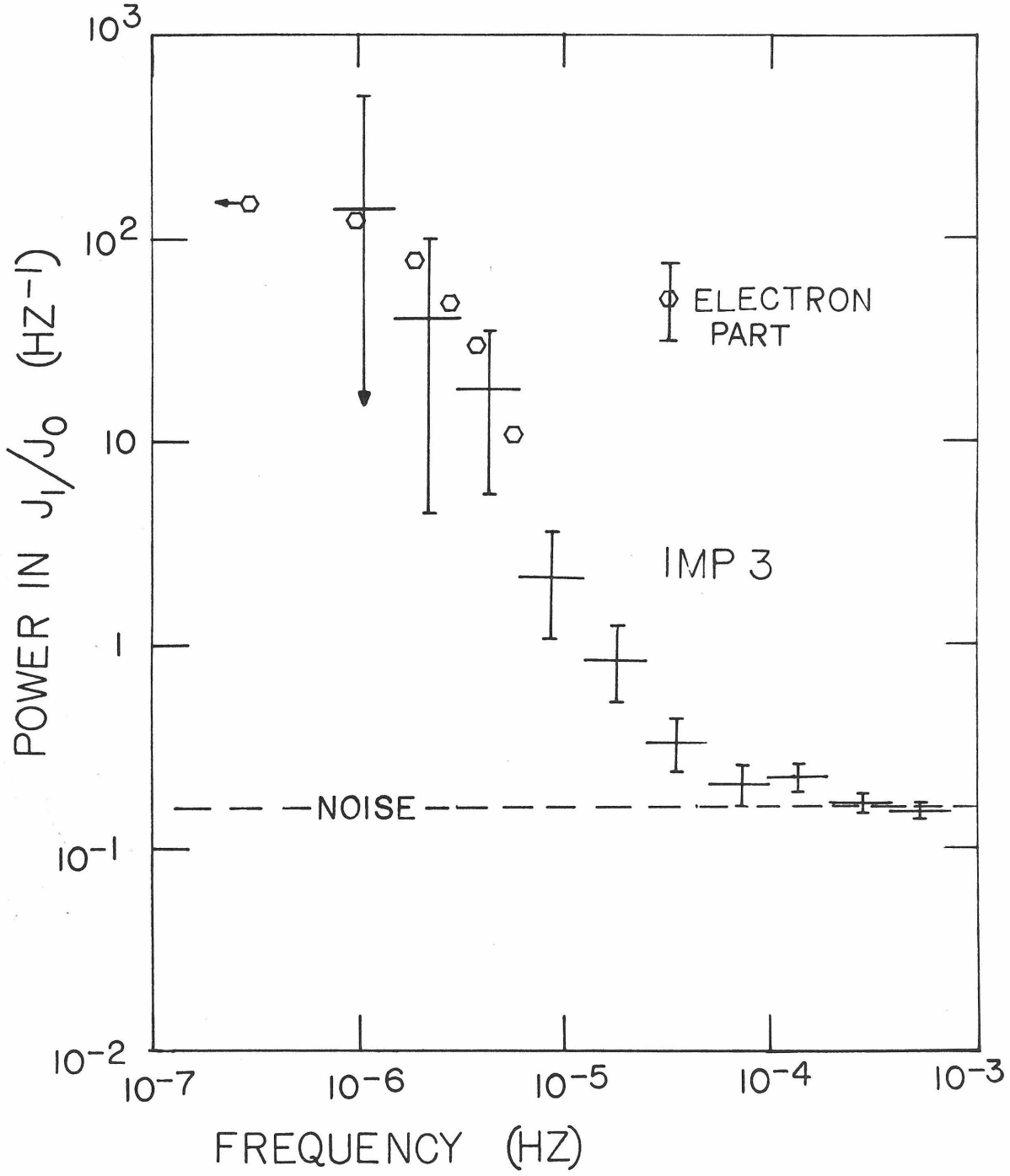
10^3
10^2
10
1
10^{-1}
10^{-2}
POWER IN J_1/J_0 (HZ-1)
ELECTRON PART
IMP 3
NOISE
10^{-7}
10^{-6}
10^{-5}
10^{-4}
10^{-3}
FREQUENCY (HZ)

Figure II-12. Power spectra of the 3-12 MeV electron flux. Raw data taken by a solid-state detector aboard IMP 3. Spectra are based on published daily averages of the electron flux. The solid lines are the power spectrum (nested-variance method) for the period Oct. 8 - Nov. 8, 1966. The points marked X are the power spectrum (correlation-function method) for the period Oct. 1 - Nov. 30, 1966. 90% confidence intervals are shown. The Poisson noise level was approximately 1×10^3 Hz^{-1}.

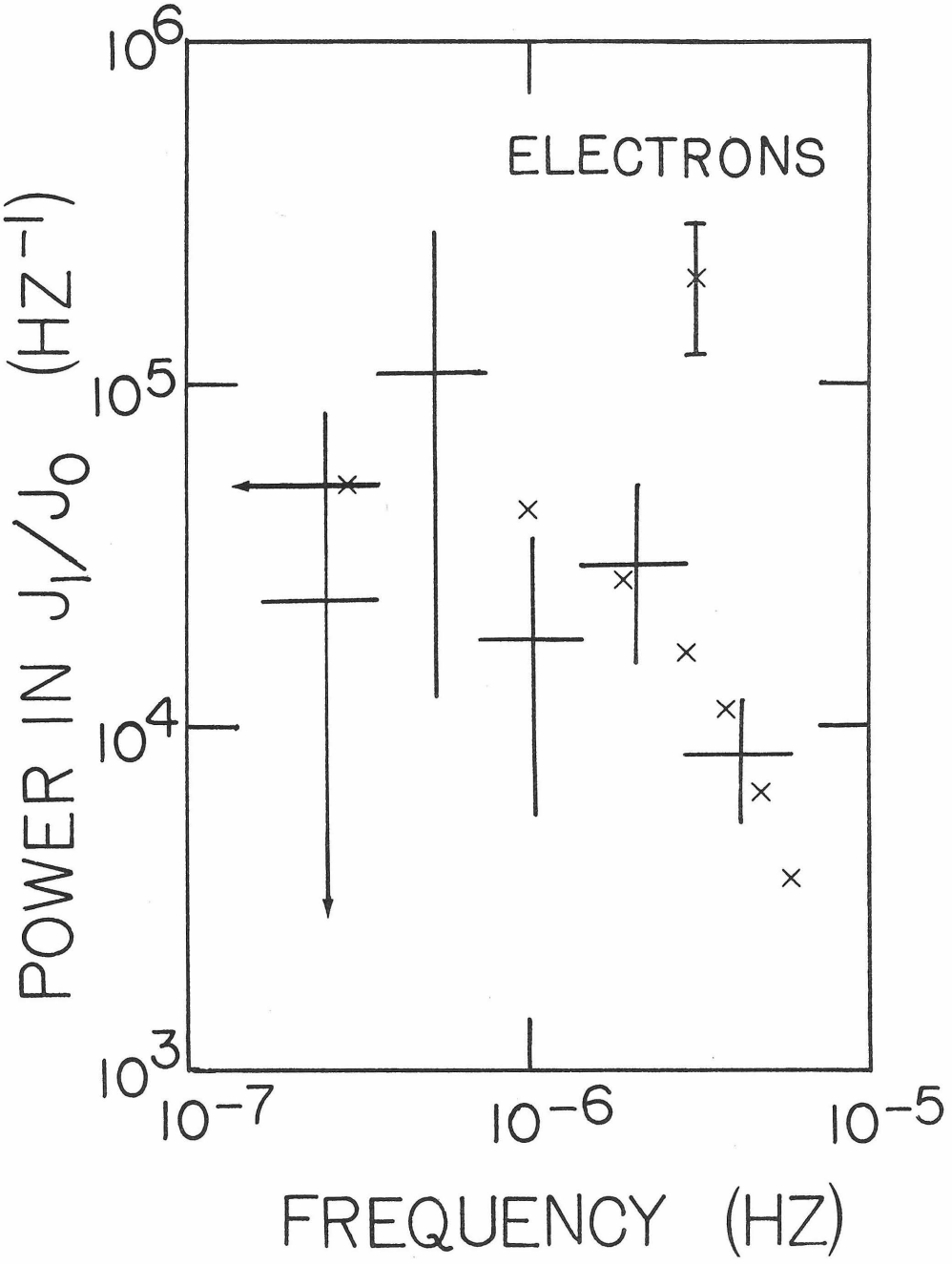
ELECTRONS
POWER IN J_1/J_0 (HZ^{-1})
10^6
10^5
10^4
10^3
10^{-7}
10^{-6}
10^{-5}
FREQUENCY (HZ)

methods of calculating the power spectrum give mutually consistent results, and the fluctuations are above the noise level. A comparison of Fig. II-12 and Fig. II-10 shows that the scintillations of 3-12 MeV electrons are several orders of magnitude larger than scintillations of ~1 GeV protons at the same frequency.

Using the power spectrum of 3-12 MeV electrons, the observation (McDonald et al., 1972) that fluctuations are small for higher-energy electrons, and measured electron and proton fluxes, I have estimated the contribution that the electrons make to the power spectrum observed by the IMP Geiger counters. The result is shown in Fig. II-11 as the hexagonal points. In addition to the statistical errors indicated on these points, there is an additional uncertainty of about 25% in the normalization of the "electrons" spectrum due to an imprecise knowledge of the average electron and proton fluxes. The striking coincidence of the electron contribution and the total spectrum implies that nearly all of the fluctuations observed with the IMP 3 Geiger counters during quiet times are due to the electrons. From comparing Fig. II-10 with Fig. II-11, one sees that scintillations in the omnidirectional proton componant of interplanetary high-energy cosmic rays (the residual of the IMP 3 spectrum when the electron componant is removed) are probably smaller than the scintillations exhibited by neutron monitors. Unfortunately, the large electron fluctuations detected by the IMP 3 Geiger counters make a more precise statement impossible. The cause of these large electron fluctuations is unknown and will not be discussed further here.

F. Conclusions

These observations indicate several possibly general characteristics of the power spectra of cosmic-ray scintillations. Briefly summarized, they are:

1) The noise level due to Poisson counting statistics is as given in equation (16). (See Fig. II-11.)
2) Scintillations in excess of the noise level are present for frequencies $f \lesssim 10^{-4}$ Hz for many types of cosmic-ray data currently available.
3) The relative size of the scintillations (that is, j_1/j_0) depends on the energy of the particles but remains the same for a given energy during typical quiet periods in the solar system.
4) For low-energy protons ($T \sim 1$ MeV), the spectrum of j_1/j_0 remains roughly the same even if the flux j_0 varies by a large factor, and the scintillations observed inside the magnetosphere are larger than those in interplanetary space.
5) The proton scintillations at ~1 GeV are much smaller than the scintillations at ~1 MeV.
6) Scintillations for all cases observed decrease markedly with increasing frequency over the range 10^{-7} Hz $\lesssim f \lesssim 10^{-4}$ Hz.
7) Fluctuations of relativistic (~5 MeV) electrons are much larger than scintillations of relativistic (~2 GeV) protons.
8) Scintillations exist in the neutron monitor flux which are not accounted for by multidiurnal anisotropies or local atmospheric effects.

III. MAGNETOSHEATH-INDUCED SCINTILLATIONS

In this Chapter, the first of two models of the phenomenon of magnetic-field-induced cosmic-ray scintillations is presented. Cosmic rays are scattered by a random magnetic field, and thus the field's fluctuations cause particle fluctuations. The simplest model, discussed in this Chapter, is one in which the cosmic rays pass from one undisturbed region to another through a "thin slab" containing plasma with a turbulent magnetic field. If the slab is thin compared with the cyclotron radius of the particles, the trajectories are nearly linear but are bent slightly by the magnetic fluctuations. The physical picture is then quite similar to those of the interplanetary scintillations of radio waves and the atmospheric scintillations of starlight.

Cosmic rays incident upon earth from interplanetary space pass through the magnetosheath before reaching the inner magnetosphere. The magnetosheath is a thin region of turbulent plasma between the relatively more quiet regions of interplanetary space and the magnetosphere, so the thin-slab model with linear unperturbed trajectories is appropriate. The theory of magnetosheath-induced cosmic-ray scintillations is developed from the thin-slab model in this Chapter. The results of the calculations are compared with some of the observations discussed in Chapter II, and it is concluded that the observed scintillations of the low-energy (1-40 MeV) proton flux observed inside the magnetosphere can be explained on the basis of the model.

The text of this Chapter is a published paper (Owens and Jokipii, 1972), and for clarity the paper is presented in its entirety.

The observations which are discussed in Section III.A were presented in Chapter II above. The discussion in the Appendix of the paper is generalized in Appendix A below. This paper presents the first quantitative discussion of cosmic-ray scintillations and develops the first physical model for the production of these scintillations.

Journal of
Geophysical Research

VOLUME 77 DECEMBER 1, 1972 NUMBER 34

Cosmic-Ray Scintillations

1. Inside the Magnetosphere

A. J. Owens and J. R. Jokipii

Downs Laboratory of Physics
California Institute of Technology, Pasadena, California 91109

Evidence is presented for the existence of statistically significant broad-band fluctuations, far above noise level, in the cosmic-ray flux observed inside the magnetosphere. The observed intensities at the polar cap at both low and high energies were analyzed, and power spectra of the cosmic-ray scintillations are presented and discussed. The low-energy data obtained during quiet times strongly suggest that, if δj is the fluctuation in intensity about the mean j_0, the spectrum of $\delta j/j_0$ is nearly constant for widely varying values of j_0. The spectra are roughly inverse power laws in frequency, with slopes of -1.5 to -2. The magnitudes of the spectra of $\delta j/j_0$ are much smaller at high energies than at low. A plausible, illustrative model for the propagation of cosmic rays through the turbulent magnetic field in the magnetosheath is presented, and a relationship between the observed cosmic-ray power spectrum and the magnetosheath magnetic-field power spectrum is obtained. It is shown that magnetic fluctuations in the magnetosheath can reasonably account for the observed cosmic-ray scintillations in the low-energy region (1 to 40 Mev), although other interpretations cannot be ruled out. Other possible mechanisms are briefly discussed. The scintillations of cosmic rays of neutron monitor energies are not explained by this model and may be interplanetary in origin.

Interest in time variations of the cosmic-ray intensity is almost as old as the study of cosmic rays itself. Time-dependent phenomena such as solar flare events, the 11-year solar-cycle variation, and Forbush decreases have been instrumental in establishing our present understanding of cosmic rays.

Until quite recently, interest has centered on large-amplitude periodic variations or large discrete events. However, inspection of a record of the cosmic-ray intensity as a function of time invariably reveals a continuous spectrum of statistically significant smaller-amplitude variations. These fluctuations are to be regarded as having a broad-band spectrum and are not directly connected with regular periodic variations such as the diurnal anisotropy. Such fluctuations have previously been discussed by *Dhanju and Sarabhai* [1967, 1970], *Jokipii* [1969], and *Williams* [1969]. Nonperiodic variations are evident even during extremely quiet times, and it is reasonable to associate them with the ever-present turbulent fluctuations of the plasma and fields in the solar wind and magnetosphere. These cosmic-ray fluctuations can be termed 'cosmic-ray scintillations,' in direct analogy with the familiar radio- and optical-frequency scintillations observed in electromagnetic radiation from space.

Just as these latter scintillations have been used to study the medium through which the electromagnetic waves propagate, one should be able to use the observed cosmic-ray scintillations to study turbulent astrophysical electric and

Copyright © 1972 by the American Geophysical Union.

magnetic fields. In this paper we first present power spectra of cosmic rays observed inside the magnetosphere, and show that the fluctuations are much larger than expected on the basis of statistical (Poisson) fluctuations alone. As one possible, illustrative interpretation of the observations, we use a model like one used in geometrical optics in order to investigate the fluctuations induced in cosmic rays during their traversal through the magnetosheath. This model is found to be consistent with observations, although other interpretations cannot be ruled out at this stage.

The organization of this paper is as follows. In the next section, the power spectra of observed counting rates for two widely different energies of cosmic rays are presented and discussed. A simplified thin-slab model of the propagation of a particle through a region of turbulent magnetic field is then presented, and the relationship between the magnetic-field power spectrum and the cosmic-ray power spectrum is deduced. This model is applied to the propagation of cosmic rays through the earth's magnetosphere, and it is shown that the model provides a reasonable interpretation of scintillations in the low-energy cosmic-ray flux. Other possible sources of the scintillations are briefly discussed.

A. Observed Cosmic-Ray Temporal Power Spectra

In order to study fluctuations of cosmic rays, we have computed power spectra from representative quiet-time data obtained inside the magnetosphere. Data for which power spectra can be calculated must satisfy several general requirements. The process must be approximately stationary; that is, the average value of the cosmic-ray counting rate must be constant or vary slowly over the time scale to be investigated. Data must be available at fixed intervals, with few data gaps. Finally, for the spectra to be physically interesting, the counting rate must be high enough so that fluctuations merely due to Poisson counting statistics are insignificant. These three restrictions limit the types of cosmic-ray data that are suitable for power spectral analysis. In this paper, we consider two types of data that are suitable: low-energy protons ($T \gtrsim 1$ Mev), and relativistic particles ($T \sim 2$ Gev).

The low-energy proton data were obtained from polar passes of a low-altitude polar orbiting satellite (Ogo 6). A solid-state detector with an effective threshold of about 1 Mev/nucleon and an upper cutoff of about 40 Mev for protons (150 Mev/nucleon for α particles) was used to sample the counting rate at terrestrial latitude greater than 74° on each polar pass. (The rigidity cutoff for 1-Mev protons in the magnetosphere during quiet times occurs at $<72°$ latitude.) The average data-collecting time was about 8 min over each pole, and the transit time between poles was 50 min. The fraction of the counting rate due to α particles was less than 5%, and there was essentially no electron contribution. The counting rate during quiet times was typically 1 c/s, or 500 counts per polar pass. The orbital parameters of the satellite were such that a certain fraction of the orbits were too far from the poles for data to be gathered and analyzed. Therefore, it was necessary to average over several polar passes in order to obtain data points that were equally spaced in time.

Although many periods showed too much activity to be suitable for power spectral analysis, several good stretches of reasonably quiet data were found. After subtracting a fitted straight line from the data, to remove the average and linear time trend, a power spectral analysis was performed. Both the correlation-function method [*Blackman and Tukey*, 1958] and the nested-variance method (called the pilot method by Blackman and Tukey) were used, and the two methods gave mutually consistent results. Since the latter method provides a larger range of frequencies in the estimates, and averages over fine structures in the frequency domain which are not of interest, it is better suited to our purposes here. In Figure 1, we plot the calculated power spectral estimates of $\delta j/j_0$ for two representative periods. We denote by δj the fluctuating part of the differential flux, and j_0 is the average flux. It is clear that the power spectra for the two periods considered coincide, indicating that the spectrum of δj is very nearly proportional to j_0^2. Since the average counting rates differed by more than a factor of 10, and the two periods of time are separated by 2 months during which the flux varied considerably, we conclude that the power spectrum of $\delta j/j_0$ for 1- to 40-Mev protons during quiet

times inside the magnetosphere does not vary significantly even if j_0 does. This is an important feature of the observations and must be accounted for in any theory. Power spectra were run for two additional quiet periods during 1969, and similar results were found. The shapes of all four spectra calculated were very nearly the same, and the amplitudes were equal to within a factor of 2. This constancy of the quiet-time, low-energy proton power spectrum over the course of a year's time places a severe constraint on possible mechanisms of production of the scintillations.

One can readily show that fluctuations due merely to Poisson counting statistics are much smaller than those observed. Consider a detector that samples an average counting rate of n particles/sec for t seconds. For Poisson statistics, the relative mean square error of the total number of particles counted will be

$$\frac{\langle \delta N^2 \rangle}{N^2} = \frac{1}{N} = \frac{1}{nt}$$

Random noise yields a flat frequency spectrum for frequencies $0 < f < f^*$, where f^* is the aliasing frequency, given by $f^* = \frac{1}{2}T$, and T is the time between data points. A property of the power spectrum is that the integral over all frequencies $0 < f < f^*$ gives the mean square error, so that in this case $f^*P(f)_p = 1/nt$, where $P(f)_p$ is the Poisson power (independent of frequency). Thus $P(f)_p = 2T/nt = 2/Dn$, where $D = t/T$ is the 'duty cycle,' the fraction of the period between data points during which data are collected. (Note that we adopt the convention that $f \geq 0$, so that $P(f) = 4\int_0^\infty R(\tau) \cos(2\pi f\tau) d\tau$.) Thus we have

$$P(f)_p = 2/Dn$$

The Poisson (noise) power level for both power spectra in Figure 1 is indicated, and it can be seen that the observed power far exceeds the expected noise level.

Our data for relativistic particles are taken from pressure-corrected hourly averages of the Alert and Deep River neutron monitor counting rates [*Steljes*, 1970]. The power spectra for both neutron monitors appear in Figure 2 for the period September 1 to November 30, 1969, a period that contains both the time periods used in the proton data given above. From Figure 2 it is evident that the power spectra

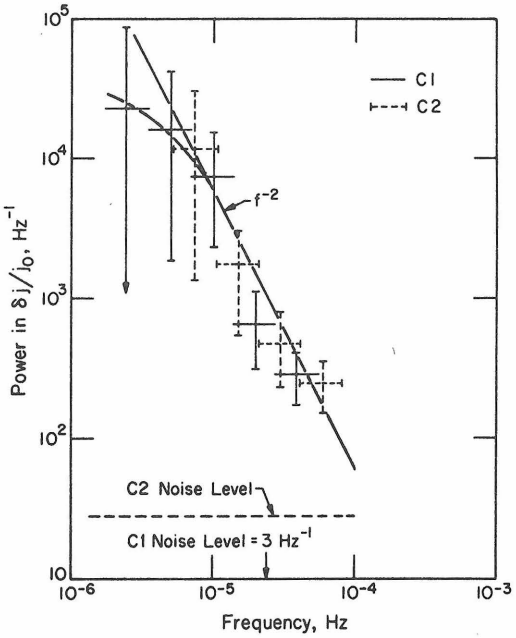

Fig. 1. Power spectrum of the low-energy proton flux. Data for 1- to 40-Mev protons taken during quiet times aboard Ogo 6, inside the magnetosphere. *C*1 refers to the period September 19–25, 1969, and *C*2 to November 11–21, 1969. The average counting rate was 5 protons/sec for *C*1 and 0.4 protons/sec for *C*2. Noise levels due to counting statistics are indicated. Error bars refer to 90% confidence intervals.

of the two neutron monitors are almost identical, to within errors, and again are far above the noise level. Power spectra for these monitors were also run for other periods in 1969, and both the shape and amplitude were the same as those in Figure 2, to within estimation errors. An important point is that the amplitude of the neutron monitor scintillations $\delta j/j_0$ is less by a factor of about 2000 than the 1-Mev power spectra of Figure 1, although the shapes are somewhat similar. The well-known diurnal and semidiurnal periodic variations make a contribution that is unimportant in all cases, as is shown by narrower-band power spectral analyses performed near the relevant frequencies. The Alert and Deep River neutron monitors were selected because of their high counting rates, their proximity to the polar region in which the 1-Mev data were taken, and the fact that they are at high enough latitude that rigidity cutoffs are unimportant and thus fluctuations due to changes in the cutoff can be

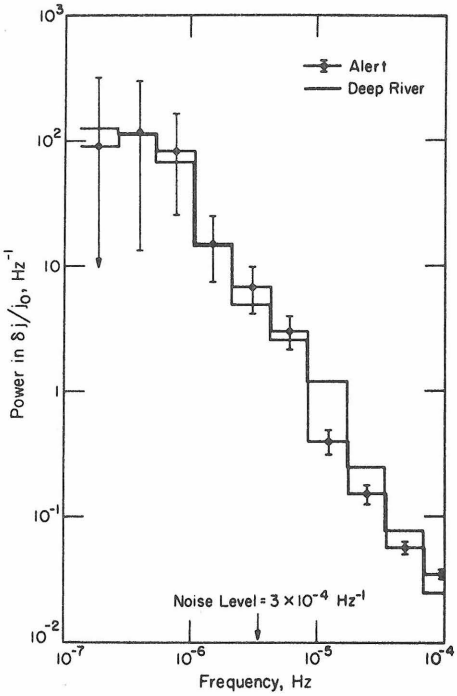

Fig. 2. Power spectra of Alert and Deep River neutron monitor counting rates. The period is September 1 to November 30, 1969. The 90% confidence intervals for Alert estimates are shown; the intervals for Deep River are the same. The average counting rates were about 6600 and 6300 c/s, respectively.

assumed to be negligible. The mean primary energy of response of these detectors is roughly 2 Gev. Although the variation in j_0 was not large enough to establish that $\delta j \propto j_0$ at relativistic energies, the data are consistent with this dependence on j_0.

These observations indicate several possibly general characteristics of the power spectra of cosmic-ray scintillations. First, scintillations much in excess on the noise level are present for frequencies less than 10^{-4} Hz. The relative size of the scintillations (that is, $\delta j/j_0$) depends on the energy of the particles involved but remains the same for a given energy during typical quiet periods. For low energies, it appears that the spectrum of $\delta j/j_0$ remains roughly the same even if the flux j_0 changes by a large factor. Scintillations are much larger for lower-energy particles, and they decrease markedly with increasing frequency for 10^{-7} Hz $\lesssim f \lesssim 10^{-4}$ Hz.

The interpretation of these scintillations is an important question. Possible causes include the turbulent magnetic fields in interplanetary space and in the vicinity of the earth, or perhaps fluctuations at the source of the particles. In the following two sections, we demonstrate that the fluctuations of the magnetic field in the magnetosheath provide one reasonable cause of the scintillation of low-energy particles observed inside the magnetosphere, although the currently available data cannot rule out other mechanisms.

B. Thin-Slab Model of Cosmic-Ray Scintillations

We first consider some general properties of the propagation of fast charged particles in the solar plasma. Because the particle speed is much greater than the Alfvén speed, electric fields can be neglected and the magnetic field can be treated in a quasi-static approximation [*Jokipii*, 1966, 1971]. It then follows directly from Liouville's theorem that the intensity I and phase space density n are constant along allowed particle trajectories. Thus, fluctuations in the counting rate due to particles in a given element of solid angle inside the magnetosphere clearly cannot be produced by local magnetic fluctuations if the particle flux in interplanetary space is uniform and isotropic and the effect of a varying cutoff is unimportant. However, it is easy to see that, if the external flux is anisotropic, fluctuations in the magnetic field can produce fluctuations in the cosmic-ray counting rate. For, as the solar wind convects the irregular magnetic field past the spacecraft, the cosmic-ray particles having access to a detector deep inside the magnetosphere will come from different directions in interplanetary space. Because of the anisotropy, these directions will have different intensities. This effect characterizes one possible family of mechanisms that can in principle produce cosmic-ray scintillations. We now illustrate this quantitatively with a simple 'thin-slab' model.

Consider a slab of plasma like that shown in Figure 3. In this slab there is an irregular frozen-in magnetic field containing spatial fluctuations that will be taken to be independent of time over the time scales of interest. Temporal fluctuations in the magnetic field are observed when the plasma is convected past a stationary observer with velocity V_w much larger than the

phase velocity of the magnetic fluctuations. We suppose that cosmic-ray particles are incident uniformly on the slab from the side $z < 0$ and that a detector, having a very narrow cone of acceptance, measures the flux of particles traveling nearly along the z axis at a position z_0. Because the geomagnetic field increases rapidly near the earth, particles detected at a given point inside the magnetosphere are characterized by a narrow asymptotic viewing cone, so that even an omnidirectional detector deep in the magnetosphere has a narrow effective cone of acceptance to particles arriving from interplanetary space.

The magnetic field inside the slab, in the frame at rest relative to the plasma in the slab, will be taken to be of the form of an average field $\mathbf{B}_0$ plus a fluctuating field $\mathbf{B}_1$,

$$\mathbf{B} = \mathbf{B}_0 + \mathbf{B}_1(\mathbf{r}) \tag{1}$$

with

$$\langle \mathbf{B}_1(\mathbf{r}) \rangle = 0 \tag{2}$$

(Angle brackets denote either an ensemble or spatial average). To simplify the algebra, we assume that the average field $\mathbf{B}_0$ is small enough that the particle cyclotron radius r_c in $\mathbf{B}_0$ is much greater than l, i.e., $r_c \gg l$, where l is the thickness of the slab. This assumption is satisfied by particles with $T \gtrsim 1$ Mev in the magnetosheath. Also, we suppose $\langle B_1^2 \rangle^{1/2} \lesssim |\mathbf{B}_0|$. Consider the particle phase-space density $n(\mathbf{r}, \mathbf{p}, t)$. (The differential intensity $I(r, \Omega, t)$ is simply related to the phase-space density n through the relation $I = np^2$, where Ω is the solid angle corresponding to the direction of $\mathbf{p}$.) We suppose that the fluctuations in the magnetic field are such that the change induced in the particle distribution function $n(\mathbf{r}, \mathbf{p}, t)$ is small as the particles traverse the slab.

The phase-space density n satisfies Liouville's equation

$$\frac{\partial n}{\partial t} + w_i \frac{\partial n}{\partial x_i} + \epsilon_{ijk} w_j \omega_k \frac{\partial n}{\partial w_i} = 0 \tag{3}$$

where $\boldsymbol{\omega} = cq\mathbf{B}/W$, $\mathbf{w}$ is the particle speed, W is its total energy, q is its charge, and c is the speed of light. Because electric fields are not important, the energy of a particle is constant, and equation 3 holds for each energy separately.

Our narrow-angle detector counts only particles with $w_x \sim 0$ and $w_y \sim 0$ below the slab, and the

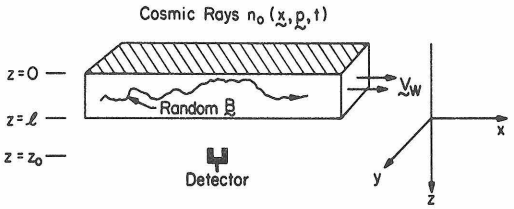

Fig. 3. Schematic illustration of the thin-slab model. Cosmic rays from $z < 0$ pass through a region of random magnetic field before being detected at $z = z_0 > l$. The region $z < 0$ will be taken to represent interplanetary space, $0 < z < l$ to represent the magnetosheath, and $z > l$ to represent the magnetosphere. The entire plasma in the thin slab is convected in the $\hat{x}$ direction with velocity $\mathbf{V}_w$.

change in trajectory is assumed to be small, so that $|w_x| \ll |w_z|$ and $|w_y| \ll |w_z|$ for the particles detected. We will later assume that the sizes of the three velocity derivatives ($\partial n/\partial w_x$, $\partial n/\partial w_y$, $\partial n/\partial w_z$) are about equal. Under these circumstances, the terms containing multiplicative factors of w_x and w_y can be ignored. In addition, we consider only the steady state, so that equation 3 becomes

$$\frac{\partial n}{\partial z} + \omega_{1x} \frac{\partial n}{\partial w_y} - \omega_{1y} \frac{\partial n}{\partial w_x} = 0 \tag{4}$$

Equation 4 can be integrated to obtain

$$n(x, y, z, \mathbf{w}) = n(x, y, z = 0, \mathbf{w}) + \int_0^z d\xi \left\{ \frac{\partial n(x, y, \xi, \mathbf{w})}{\partial w_x} \omega_{1y}(x, y, \xi) - \frac{\partial n(x, y, \xi, \mathbf{w})}{\partial w_y} \omega_{1x}(x, y, \xi) \right\} \tag{5}$$

Now, we are interested in the fluctuating part of n (or I), and so we define

$$\delta n = n - \langle n \rangle$$

Taking δn to be zero at $z = 0$, equation 5 becomes, upon defining

$$\delta_i = (w/n)[\partial n(x, y, 0)/\partial w_i]_{\text{const energy}} \tag{6a}$$

$$\frac{\delta n}{n} = \int_0^z d\xi \cdot \left\{ \frac{\delta_x}{w} \omega_{1y}(x, y, \xi) - \frac{\delta_y}{w} \omega_{1x}(x, y, \xi) \right\} \tag{6b}$$

where only terms through first order in the small

quantities δn and ω_1 are retained. Note that δn is a function of x and y at a given depth z. The vector $\boldsymbol{\delta}$ as defined in equation 6a is essentially the vector anisotropy of the cosmic-ray flux just outside the thin slab. For example, suppose

$$n(\mathbf{x}, \mathbf{w}, t) = n_0(\mathbf{x}, t) \cdot \left\{1 + \epsilon_i^{(1)}(\mathbf{x}, t)\frac{w_i}{w} + \epsilon_{ij}^{(2)}(\mathbf{x}, t)\frac{w_i w_j}{w^2} + \epsilon_{ijk}^{(3)}(\mathbf{x}, t)\frac{w_i w_j w_k}{w^3} + \cdots\right\}$$

where $1 \gg |\epsilon^{(1)}| \gg |\epsilon^{(2)}|, |\epsilon^{(3)}|, \cdots$. The diurnal and multidiurnal anisotropies observed at neutron monitor energies have this form, as does the Compton-Getting anisotropy that dominates for low-energy cosmic rays. Then

$$\delta_i \equiv \frac{w}{n}\left[\left(\frac{\partial n}{\partial w_i}\right)\right]_{|w|} \sim \epsilon_i^{(1)} + O(\epsilon^{(2)})$$

gives the same result as the usual definition of the anisotropy.

We write the random field inside the slab in the form $\omega_1(\mathbf{r})\theta(z)\theta(l - z)$, where $\omega_1(\mathbf{r})$ is a homogeneous random function of $\mathbf{r}$, and $\theta(z)$ is the unit step function. Then $\omega_1(\mathbf{r})$ can be written in the form

$$\omega_{1i}(\mathbf{r}) = \int e^{-i\mathbf{k}\cdot\mathbf{r}}\, d\omega_i(\mathbf{k}) \tag{7}$$

where $d\omega_i(\mathbf{k})$ is a random Fourier-Stieltjes increment [*Yaglom*, 1962]. In the following, $d\omega_i(\mathbf{k})$ will be written in the form $\tilde{\omega}_i(\mathbf{k})\, d^3k/(2\pi)^3$. For the power spectrum of $\mathbf{B}_1(\mathbf{r})$, defined by

$$P_{ij}(\mathbf{k}) = \int_{-\infty}^{\infty}\int_{-\infty}^{\infty}\int_{-\infty}^{\infty} d\xi_x\, d\xi_y\, d\xi_z e^{i\mathbf{k}\cdot\boldsymbol{\xi}} \cdot \langle B_{1i}(\mathbf{r})B_{1j}(\mathbf{r} + \boldsymbol{\xi})\rangle \tag{8a}$$

we have the relation

$$(2\pi)^3 \frac{c^2q^2}{W^2} P_{ij}(\mathbf{k})\, \delta(\mathbf{k} - \mathbf{k}')\, d^3k'\, d^3k = \langle \tilde{\omega}_i^*(\mathbf{k})\tilde{\omega}_j(\mathbf{k})\rangle\, d^3k\, d^3k' \tag{8b}$$

Equation 8b is a statement of the Wiener-Khinchine theorem [*Yaglom*, 1962] with appropriate normalization. We consider the variation of δn with x and y for a given z. The Fourier transform of δn in the x-y plane for a given z can be written

$$\delta n(x, y, z, \mathbf{w}) = \int_{-\infty}^{\infty}\int_{-\infty}^{\infty} e^{i(k_x x + k_y y)} \cdot \tilde{\delta n}(k_x, k_y, z, \mathbf{w})\frac{dk_x}{2\pi}\frac{dk_y}{2\pi} \tag{9}$$

With these definitions, equation 6b becomes, if one changes the order of integration,

$$\frac{\delta n(k_x, k_y, z, \mathbf{w})}{n} = \frac{1}{w}\int_{-\infty}^{\infty}\frac{dk_z}{2\pi}\frac{-1}{ik_z} \cdot [e^{ik_z z} - 1]\{\delta_x\omega_y(\mathbf{k}) - \delta_y\omega_x(\mathbf{k})\} \tag{10}$$

Next we multiply equation 10 by its complex conjugate, take the ensemble average, and use the Wiener-Khinchine theorem to obtain, after some reduction,

$$\frac{P^{\delta n}(k_x, k_y, z)}{n^2} = \frac{z^2}{w^2}\frac{q^2c^2}{W^2}\int_{-\infty}^{\infty}\frac{dk_z}{2\pi}\frac{\sin^2(k_z z/2)}{(k_z z/2)^2} \cdot \{\delta_x{}^2 P_{yy}(\mathbf{k}) + \delta_y{}^2 P_{xx}(\mathbf{k}) - \delta_x\delta_y[P_{xy}(\mathbf{k}) + P_{yx}(\mathbf{k})]\} \tag{11}$$

This equation is true for any value of z inside the slab, including the lower edge $z = l$. From that point onward toward $z > l$, the particle trajectory is a straight line, so that δn is constant, by Liouville's theorem. (For a detector with finite solid angle, some correction would have to be made for crossing beams of particles, but we will not consider this here.) Hence a detector sensitive over a small solid angle centered on the z direction will measure the power given by equation 11 with $z = l$, no matter where it is situated, as long as $z > l$. Similarly, the power given in (11) will be constant along any allowed trajectory for $z > l$, if magnetic-field fluctuations are negligible in that region. Therefore, a detector just beneath the magnetosphere and another deep inside the magnetosphere along the same trajectory will observe the same power spectrum.

We see from equation 11 that the power in the density fluctuations is determined by the power in the magnetic-field fluctuations. The equation is basically quite similar to the thin-screen equation used in discussing interplanetary scintillation of radio waves [*Salpeter*, 1967; *Jokipii*, 1970].

In the next section, we will argue that the observed scintillations in the low-energy cosmic-ray intensity can be reasonably interpreted in

terms of this model if the slab is taken to represent the magnetosheath. The temporal variations are caused by the slab (magnetosheath plasma) being rigidly convected past the observer. Hence, we will convert equation 11 to a frequency spectrum by assuming that the slab is translated in the x direction at a speed V_w which is taken to be much greater than the Alfvén speed in the plasma. It is then seen that any two-dimensional wave-number spectrum $P(k_x, k_y)$ gives rise to a frequency spectrum

$$P(f) = \frac{1}{V_w}\int_{-\infty}^{\infty}\frac{dk_y}{2\pi}\,P\left(k_x = \frac{2\pi f}{V_w}, k_y\right) \quad (12a)$$

[e.g., *Jokipii*, 1971, Appendix 1]. Similarly, a three-dimensional spectral tensor $P_{ij}(k_x, k_y, k_z)$ such as that of the magnetic field gives rise to a temporal frequency spectrum

$$P_{ij}(f) = \frac{1}{V_w}\int_{-\infty}^{\infty}\int_{-\infty}^{\infty}\frac{dk_y}{2\pi}\frac{dk_z}{2\pi} \cdot P_{ij}\left(k_x = \frac{2\pi f}{V_w}, k_y, k_z\right) \quad (12b)$$

Thus, equation 11 becomes

$$\frac{P^{\delta n}(f)}{n^2} = \frac{l^2}{w^2}\frac{q^2c^2}{W^2}\frac{1}{V_w}\int_{-\infty}^{\infty}\frac{dk_y}{2\pi} \cdot\int_{-\infty}^{\infty}\frac{dk_z}{2\pi}\frac{\sin^2(k_z l/2)}{(k_z l/2)^2} \cdot\left\{\delta_x{}^2 P_{yy}\left(k_x = \frac{2\pi f}{V_w}, k_y, k_z\right) + \delta_y{}^2 P_{xx}\left(k_x = \frac{2\pi f}{V_w}, k_y, k_z\right) - \delta_x\,\delta_y\left[P_{xy}\left(k_x = \frac{2\pi f}{V_w}, k_y, k_z\right) + P_{yx}\left(k_x = \frac{2\pi f}{V_w}, k_y, k_z\right)\right]\right\} \quad (13)$$

Equation 13 is the general result for the slab model. To carry out the integrations explicitly requires specification of the power spectrum tensor of the magnetic field. To illustrate the basic character of the phenomenon, we take a specific form of this tensor that is consistent with present knowledge of the magnetosheath magnetic field. We suppose that the turbulent field is statistically homogeneous and isotropic. Hence, as is shown in the Appendix, we have

$$P_{ij}(\mathbf{k}) = G(|\mathbf{k}|)[k^2\,\delta_{ij} - k_i k_j] \quad (14a)$$

where $G(|\mathbf{k}|)$ is an arbitrary function of $|\mathbf{k}| = k$ (subject to the condition that $P_{ij}X_iX_j > 0$ for any vector X_i). Further, we suppose $G(k)$ to be of the form

$$G(k) = \frac{G_0}{(A^2 + k^2)^{\beta/2+2}} \quad (14b)$$

For this form of $P_{ij}(\mathbf{k})$, the observed frequency spectrum for the fluctuating magnetic field is (see equation 12b)

$$P_{xx}(f) = H_0/(f^2 + f_A{}^2)^{\beta/2} \quad (15a)$$

$$P_{yy}(f) = \tfrac{1}{2}[H_0/(f^2 + f_A{}^2)^{\beta/2}] \cdot\left[1 + \beta\frac{f^2}{f^2 + f_A{}^2}\right] \quad (15b)$$

$$P_{xy}(f) = P_{yx}(f) = 0 \quad (15c)$$

with

$$H_0 = \frac{1}{\pi V_w}\frac{G_0}{\beta(\beta+2)}\left(\frac{V_w}{2\pi}\right)^{\beta}$$

Here $f_A = V_w A/2\pi$ is a characteristic frequency. Note that, for $f \gg f_A$, $P_{ii} \propto f^{-\beta}$ which, for $\beta \sim 1.5$ to 2, is what is observed for the interplanetary and magnetosheath fields. For $f \ll f_A$, the spectra are flat.

Using equations 14 for the form of the spectrum to be inserted into equation 13 yields a result for the cosmic-ray power spectrum in terms of two well-defined integrals, over k_y and k_z. The k_y integral is trivial, and although the general form of the integration over k_z can be written in terms of Hankel transforms of zero order and modified Bessel functions of the second kind, such solutions are mathematically quite complex and obscure the physics involved. An alternative approach, to be used here, is to notice that the two functions $\sin^2(k_z l/2)/(k_z l/2)^2$ and $G(|\mathbf{k}|)$, when considered as functions of k_z, are both rather sharply peaked functions. Then in the limit that $k_x{}^2 + A^2$ is much smaller than $(2/l)^2$, the first function is essentially constant over the region in which the second contributes. In the other limit, $k_x{}^2 + A^2 \gtrsim\gtrsim (2/l)^2$, the $G(k)$ term can be considered a constant during the integration over k_z. The integrals in both limits can be evaluated, and the argument suggested here can be made with complete mathematical rigor. Using this technique, and transforming

k_x to $2\pi f/V_w$ at the end of the calculation as is required by equation 13, one obtains

$$P^{\delta n}(f)/n^2 = (l/w)^2 \frac{q^2c^2}{W^2} \cdot \{\delta_x{}^2 P_{yy}(f) + \delta_y{}^2 P_{xx}(f)\} \quad (16a)$$

$$\text{for} \quad f^2 + f_A{}^2 \lesssim\lesssim (V_w/\pi l)^2$$

$$P^{\delta n}(f)/n^2 = (l/w)^2 \frac{q^2c^2}{W^2} \cdot \{\delta_x{}^2 P_{yy}(f) + \tfrac{1}{2}\,\delta_y{}^2 P_{xx}(f)\} \quad (16b)$$

$$\cdot (V_w/\pi l f) \frac{\Gamma(1/2)\Gamma(\beta/2 + 1/2)}{\Gamma(\beta/2)}$$

$$\text{for} \quad f \gtrsim\gtrsim V_w/\pi l,\ f_A$$

In these equations, the power spectra of $\mathbf{B}_1$ are as given in equations 15*a* and 15*b*, and $\Gamma(a)$ is the gamma function with argument a. The principal result is that the cosmic-ray power spectrum has the same shape as the magnetosheath magnetic-field power spectrum at low frequencies, but at high frequencies the cosmic-ray power spectrum decreases by one additional power of frequency. Notice that the amplitude depends on the three parameters δ_x, δ_y, and l at low frequencies, the additional parameter V_w entering at higher frequencies. All these parameters are known from conditions near the earth. For example, near the earth the thickness of the magnetosheath is typically 5 or 10 R_E, and the convection velocity V_w is of the order of 100 or 200 km/sec. The interplanetary cosmic-ray anisotropies $|\boldsymbol{\delta}|$ are typically 15% at energies of 1 Mev/nucleon and 0.5% at energies greater than 1 Gev. The other parameters in equations 16, the frequency f_A below which the magnetic-field power spectrum becomes flat with decreasing f, and the spectral index β, are determined by the magnetic fluctuations.

It is interesting, and quite important, to note that the result of equations 16 is not strongly influenced by the assumed symmetry of the magnetic-field fluctuations. The more general case of axially symmetric magnetic-field fluctuations is considered in the Appendix. Equation 14*a* is based on the spherically symmetric limit, in which $G' = 0$ in equation A3. In the opposite limit of cylindrical symmetry, $G = 0$ and $G'(k) \neq 0$, and the power spectrum has the form given in (A5). We have performed the integrals in equation 13 for this case, with the axis of symmetry chosen along the convection ($\hat{x}$) direction and $G'(k)$ of the form in equation 14*b*. Since the reasoning proceeds along the same lines as above, we only quote the results:

$$P^{\delta n}(f)/n^2 = (l/w)^2 \frac{q^2c^2}{W^2} \cdot \{\delta_x{}^2 P_{yy}(f) + \delta_y{}^2 P_{xx}(f)\} \quad (17a)$$

$$\text{for} \quad f^2 + f_A{}^2 \lesssim\lesssim (V_w/\pi l)^2$$

$$P^{\delta n}(f)/n^2 = (l/w)^2 \frac{q^2c^2}{W^2} \cdot \left\{\left(\frac{\beta+1}{\beta}\right)\delta_x{}^2 P_{yy}(f) + \tfrac{1}{2}\,\delta_y{}^2 P_{xx}(f)\right\} \quad (17b)$$

$$\cdot (V_w/\pi l f) \frac{\Gamma(1/2)\Gamma(\beta/2 + 1/2)}{\Gamma(\beta/2)}$$

$$\text{for} \quad f \gtrsim\gtrsim V/\pi l,\ f_A$$

Comparison of equations 16 and 17 shows that the weak assumption of axial symmetry of the magnetic turbulence is sufficient to obtain the same result, to within a factor of 2, as that given by equations 16. Because of this fact, we use equations 16 as the predictive model in the rest of this paper.

We first note that the power spectrum of δn (or δj) is proportional to $n_0{}^2$ (or $j_0{}^2$). This feature was shown to be consistent with data presented in an earlier section. Furthermore, in the case of both symmetries discussed here, the observed power spectrum of density scintillations is proportional to the magnetic-field power spectrum at low frequencies and proportional to $1/f$ times the magnetic spectrum at high frequencies. These results should be quite general and it is appropriate to consider their physical interpretation.

The low-frequency result can be readily interpreted as follows. Low frequencies correspond to wave numbers much less than $1/l$, where l is the thickness of the slab. Hence, for any given x and y, the field fluctuations in the slab are essentially independent of z and the only effect on the particle is a slight bending of the trajectory in this nearly constant field. As x and y change, this field changes and the associated deflection changes. By Liouville's theorem, the detector then samples a different part of the initial angular distribution and thus sees a different

density if the interplanetary particle anisotropy δ is nonzero. As the field slowly changes due to convection by the wind, the intensity observed changes in phase with $\mathbf{B}_1(\mathbf{r})$ as different parts of the angular distribution are sampled. Hence the proportionality to $P_{ij}(f)$. A slight extension of this reasoning will even give the correct constant of proportionality.

However, at high frequencies, there are many wavelengths of the field fluctuations in the distance l. In this case, the bending of one element Δz will be partly canceled by the next, in a sort of random walk, and so, as f increases, the amplitude of the fluctuation δn will decrease more rapidly than $P_{ij}(f)$. The precise dependence on f and the constants do not follow readily from such a simple qualitative discussion.

Hence, equations 16 can be regarded as quite general for reasonable magnetic-field power spectrum tensors.

C. Interpretation of the Observations

For illustration, we apply the results of the thin-slab model discussed above to the propagation of cosmic rays through the earth's magnetosheath and magnetosphere. We will investigate the hypothesis that fluctuations observed inside the magnetosphere are due solely to the magnetosheath-induced scintillations. We begin by discussing the characteristics of the magnetosheath that are relevant to our model.

Features of the magnetosheath. The general features of the earth's magnetosheath are represented in Figure 4. The outer boundary is a shock front caused by the interaction of the solar-wind plasma with the geomagnetic field. The plasma velocity decreases from its interplanetary value (typically 350 km/sec) upon crossing the shock and then increases again. The wind velocity over the poles is of the order of 100–200 km/sec, directed essentially outward away from the sun. The magnetic field from interplanetary space is carried into the magnetosheath, but the relative amplitude of the fluctuations is greatly increased. The inner boundary is defined by the magnetopause, a point at which the magnetic field becomes steady and is due to the earth's field. The fluctuations $\delta B/B_0$ are generally much smaller in the magnetosphere than in the magnetosheath, and so the magnetospheric fluctuations will have a much smaller effect on cosmic rays. The thickness of the magnetosheath, from the sunward side to the poles, is approximately 5 R_E, and the inner boundary is some 10 or 15 R_E from the surface of the earth.

Magnetic-field characteristics of the magnetosheath have been measured by several satellites. A typical set of measurements, [*Siscoe et al.*, 1967] taken aboard Mariner 4, shows that the average magnetic-field strength decreases from ~15 γ at the inner boundary to 4 γ near the outer boundary, the average value being ~7 γ, only slightly higher than the 5 γ com-

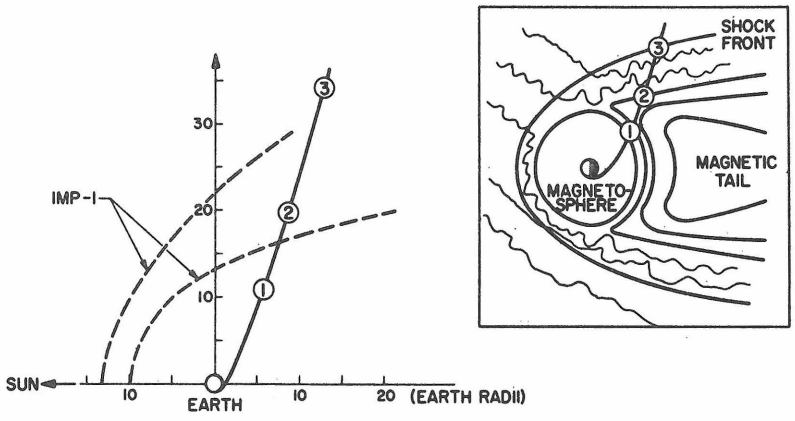

Fig. 4. The earth's magnetosheath. Dashed lines indicate average positions of the shock front and magnetopause as determined by Imp 1. Circled numbers in the left diagram identify, respectively, the three regions: magnetosphere, magnetosheath, and the undisturbed interplanetary medium. Wavy lines in the right diagram represent interplanetary magnetic-field lines.

monly encountered in the nearby interplanetary medium. (The path of Mariner 4 is shown by the dashed line in Figure 4.) The power spectrum of the magnetic-field fluctuations for a quiet time in the magnetosheath [*Siscoe et al.*, 1967] is shown in Figure 5. The features that concern us are the amplitude and shape of the power spectrum for frequencies less than 10^{-3} Hz. The shape for $f < 10^{-3}$ Hz is approximately a power law with $P_{|B|}(f) \sim f^{-2}$. Figure 5 gives the power spectrum of the magnitude of the magnetic field, not of one component; the spectrum of the latter is expected to have approximately the same shape and be larger in magnitude by a factor of 2 to 6. (This result is typical of the interplanetary fluctuations, as was discussed by *Coleman* [1966].) We do not know the spectrum below 3×10^{-4} Hz. Since there is no indication of a change in slope, we can confidently extrapolate down to the frequencies ($\sim 10^{-4}$ Hz) of interest. If future measurements should show an appreciably dif-

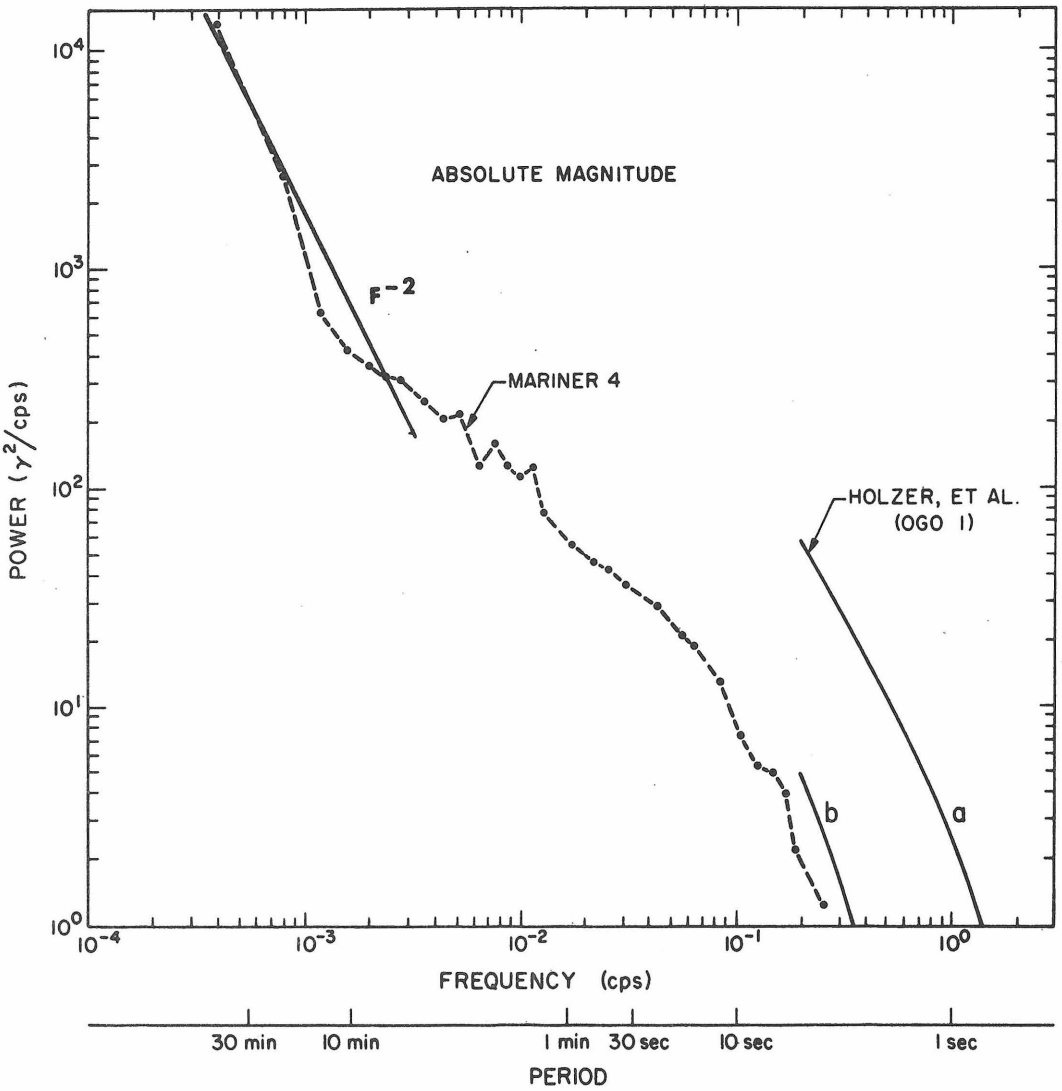

Fig. 5. Power spectrum of absolute magnitude of the magnetic field in the magnetosheath. Dashed curve obtained during quiet time aboard Mariner 4, by *Siscoe et al.* [1967]. Curve *a* was obtained from a noisy region and curve *b* from a quiet region of the magnetosheath by *Holzer et al.* [1966] from Ogo 1 data.

ferent spectrum at $\sim 10^{-4}$ Hz, our discussion would have to be modified.

In the interplanetary medium, the power spectrum of the fluctuations in the magnetic-field amplitude is smaller by roughly a factor of 100 than the corresponding power spectrum in the magnetosheath [e.g., *Coleman*, 1966, Figure 16]. Since the average magnetic field has about the same magnitude in both regions, it is evident that in the magnetosheath the fluctuations in the magnetic field are much larger than in interplanetary space. It is for this reason that the 'thin-slab' model is adopted and the magnetosheath is considered as a turbulent transition region between the more quiet regions of interplanetary space and the magnetosphere.

Thin-slab model with idealized particle access. The actual problem of particle access to the polar caps is quite complicated, particularly at low energies. We first adopt an idealized model of particle access in order to obtain an illustration of the possible effects of the magnetosheath turbulence on cosmic rays. A more realistic model of low-energy particle propagation near the earth is discussed below. In our simplified model, we neglect the inclination of the ecliptic and assume that particles which reach a point deep in the magnetosphere are incident with velocities in interplanetary space directed essentially toward the poles. For this reason, it is reasonable to use the free-space anisotropy $\boldsymbol{\delta}$ in the calculations. We assume that the solar-wind velocity in the magnetosphere is radially outward from the sun. Recalling the geometry of the thin-slab model in Figure 3, these assumptions allow the identification of the axes $\hat{x} \sim \hat{r}$, $\hat{y} \sim \hat{\varphi}$, and $\hat{z} \sim \hat{\theta}$, where (r, θ, φ) are solar spherical polar coordinates. This idealized model of particle access to the polar caps is grossly oversimplified for $\sim$1-Mev particles, but it is reasonable for high-energy particles ($\sim$1 Gev) and it greatly simplifies both the calculations and the conceptual picture.

Now consider the theoretical result given in equations 16, for frequencies less than 10^{-3} Hz. The frequency f_A, corresponding to the low frequency at which the magnetic-field power spectrum flattens out, has not been observed in the magnetosheath. However, in the interplanetary magnetic field, observations place $f_A \sim 2 \times 10^{-5}$ Hz, corresponding to a wave number of $k \sim 6 \times 10^{-12}$ cm^{-1} if the convection velocity is 350 km/sec. (For convected spatial fluctuations, $k_x = 2\pi f/V_w$.) If the same wave-number structure of fluctuations exists in the magnetosheath as in the interplanetary plasma, it might be expected that in the magnetosheath the frequency f_A is reduced by the ratio of the convection velocities, or by a factor of (350/(100 or 200)) $\sim$ 2 to 4. We therefore expect $f \sim 10^{-5}$ Hz. The upper-frequency f for which equation 16*a* remains applicable is then given by $f^{*2} + f_A^2 = (V_w/\pi l)^2$. Putting in values $V_w = 100$ km/sec and $l = 5\ R_E$, one obtains $f^* \cong 10^{-3}$ Hz. Therefore, equation 16*a* can be considered valid for frequencies less than about 10^{-3} Hz. Putting in numerical values, we obtain

$$P^{\delta n}(f)/n^2 = (l/5\ R_E)^2(w/c)^{-2} \cdot (T + 0.938)^{-2}(Z^2/A^2) \cdot \{(\delta_r/1\%)^2 P_{\varphi\varphi}(f) + (\delta_\varphi/1\%)^2 P_{rr}(f)\} \cdot (9.1 \times 10^{-9}) \quad (18)$$

In this equation, T is the particle's kinetic energy in Gev/nucleon, the particle's charge is Ze, and its mass number is A. The magnetic field is measured in gammas, $1\ \gamma = 10^{-5}$ gauss. In the next two sections, we compare the observations of Ogo 6 and the neutron monitors with the theoretical model and its result as given in equation 18.

Low-energy cosmic rays: $T \sim 1$ Mev/nucleon. Although the direct access picture of the preceding section is an oversimplification for particles with $T \sim 1$ Mev, we use this model as an illustration of the general magnitude of the magnetosheath-induced scintillations. A discussion of the complicating factors and an attempt at a slightly more realistic calculation is given later. For the present, we consider the idealized access model as expressed in equation 18. At 1 Mev, protons dominate the flux of cosmic rays, and so $Z/A = 1$. Both observations and theory [*Gleeson et al.*, 1971] indicate that at low energies ($T \lesssim 10$ Mev) the dominant anisotropy of cosmic rays in interplanetary space near earth is due to convection, and thus is radial. The anisotropy of the differential flux is then given simply by the Compton-Getting anisotropy,

$$\boldsymbol{\delta}_{cv} = (V/w)(2 + \alpha(T)\gamma)\hat{r}$$

where γ is the exponent of the energy spectrum,

$\alpha(T) = 2$ for nonrelativistic particles, and V is the (interplanetary) solar-wind velocity.

Using this radial anisotropy and evaluating the constants in equation 18 for low-energy protons, one obtains

$$P^{\delta i}(f)/j_0^2 = (3.1 \times 10^{-5})(1+\gamma)^2(1\ \text{Mev}/T) \cdot (l/5\ R_E)^2(V/350\ \text{km/sec})^2 P_{\varphi\varphi}(f) \qquad (19)$$

This equation gives the theoretical power expected for particles of given energy T. If the detector is an integral detector, the measured power will be the integral of (19) over all energies greater than threshold T_0. Assuming that the energy exponent of the differential flux (γ) remains constant over the region of importance, the integral relation similar to (19) is given by

$$P_I^{\delta i}(f)/j_0^2 = \int_{T_0}^{\infty} (P^{\delta i}(f)/j_0^2) j(T)\, dT \Big/ \int_{T_0}^{\infty} j(T)\, dT \qquad (20a)$$

or

$$P_I^{\delta i}(f)/j_0^2 = (3.1 \times 10^{-5})(1+\gamma)^2 \cdot ((\gamma-1)/(\gamma+1))(1\ \text{Mev}/T_0)(l/5\ R_E)^2 \cdot (V/350\ \text{km/sec})^2 P_{\varphi\varphi}(f) \qquad (20b)$$

In equations 20 and below, the subscript I on the power spectrum indicates that the measurement has been made with an integral-energy detector. Using the typical magnetosheath power spectrum of Figure 5, and extrapolating the figure downward slightly in frequency, we see that at $f = 10^{-4}$ Hz the predicted power spectrum for 1-Mev protons has a shape of f^{-2} and an amplitude of

$$P_I^{\delta i}(f = 10^{-4})/j_0^2 = (3.1/\text{Hz})(\gamma-1)(\gamma+1)(l/5\ R_E)^2 \cdot (V/350\ \text{km/sec})^2 (P_{\varphi\varphi}/P_{|B|}) \qquad (21)$$

We wish to apply the model to the 1-Mev proton data from Ogo 6. We choose the typical parameter values $V = 350$ km/sec, $l = 5\ R_E$, $P_{\varphi\varphi}/P_{|B|} = 4$, and $\gamma = 3$ (the energy exponent during quiet times measured in the Ogo 6 experiment). The model predicts a spectral shape of f^{-2} near 10^{-4} Hz, leveling off at about $f_A \sim 10^{-5}$ Hz, with an amplitude given by

$$P_I^{\delta i}(f = 10^{-4}\ \text{Hz})/j_0^2 \sim 100\ \text{Hz}^{-1}\ \text{(theoretical)} \qquad (22a)$$

The amplitude is accurate to perhaps a factor of 4 due to uncertainties in the parameter estimates. The observed power spectrum, given in Figure 1, has precisely the predicted slope and an amplitude of

$$P_I^{\delta i}(f = 10^{-4}\ \text{Hz})/j_0^2 \sim 60\ \text{Hz}^{-1}\ \text{(observational)} \qquad (22b)$$

accurate to a factor of 2. Thus the thin-screen model of magnetosheath-induced cosmic-ray scintillations gives good agreement with the observed fluctuations of ~1-Mev protons, with realistic parameters.

Williams [1969] has obtained power spectra of 1- to 10-Mev protons in interplanetary space during solar-flare events. A typical spectrum, for November 15–16, 1967, is shown in Figure 6. Although this spectrum was taken during a nonquiet time in the interplanetary

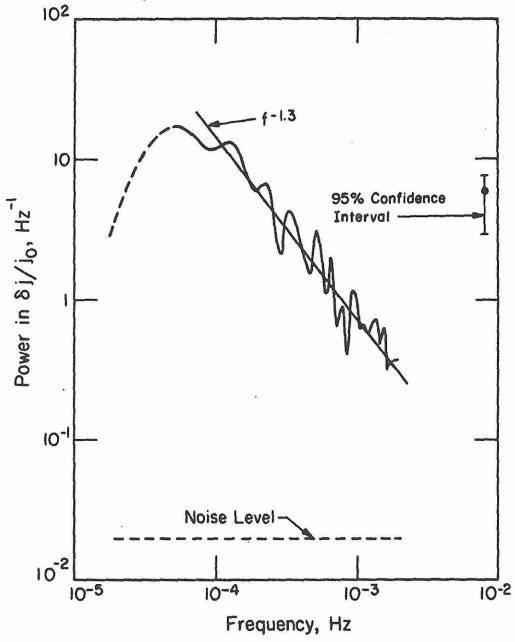

Fig. 6. Power spectrum of the interplanetary low-energy proton flux. Data for 1- to 10-Mev protons taken aboard Explorer 34, during later stages of a flare event, November 15–16, 1967. The average counting rate was 100 protons/sec. Power spectrum given by *Williams* [1969]. Power falls off below 5×10^{-5} Hz because of filtering of the data before analysis; the falloff is not a feature of the cosmic-ray flux power spectrum.

medium, so that the fluctuations might be expected to be larger than normal, a comparison with Figure 1 (for 1- to 40-Mev protons inside the magnetosphere) shows that the interplanetary spectrum (even though obtained during a disturbed period) is more than an order of magnitude lower in amplitude than the spectrum observed near earth. This may be an additional indication that the major source of low-energy cosmic-ray scintillations near earth is the turbulent magnetosheath field. Further data, particularly simultaneous measurements at similar energies inside and outside the magnetosheath, are necessary before any definite conclusion can be drawn.

High-energy cosmic rays: $T > 1$ Gev/nucleon. For high-energy cosmic rays, both theory and experiment indicate that the dominant anisotropy is due to corotation of the solar-wind plasma with the sun [e.g., *Jokipii*, 1971]. This anisotropy is in the φ direction, and of magnitude $\sim 0.5\%$, essentially independent of energy. Setting $w = c$ and $T > 1$ Gev in equation 18, we obtain approximately

$$P^{\delta i}(f)/j_0^2 = (2.3 \times 10^{-9})(Z^2A^2)(1 \text{ Gev}/T)^2 \cdot (\delta_\varphi/0.5\%)^2(l/5\ R_E)^2 P_{rr}(f) \qquad (23)$$

For protons of about 2-Gev energy, using the magnetosheath power spectrum as given in Figure 5, this equation gives an amplitude at $f = 10^{-4}$ Hz of

$$P^{\delta i}(f = 10^{-4} \text{ Hz})/j_0^2 = 6 \times 10^{-5} \cdot (\delta_\varphi/0.5\%)^2(P_{rr}/P_{|B|}) \quad \text{Hz}^{-1} \qquad (24)$$

assuming $l = 5\ R_E$, as above. If an integral detector is used, there is an additional factor of $(\gamma - 1)/(\gamma + 1)$ in this equation, as in equation 20*b*. Thus the expected contribution of the magnetosheath scattering to cosmic-ray scintillations for a detector with mean energy $T \sim 2$ Gev is given by

$$P^{\delta i}(f = 10^{-4} \text{ Hz})/j_0^2 = 2 \times 10^{-4} \text{ Hz}^{-1} \qquad (25)$$

In this equation, we have used $\gamma = 2.6$ and $\delta_\varphi = 0.5\%$, as observed, and $(P_{rr}/P_{|B|}) \sim 4$. Notice by comparison of equations 22*a* and 25 that the relative fluctuations due to the magnetosheath scattering are much lower at high energies than at low energies.

We refer to the power spectra for the Alert and Deep River neutron monitor counting rates, given in Figure 2, and recall that these neutron monitors can be idealized as detectors with mean energy $T \sim 2$ Gev. At 10^{-4} Hz, the observed power is 200 times larger than that predicted by equation 25 and the thin-slab magnetosheath model. This indicates that there is another source responsible for the scintillations observed by neutron monitors. A possible candidate is the interplanetary magnetic field, the same fluctuating field that scatters the cosmic rays.

Effects of particle access. The access of particles of moderate or high energies ($\gtrsim$100 Mev) to the polar caps is relatively simple. The particles come from interplanetary space and traverse the magnetosheath and magnetosphere essentially directly to strike a detector. The idealized particle access model discussed above is appropriate for these particles. The access of low-energy particles, such as 1-Mev protons, is more complicated. Although the entire polar cap ($\lambda \gtrsim 72°$) is accessible to these particles, only those particles observed near the edge of the polar cap passed through the magnetosheath at a short distance (less than $\sim 50\ R_E$) from the earth. Experiments indicate that particles observed at higher latitudes, in the region containing open magnetic-field lines that extend into the geomagnetic tail, come from a region of interplanetary space far behind the earth. A schematic model for the access of 1- to 40-Mev protons into the magnetosphere is shown in Figure 7 [*Evans*, 1972]. The low-polar-latitude (LPL) access region is the one for which particles traverse the magnetosheath directly, and the one for which the thin-slab model and discussion of low-energy cosmic rays are appropriate. The other two access regions (α-HPL and β-HPL) are several hundred earth radii past the earth, in a region that has not been explored systematically by space probes. The structure of the magnetosheath in this region is not known, although its sharp boundaries and qualitatively different character are probably no longer well defined. It is doubtful that the simple thin-slab model is appropriate for these particles.

The expected power spectrum of the particles entering by the HPL access regions can be qualitatively estimated as follows. As was dis-

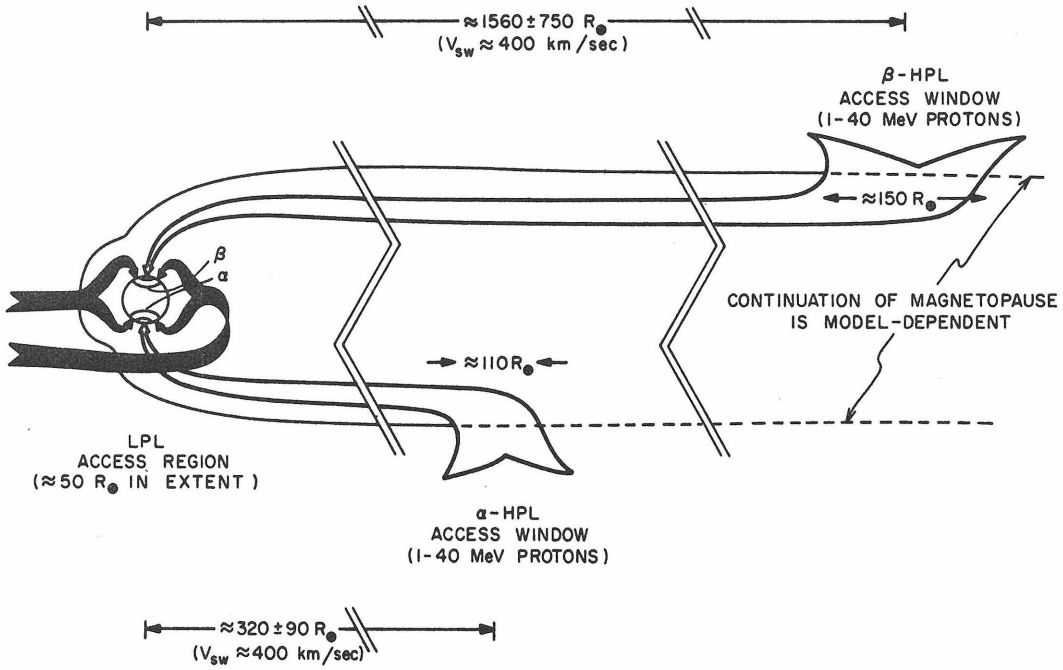

Fig. 7. Access of 1- to 40-Mev protons to the polar caps. Direct access at low polar latitudes (LPL) is shown in black. Distances to the two high polar latitude (HPL) access windows are determined by association with time delays of features in the high-latitude flux observed during energetic delayed particle events [*Evans*, 1972]. Arrows represent interplanetary proton fluxes.

cussed above, Liouville's theorem is applicable for low-frequency fluctuations. We imagine that an observer at a given polar latitude sees a fluctuating counting rate because the particular open field line through his point of observation is reconnecting with different interplanetary field lines as time progresses. Thus his effective sampling direction in interplanetary space is being shifted slowly in time by the fluctuating interplanetary magnetic field, and he sees fluctuations if the particle anisotropy is nonzero. Therefore, the HPL cosmic-ray scintillations for low frequencies are proportional to the particle anisotropy and the relative size of the interplanetary field fluctuations. By dimensional analysis, we argue that for this process

$$P^{\delta i}(f)/j_0{}^2 = \eta \delta_\perp{}^2 P_\perp(f)/B_0{}^2 \qquad (26)$$

where $\delta_\perp$ is the cosmic-ray anisotropy and $P_\perp(f)$ is the power spectrum of a component of the interplanetary magnetic field in a direction perpendicular to the asymptotic sampling direction, and η is a dimensionless constant of order unity. For a 1-Mev proton, $\delta_\perp \sim 15\%$, $B_0 \sim 5\ \gamma$ is the average interplanetary magnetic field, and, in the vicinity of $f \sim 10^{-4}$ Hz, the power spectrum of *Coleman* [1966] gives $P_{\theta\theta}(f \sim 10^{-4}\ \text{Hz}) \approx 10^4\ (f/10^{-4}\ \text{Hz})^{-1.5}\ \gamma^2/\text{Hz}$, so that equation 26 gives

$$P^{\delta i}(f \sim 10^{-4}\ \text{Hz})/j_0{}^2 \approx 9(f/10^{-4}\ \text{Hz})^{-1.5}\ \text{Hz}^{-1} \qquad (27)$$

Comparison of equations 22*a* and 27 indicates that scintillations due to particles from the near (LPL) access region are somewhat larger than those for particles which enter via the far (HPL) access regions. An analysis of the orbit parameters of the Ogo 6 trajectory for the epochs considered in Figure 1 indicates that approximately half the detected flux was obtained in the low polar latitudes and half in the high polar latitudes. Taking the flux-weighted averages of equations 22*a* and 27, we obtain a theoretical value of $P^{\delta j}/j_0{}^2 \sim 50\ \text{Hz}^{-1}$ for $f = 10^{-4}$ Hz, in good agreement with the data shown in Figure 1. We note that the complications in the argument due to the existence of several access windows for low-energy

protons do not appreciably alter our conclusion that magnetic irregularities in the magnetosheath can account for the observed scintillations of low-energy cosmic rays. The contribution of the far access region is probably not important.

Other sources of scintillations. Fluctuations of cosmic rays could conceivably be due to variations of the sources or to interactions with the plasma through which the cosmic rays propagate. Because of the large distances and the scattering involved in propagating from nonsolar sources, variations on the order of hours to days could not persist for galactic sources. Therefore the only source of cosmic rays whose quasiperiodic variations might be significant is the sun. Since the sun produces appreciable numbers of cosmic rays of energies $\gtrsim$20 Mev only during flare events, it is clear that scintillations in high-energy cosmic rays must be due to interactions during propagation. Magnetic forces dominate cosmic-ray trajectories, and it appears that interplanetary magnetic fluctuations are much stronger than interstellar variations for these time scales, and so interaction with magnetic irregularities inside the solar system is the most likely mechanism for the scintillation of high-energy cosmic rays. Scintillations due to the magnetosheath were shown to be negligible for these energies. A rough estimate of the power in the scintillations due to interplanetary magnetic-field fluctuations can be obtained by an argument similar to the one used in obtaining equation 26 above. For low frequencies, Liouville's theorem applies, and the cosmic-ray scintillations are caused by an anisotropic cosmic-ray flux being guided across the asymptotic viewing cone by magnetic irregularities. For a detector with a narrow asymptotic viewing cone, and therefore for any detector deep inside the magnetosphere, the estimate of equation 26 is applicable. With $\delta \sim 0.5\%$, typical for energies $\sim$1 Gev, this equation yields

$$P^{\delta j}(f \sim 10^{-4}\ \mathrm{Hz})/j_0^2 \sim 0.01(f/10^{-4}\ \mathrm{Hz})^{-1.5}\ \ \mathrm{Hz}^{-1} \qquad (28)$$

in qualitative agreement with the observations for neutron monitors (Figure 2). A more quantitative theory of interplanetary scintillations, taking into account the resonant interactions between cosmic rays and hydromagnetic waves at higher frequencies, is required before any conclusions can be drawn.

The modified quantitative theory indicates that low-energy ($\sim$1-Mev) cosmic-ray scintillations can be interpreted by a model considering the contribution due to the scattering in the random magnetic fields of the magnetosheath. A possible alternative mechanism is a variation in the rate of solar production of these cosmic rays. If the mechanism is solar, the observational data indicate that the source must be variable over a wide range of times of the order of hours to days, and the mechanism must not change significantly over the course of a year's time. Also, the mechanism is severely constrained by the observation that $\delta j/j_0$ is constant. It is also clear that, in propagating from the sun to the observation point near earth, much of the temporal coherence will be lost. The small ($\sim$15%) anisotropies observed near earth indicate that, even if the low-energy quiet-time cosmic rays are produced near the sun, they have scattered considerably by the time they are detected. Particles lose most of their initial temporal correlation (for the time scales of interest here) in approximately one scattering length, $\lambda = 3\kappa/w \sim 2 \times 10^{11}$ cm, where κ is the diffusion coefficient, and $\kappa \sim 10^{20}$ cm^2/sec and $w = 1.5 \times 10^9$ cm/sec are typical parameters for $\sim$1-Mev protons. Since the scattering mean free path is much smaller than 1 AU, solar particles are scattered many times before reaching the earth and therefore have their initial coherence destroyed. Even in the absence of significant scattering, the finite-energy bandwidth of the detector means that particles of different velocities and hence different production times at the source are detected simultaneously. It is easy to show that, for a detector with $\Delta T \sim T_0$, oscillations with frequencies greater than $1/t_0$ are strongly attenuated, where t_0 is the rectilinear transit time of a particle with kinetic energy T_0. Although these arguments cannot entirely rule out a solar origin for low-energy cosmic-ray scintillations, they indicate that such an origin is at present less attractive than the alternative discussed above.

D. Discussion and Conclusions

The purpose of this paper has been to present a discussion of cosmic-ray scintillations.

We presented power spectra of time-series data for low-energy (~1-Mev) protons and for particles of neutron monitor energy (~1 Gev), and we found that the fluctuations are much more than would be expected if the source were purely statistical (Poisson) noise. The scintillations decrease in amplitude from $\sim 10^{-7} \lesssim f \lesssim 10^{-4}$ Hz, and they are much stronger at 1 Mev than at 1 Gev. We suggested that these scintillations can be interpreted as originating in the interaction of the cosmic rays with the turbulent magnetic fields through which they propagate.

As a first example of the generation of cosmic-ray scintillations, we considered a simple thin-slab model of the magnetosheath and used this model to interpret the enhanced scintillations of ~1-Mev protons inside the magnetosphere. Reasonable values of the parameters give a good fit to the observed data at these low energies. Because of the strong rigidity dependence of the result, scintillations of neutron monitor counting rates are not appreciably affected by the fields in the magnetosheath. The much smaller amplitude of scintillations that do exist at these higher energies may be interplanetary in origin.

These conclusions are based on a small set of data, and the model must at present be regarded as an attractive possibility. Further detailed analyses of power spectra of cosmic-ray counting rates (at all energies, inside and outside the magnetosphere, from spinning and stationary space probes) will provide additional checks on the ideas that we have developed. Our major conclusion is that power spectral analyses of all types of cosmic-ray data could provide useful information about the interaction of cosmic rays with astrophysical electromagnetic fields.

APPENDIX: AXISYMMETRIC POWER SPECTRUM

In this Appendix, we consider the conditions that axial symmetry and a divergence-free magnetic field require of the magnetic-field power spectrum. After *Batchelor* [1946], let the power spectral tensor $P_{ij}(\mathbf{k})$ be a function of the only two available vectors, $\mathbf{k}$ and ξ, where ξ is a unit vector along the axis of symmetry. The most general form that P_{ij} can have, since it must be a symmetric tensor, is

$$P_{ij}(\mathbf{k}) = Ak_ik_j + B\xi_i\xi_j + C\delta_{ij} + D(k_i\xi_j + k_j\xi_i) \quad \text{(A1)}$$

where A, B, C, and D are functions of the only two invariants, k^2 and $\mathbf{k}\cdot\xi$. If one takes $\xi \rightarrow -\xi$, the power spectrum must be unchanged, and this condition requires A, B, and C to be even functions of $\mathbf{k}\cdot\xi$ and D an odd function of $\mathbf{k}\cdot\xi$. For isotropic turbulence, or spherical symmetry, $P_{ij}(\mathbf{k})$ can be a function only of $\mathbf{k}$, so that $B = D = 0$ in equation A1. The condition $\nabla\cdot\mathbf{B} = 0$ requires

$$P_{ij}(\mathbf{k})k_j = 0 \quad \text{(A2)}$$

Using this relation to eliminate B and D in equation A1, and introducing the functions $G = A$ and $G' = B/k^2$, we obtain

$$[P_{ij}(\mathbf{k})] = \begin{vmatrix} (k_y^2 + k_z^2)G + k_z^2G' & -k_xk_yG & -k_xk_z(G + G') \\ -k_xk_yG & (k_x^2 + k_z^2)G + k_z^2G' & -k_yk_z(G + G') \\ -k_xk_z(G + G') & -k_yk_z(G + G') & (k_x^2 + k_y^2)(G + G') \end{vmatrix} \quad \text{(A3)}$$

In this equation, the axis of symmetry is along the z direction and the arbitrary functions G and G' depend only on $k_\perp^2 = (k_x^2 + k_y^2)$ and $k_\parallel^2 = k_z^2$.

If the symmetry is spherical, (i.e., the turbulence is isotropic), then $G' = 0$ and G is a function only of $|\mathbf{k}|$. In this case,

$$P_{ij}(\mathbf{k}) = G(|\mathbf{k}|)(k^2\delta_i\delta_j - k_ik_j) \quad \text{(A4)}$$
(spherical symmetry)

We define the term cylindrical symmetry (about the z axis) to mean that $P_{xx}(\mathbf{k}) = P_{yy}(\mathbf{k})$ for all $\mathbf{k}$, which requires $G = 0$ via inspection in (A3), leaving

$$P_{ij}(\mathbf{k}) = G'(k_z^2, k_\perp^2 = k_x^2 + k_y^2) \cdot \begin{vmatrix} k_z^2 & 0 & -k_xk_z \\ 0 & k_z^2 & -k_yk_z \\ -k_xk_z & -k_yk_z & k_\perp^2 \end{vmatrix} \quad \text{(A5)}$$
(cylindrical symmetry)

Acknowledgments. We would like to thank J. Earl and E. C. Stone for helpful suggestions. The low-energy proton data were graciously provided by Stone and R. Vogt.

This research was supported, in part, by the National Aeronautics and Space Administration through grant NGR-05-002-160, the National Science Foundation (Owens), and the Alfred P. Sloan Foundation (Jokipii).

* * *

The Editor wishes to thank L. A. Fisk and E. N. Parker for their assistance in evaluating this paper.

REFERENCES

Batchelor, G. K., The theory of axisymmetric turbulence, *Proc. Roy. Soc., Ser. A, 186,* 480, 1946.

Blackman, R. B., and J. W. Tukey, *The Measurement of Power Spectra,* Dover, New York, 1958.

Coleman, P. J., Jr., Variations in the interplanetary magnetic field: Mariner 2, observed properties, *J. Geophys. Res., 71,* 5509, 1966.

Dhanju, M. S., and V. A. Sarabhai, Short-period variations of cosmic-ray intensity, *Phys. Rev. Lett., 19,* 252, 1967.

Dhanju, M. S., and V. Sarabhai, Short-period fluctuations of cosmic ray intensity at geomagnetic equator and their solar terrestrial relationship, *J. Geophys. Res., 75,* 1795, 1970.

Evans, Lawrence Curtis, Magnetospheric access of solar particles and the configuration of the distant geomagnetic field, Ph.D. thesis, Calif. Inst. of Technol., Pasadena, 1972.

Gleeson, L. J., S. M. Krimigis, and W. I. Axford, Low-energy cosmic rays near earth, *J. Geophys. Res., 76,* 2228, 1971.

Holzer, R. E., M. G. McLeod, and E. J. Smith, Preliminary results from the Ogo 1 search coil magnetometer; Boundary positions and magnetic noise spectra, *J. Geophys. Res., 71,* 1481, 1966.

Jokipii, J. R., Cosmic-ray propagation, 1, Charged particles in a random magnetic field, *Astrophys. J., 146,* 480, 1966.

Jokipii, J. R., Stochastic variations of cosmic rays in the solar system, *Astrophys. J., 156,* 1107, 1969.

Jokipii, J. R., On the 'thin screen' model of interplanetary scintillations, *Astrophys. J., 161,* 1147, 1970.

Jokipii, J. R., Propagation of cosmic rays in the solar wind, *Rev. Geophys. Space Phys., 9,* 27, 1971.

Salpeter, E. E., Interplanetary scintillations, 1, Theory, *Astrophys. J., 147,* 433, 1967.

Siscoe, G. L., L. Davis, Jr., E. J. Smith, P. J. Coleman, Jr., and D. E. Jones, Magnetic fluctuations in the magnetosheath: Mariner 4, *J. Geophys. Res., 72,* 1, 1967.

Steljes, J. R., Cosmic ray NM-64 neutron monitor data XIV, *AECL-3560,* Atomic Energy of Canada, Ltd., Chalk River, Ontario, 1970.

Williams, D. J., Solar proton observations, 1–10 Mev, in *Proceedings of the Seminar on Interplanetary Physics Using Cosmic Rays,* A. I. Ioffe Physical Technical Institute, Leningrad, USSR, 1969.

Yaglom, A. M., *An Introduction to the Theory of Stationary Random Functions,* Prentice-Hall, Englewood Cliffs, N. J., 1962.

(Received June 6, 1972;
accepted August 21, 1972.)

E. Summary

The paper in this Chapter deals with the thin-slab model of magnetosheath-induced cosmic-ray scintillations. The model is appropriate for cosmic rays with cyclotron radius large compared to the thickness of the magnetosheath, or for protons with energies $T \gtrsim 1$ MeV. Although more data - especially from simultaneous magnetospheric and interplanetary measurements of particles with the same energy - are needed before a definitive test of the theory can be made, several tentative conclusions can be drawn:

1) The random fluctuations of the magnetic field inside the magnetosheath can account for the frequency spectrum of the low-energy (1-40 MeV) proton scintillations observed inside the magnetosphere.
2) Scintillations at neutron-monitor energies are much larger than predicted by the magnetosheath model, indicating that higher-energy cosmic-ray scintillations are produced by another source.

If these tentative conclusions are accepted, the proton observations discussed in Chapter II can be interpreted simply. At low energies (~1 - 10 MeV), interplanetary scintillations (Fig. II-7) are much smaller than those induced by the magnetosphere (Fig. II-3 through II-6). At higher energies (~1 GeV), because the magnetosheath contribution falls off rapidly with energy (compare equations 22a and 25), the scintillations which occur are probably interplanetary in origin.

The theory of the interplanetary scintillations of cosmic rays will be considered in Chapter IV and V. As shown below (see equation IV-8), the order-of-magnitude estimate of equation (26) in this Chapter is approximately correct in the low-frequency limit if $\delta_\perp$ is interpreted

as the magnetic-field-aligned particle anisotropy in the rest frame of the solar wind.

Erratum to Cosmic-Ray Scintillations I.

In Fig. 2, the noise levels should be 1×10^{-2} Hz^{-1} for Alert and 4×10^{-3} Hz^{-1} for Deep River. In the caption to this figure, the average counting rates should be 180 sec^{-1} and 510 sec^{-1}, respectively. These errors, which were pointed out by Martin H. Israel, are due merely to an incorrect normalization of the neutron-monitor counting rates and in no way influence any of the results discussed in the paper.

IV. INTERPLANETARY SCINTILLATIONS I: LOW-FREQUENCY LIMIT

This Chapter is the first of two dealing with the theory of interplanetary scintillations of cosmic rays. The model deals with the generation of scintillations by the stochastic interplanetary magnetic field, and it assumes that the typical cosmic ray scatters many times in propagating from the boundaries of the interplanetary medium to the point of observation. In Section IV.A, I present the theory of interplanetary scintillations, assuming that the fluctuations are a function only of distance along the average magnetic field and are characterized by wavenumbers k satisfying the inequality $k < \omega_0/w$, where ω_0 is the cyclotron frequency. The physical mechanism for interplanetary scintillations is discussed, and a simple proportionality between the cosmic-ray flux power spectrum and the magnetic-field power spectrum is derived (equation 8).

Section IV.B deals with the effect that the earth's rotation has on the interplanetary scintillations observed by neutron monitors. The low-frequency limit is used, and the temporal variation due to the neutron monitor's viewing cone being swept across the sky is considered in detail for a simplified model. The result of the theory is a prediction that neutron monitors with asymptotic geographic latitudes near the poles are uneffected by the rotation, but neutron monitors with asymptotic viewing directions near the geographic equator have a broad peak in their scintillations power spectrum near one cycle per day. The results of the calculations (equations 19 and 24) are compared with observed power spectra from the Alert and Deep River Neutron Monitor

fluxes, and detailed agreement between theory and observations is found (Fig. IV-3 and IV-5).

A. Interplanetary Scintillations of Cosmic Rays in the Low-Frequency Limit

In this Section, I present a simple model for the production of broad-band cosmic-ray fluctuations ("scintillations") by magnetic irregularities in interplanetary space. Portions of the work discussed in this section have previously been published (Owens and Jokipii, 1973). I work initially in the rest frame of the plasma where the electric field $\underset{\sim}{E} \sim 0$, and regard the magnetic field $\underset{\sim}{B}$ as a stationary, random function of time and position (e.g. Jokipii 1966, 1971). Consider particles of a given mass γm, charge q, velocity $\underset{\sim}{w}$, and let $n(\underset{\sim}{x},\underset{\sim}{w},t)$ be the distribution function. Define $\underset{\sim}{B}_0$ and n_0 as the ensemble averages of $\underset{\sim}{B}$ and n, respectively, and let $\underset{\sim}{B}_1$ and n_1 be the fluctuations about the mean. The average distribution function n_0 satisfies the full Fokker-Planck equation of Jokipii (1966, 1971) and Appendix B. Assume that the scales of variation of the means are much larger than those of interest. Liouville's equation may be written

$$\left[\frac{\partial}{\partial t} + w_i \frac{\partial}{\partial x_i} + \epsilon_{ijk} w_j \left(\omega_{0k} \frac{\partial}{\partial w_i} + \omega_{1k} \frac{\partial}{\partial w_i}\right)\right] (n_0 + n_1) = 0 \qquad (1)$$

where $\underset{\sim}{\omega}_0 = q\underset{\sim}{B}_0/\gamma mc$ and $\underset{\sim}{\omega}_1 = q\underset{\sim}{B}_1/\gamma mc$. Next assume that $\underset{\sim}{\omega}_1$ and n_1 are small, work only to lowest order in small quantities, and let $\underset{\sim}{B}_0 = B_0 \hat{e}_z$. Subtract the ensemble average of equation (1) from equation (1), neglect the second-order terms, and Fourier transform the resulting equation in t, $\underset{\sim}{x}$ space, obtaining as a function of frequency ω and wave vector $\underset{\sim}{k}$,

$$\left[i(\omega - \underset{\sim}{k}\cdot\underset{\sim}{w}) - \omega_0 \frac{\partial}{\partial\varphi}\right] n_1(\underset{\sim}{k},\omega,\underset{\sim}{w}) = -\epsilon_{ijk} w_j \omega_{1k}(\underset{\sim}{k},\omega) \frac{\partial n_0}{\partial w_i}, \qquad (2)$$

where $\varphi = \tan^{-1}(w_y/w_x)$.

Now restrict consideration to the low-frequency limit, which for the remainder of this Thesis will be defined by the relations

$$\omega \ll \omega_0 \qquad (3a)$$

$$|\underset{\sim}{k}|\ |\underset{\sim}{w}| \ll \omega_0 . \qquad (3b)$$

The condition (3a) is well satisfied for the waves which interact with cosmic rays in all relevant astrophysical situations, and the second condition (3b) can be viewed as a small-wavenumber limit for particles with a given energy. The limit (3b) restricts the discussion of this Chapter to wavenumbers smaller than the cyclotron resonant wavenumber $k_r \sim \omega_0/w$. The case of general $\underset{\sim}{k}$ will be discussed in Chapter V.

For simplicity, I introduce two more assumptions. First, let $\underset{\sim}{B}_1$ vary only with distance along $\underset{\sim}{B}_0$, so that $\underset{\sim}{k} = k_{\parallel} \hat{e}_z$. This is equivalent to assuming that fluctuations propagate only along the average field direction. Finally, assume that to lowest order the average distribution function $n_0(\underset{\sim}{x},\underset{\sim}{w},t)$ depends on velocity only through the particle pitch-angle $\mu = w_{\parallel}/w$. The generalization to arbitrary $n_0(\underset{\sim}{x},\underset{\sim}{w},t)$, will also be considered in Chapter V. The present limits serve to illustrate the major features of the model and allow a simple analytic solution to equation (2) for the cosmic-ray scintillations.

In the limit discussed here, equation (2) becomes

$$-\omega_0 \frac{\partial n_1(k_\parallel, \underset{\sim}{w})}{\partial \varphi} = w_\perp [\omega_{1x}(k_\parallel)\sin\varphi - \omega_{1y}(k_\parallel)\cos\varphi]\frac{n_0}{w}\delta_\parallel , \qquad (4)$$

where $w_\perp = \sqrt{1 - \mu^2}\, w$ and $\delta_\parallel$ is the field-aligned anisotropy,

$$\delta_\parallel = \frac{w}{n_0}\left(\frac{\partial n_0}{\partial w}\right)_{\parallel \text{ const } w} . \qquad (5)$$

Since n_0 is independent of φ, equation (4) is a simple first-order differential equation in φ. The solution is given by

$$n_1(k_\parallel, \underset{\sim}{w}) = \delta_\parallel n_0 \frac{w_\perp}{w}\left[\frac{\omega_{1x}(k_\parallel)}{\omega_0}\cos\varphi + \frac{\omega_{1y}(k_\parallel)}{\omega_0}\sin\varphi\right]. \qquad (6)$$

A constant of integration has been set equal to zero in equation (6) so that n_1 is linear in $\underset{\sim}{\omega}_1$ and $\langle n_1 \rangle = 0$. This procedure assumes that the scintillation region is "thick" enough that the initial conditions have no effect on the fluctuations. It will be shown in Chapter V that this requires that the region in which the scintillations occur be many scattering lengths thick, as is true for cosmic rays with energies $T \lesssim 50$ GeV in interplanetary space.

Application of the Wiener-Khinchin theorem (Yaglom, 1962) to equation (6) yields the power spectrum of n_1 in the rest frame of the plasma,

$$P^n(k_\parallel, w_\parallel, \varphi) = \frac{w_\perp^2}{B_0^2}\frac{n_0^2}{w^2}\delta_\parallel^2 \left\{ P^B_{xx}(k_\parallel)\cos^2\varphi + P^B_{yy}(k_\parallel)\sin^2\varphi + [P^B_{xy}(k_\parallel) + P^B_{yx}(k_\parallel)]\sin\varphi\cos\varphi \right\} , \qquad (7)$$

where $P^B_{ij}(k_\parallel)$ is the power spectrum of B_1. If I assume that

$P^B_{xx} \sim P^B_{yy} = P^B_{\perp}$ and $P^B_{xy} \sim P^B_{yx} \sim 0$, I get

$$\frac{P^n(k_\parallel,w,\mu)}{n_0^2} = \frac{P^j(k_\parallel,w,\mu)}{j_0^2} = (1 - \mu^2)\,\frac{P^B_\perp(k_\parallel)}{B_0^2}\,(\delta_\parallel)^2 \qquad (8)$$

where j is the cosmic-ray differential intensity, $j = (\gamma mw)^2 n$ and j_0 is the average value of j.

Equation (8) is appropriate for a detector which samples particles from a <u>given</u> direction with a given pitch-angle and energy. In some cases, particularly for detectors on rapidly-rotating spacecraft, this limit is not appropriate and the level of the fluctuations will depend on how the viewing cone of the detector is being swept across the sky. It can easily be shown from the model (average n_1 from equation 6 over φ) that a perfectly <u>omnidirectional</u> detector at rest with respect to the plasma would see <u>no</u> fluctuations at these low wavenumbers and to lowest order in B_1/B_0.

Now, if one transforms from the rest frame of the plasma to the frame of a stationary observer in interplanetary space, it is well known that the spatial fluctuations are observed as temporal fluctuations with a frequency

$$f = \underset{\sim}{k}\cdot\underset{\sim}{V}/2\pi \qquad (9)$$

(Jokipii, 1971, Appendix 1) where $\underset{\sim}{V}$ is the solar wind velocity. Equations (6) - (8) remain valid in the rest frame, if terms of order V/w are neglected compared to unity, with the wavenumber being replaced by the appropriate observing frequency according to equation (9). Equation (8) thus relates the spectra of $\underset{\sim}{B}_1$ and n_1 at a given frequency.

For ~1 GeV particles the above low-frequency limit, $|\underset{\sim}{k}||\underset{\sim}{w}| \ll \omega_0$, is valid for observing frequencies $f \ll \frac{V}{w}\,\omega_0/2\pi \approx 5 \times 10^{-5}$ Hz.

Now consider a simple interpretation of the result. At low frequencies and long wavelengths the particles are guided along the magnetic field, and the angular distribution swings to follow the field direction. If there is an anisotropy, the intensity observed in a fixed direction Ω will vary as the direction of the field varies. For small fluctuations the factor $P_{\perp}(k_{\parallel})/B_0^2$ is simply the mean square angle θ corresponding to magnetic fluctuations with wavenumber $k_{\parallel}$. In actual fact, of course, the fluctuations in the interplanetary magnetic field are appreciable, with $\langle B_1^2\rangle^{1/2}/B_0 \simeq 1/3$, and equation (8) must be regarded only as a first approximation.

As an example of the application of results of the theory, I consider the quantitative relation (8) and compare the theory with the observations of scintillations for the Alert Neutron Monitor discussed in Chapter II. Although the earth is rotating, the Alert Neutron Monitor has an asymptotic viewing direction which is essentially constant, corresponding to latitude $\gtrsim 60^{\circ}$ (Shea, private communication). I choose 2/3 as a typical value of $(1 - \mu^2)$ and evaluate $\delta_{\parallel}$ for the typical energy (~1 GeV) of the cosmic rays detected. The value of $P_{\perp}^{B}(f)/B_0^2$ can be obtained from direct observations of the interplanetary magnetic field, and the spectra presented by Quenby and Sear (1971) for a quiet period during 1969 are used. For an average spiral angle $\psi \sim 45^{\circ}$ at 1 A.U. (Parker, 1963) one may obtain for $P_{\perp}$ (see Section V.E below for details)

$$P_{\perp}^{B} \simeq 1/4\ (2P_{\theta\theta}^{B} + P_{rr}^{B} + P_{\varphi\varphi}^{B}). \tag{10}$$

Recently Fisk and Sari (1973) have argued that much of the observed low-frequency power in the magnetic field is due to tangential discontinuities. I will proceed, keeping in mind that inferring $P_{\perp}(k_{\parallel})$ from $P_{ij}(f)$ is subject to some uncertainty. The value of $\delta_{\parallel} \sim 1\%$ at ~1 GeV can be estimated with some confidence from the solution to the cosmic-ray modulation equation in the high-energy limit. The anisotropy is due to diffusion and is given by

$$\delta_{\parallel} = - \frac{3K_{\parallel}}{wn_0} \frac{\partial n_0}{\partial z} \tag{11}$$

where z is distance along the average magnetic field, $K_{\parallel}$ is the parallel cosmic-ray diffusion coefficient, and $\frac{\partial n_0}{\partial z} = \cos\psi \frac{\partial n_0}{\partial r}$ since to lowest order n_0 is a function only of radius at a given energy. In the high-energy limit ($T \gtrsim 0.5$ GeV), the radial gradient of the cosmic-ray intensity (see equation 92 of Jokipii, 1971) for $K_{\perp} \ll K_{\parallel}$ is given by

$$\frac{1}{n_0} \frac{\partial n_0}{\partial r} = \frac{2+\alpha\Gamma}{3} \frac{V}{K_{\parallel} \cos^2\psi} . \tag{12}$$

Here I define $\Gamma = - \frac{\partial\ \ell n\ j_0}{\partial\ \ell n\ T}$ and $\alpha = \frac{\gamma+1}{\gamma}$. Combining equations (11) and (12), one has

$$\delta_{\parallel} = \frac{2+\alpha\Gamma}{\cos\psi} \frac{V}{w}. \tag{13}$$

Choosing V = 350 km/sec, and noting that $\Gamma \sim 1.4$ for ~1 GeV protons, one obtains $\delta_{\parallel} \sim 0.9\%$. Since the calculated anisotropy varies little for

energies 0.5 GeV $\lesssim T \lesssim$ 10 GeV this value can be used with some confidence.

The result of the theory, equation (8), with the perpendicular power spectrum calculated from equation (10) and the anisotropy from equation (13), is displayed in Fig. IV-1. The dashed portion of the theoretical curve signifies extrapolation into a region in which $|\underset{\sim}{k}|\ |\underset{\sim}{w}| \ll \omega_0$ is not satisfied. Similarly, at wavelengths comparable with or larger than the ~1 A.U. scale of $\underset{\sim}{B}_0$, ($f \lesssim 5 \times 10^{-7}$ Hz) the theory is not applicable. Also plotted on Fig. IV-1 is the observed power spectrum of the flux of the Alert Neutron Monitor, taken from Fig. II-8. The agreement between theory and observation is quite good, in support of the suggestion that scintillations of high-energy ($T \gtrsim 100$ MeV) cosmic rays are of interplanetary origin. Because of the relation between cosmic-ray scintillations and magnetic-field fluctuations (e.g., equation 8) which the model provides, it may be possible to monitor properties of the interplanetary magnetic field from ground-based (i.e., neutron monitor) observations. Because of the possible use of neutron-monitor data from detectors with asymptotic viewing directions far from the geographic poles, in the next Section I consider the effect that the earth's rotation will have on the scintillations seen by neutron monitors.

Figure IV-1: Power spectrum of cosmic-ray scintillations. The data are the spectrum of the Alert Neutron Monitor flux ($T \gtrsim 0.5$ GeV) for a 90-day quiet period in 1969. Other periods give similar spectra. The Poisson noise level $P_p(f) = 2/I$ for the spectrum is $\sim 10^{-2}\,\mathrm{Hz}^{-1}$. 90% confidence intervals are shown. The curve labeled "theory" is the prediction of the model developed in the text. j_1 is the fluctuation in intensity about its mean, j_0.

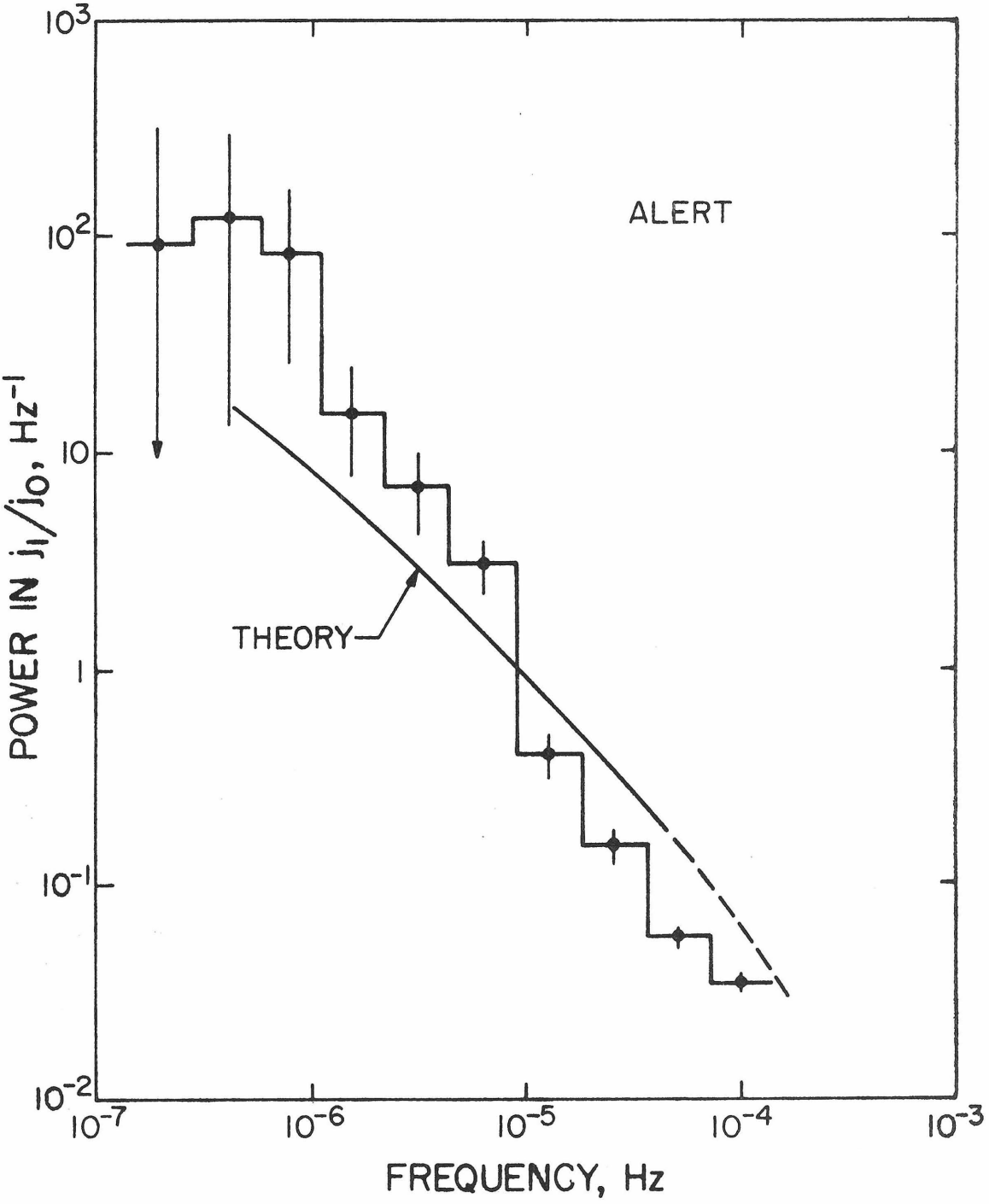
ALERT
THEORY
POWER IN j_1/j_0, Hz^{-1}
FREQUENCY, Hz
10^3
10^2
10
1
10^{-1}
10^{-2}
10^{-7}
10^{-6}
10^{-5}
10^{-4}
10^{-3}

B. Effect of Rotation on Interplanetary Neutron-Monitor Scintillations

Neutron monitors are essentially narrow-angle detectors with asymptotic viewing cones which depend on energy and point in a fixed direction with respect to the earth. As the earth rotates, the viewing cones are swept across the sky. In order to demonstrate the essential effects which the earth's rotation will have, I consider the simplest possible model, as shown in Fig. IV-2. A neutron monitor is idealized as having a single narrow-angle asymptotic viewing cone which looks in a given direction with geographic latitude λ. The inclination of the ecliptic is ignored, and the average interplanetary magnetic field is taken to be along the earth's equator ($\lambda = 0$). The azimuthal angle Φ of the viewing cone with respect to a non-rotating coordinate system is assumed to vary uniformly with time, so that

$$\Phi(t) = 2\pi f_e t + \Phi_0, \tag{14}$$

where f_e is the earth's rotation frequency, 1/day. This model thus ignores effects which the geomagnetic tail might have on asymptotic viewing cones of the neutron monitors.

Assume that the cosmic-ray scintillations seen by neutron monitors are interplanetary in origin, and consider the low-frequency limit discussed in the previous Section. It will be shown that the effect of the earth's rotation is negligible for frequencies $f \gtrsim f_e \sim 10^{-5}$Hz. Recalling that the low-frequency limit is valid for ~1 GeV protons for frequencies up to ~5×10^{-5}Hz, one sees that the low-frequency limit is an adequate description of the interplanetary scintillations for those frequencies which are effected by the earth's

Figure IV-2: Simplified model for neutron monitors. A narrow asymptotic viewing cone with geographic latitude λ is swept uniformly across the sky as the earth rotates. The inclination of the ecliptic is ignored, and the average interplanetary magnetic field is equatorial. The influence of the magnetosheath is ignored. A cosmic ray entering the asymptotic viewing cone with the appropriate velocity is guided by the earth's magnetic field to the detector.

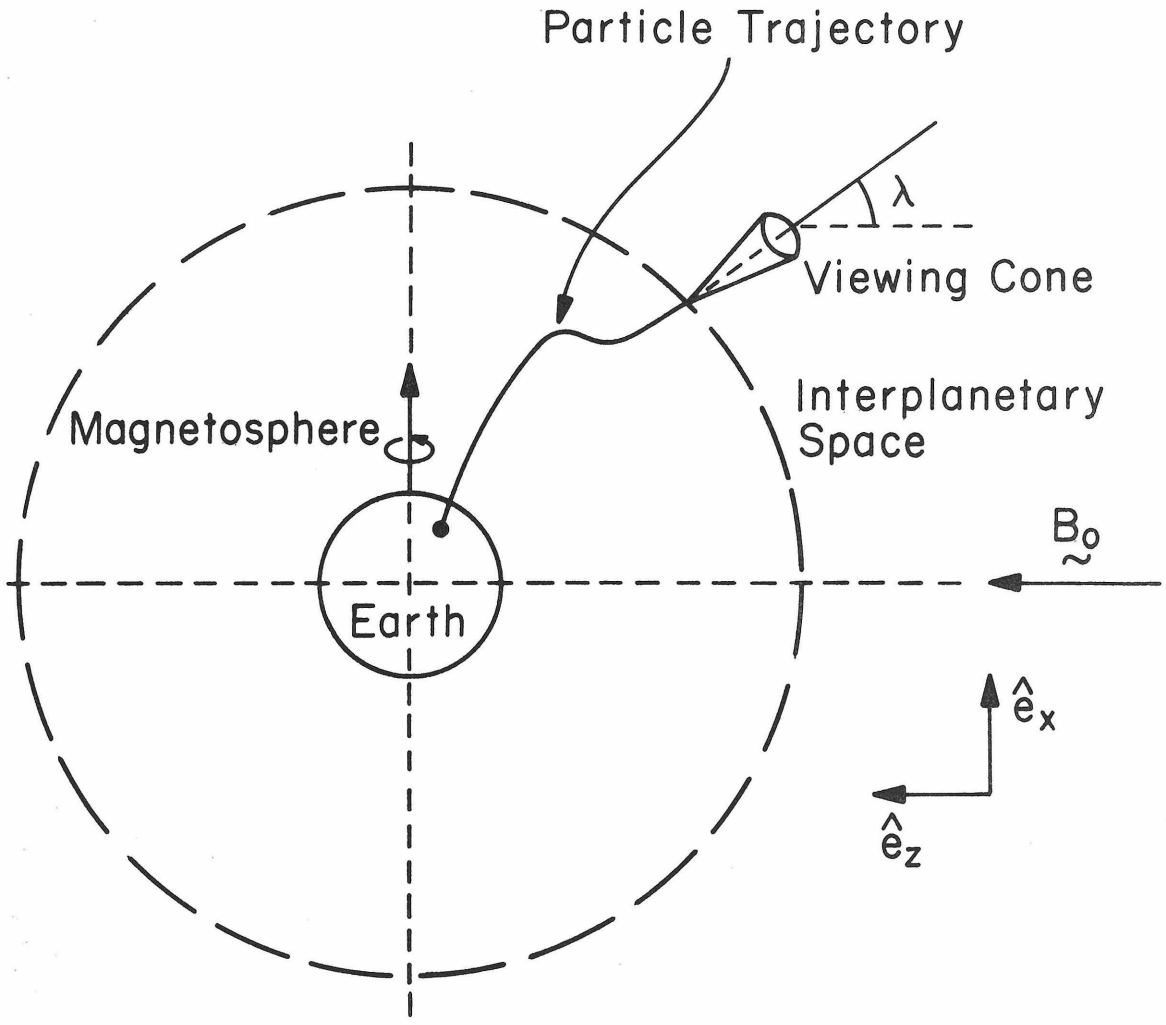
Particle Trajectory
λ
Viewing Cone
Interplanetary
Space
Magnetosphere
B0
Earth
êx
êz

rotation.

Choose coordinates such that the average magnetic field is along the z-axis and the earth's rotation axis is along the x-axis, as shown in Fig. IV-2. In a non-rotating reference frame which is stationary at the orbit of earth, the low-frequency limit of equation (6) gives

$$n_1(\underset{\sim}{w},t) = \delta_{\parallel} n_0 \left[\frac{\omega_{1x}(t)}{\omega_0}\frac{w_x}{w} + \frac{\omega_{1y}(t)}{\omega_0}\frac{w_y}{w}\right]. \tag{15}$$

In the rest frame mentioned, the cosmic-ray flux is very nearly isotropic, with an anisotropy of $\frac{1}{2}\%$ or less at neutron-monitor energies. Therefore $n_0(\underset{\sim}{w}) \tilde{=} n_0(|\underset{\sim}{w}|)$ and n_0 is essentially constant for all viewing directions. Since the neutron monitor is rotating and has a narrow asymptotic viewing cone for each energy of cosmic ray, from the geometry of Fig. IV-2 it can be seen that the neutron monitor sees only particles with velocities given by

$$\begin{aligned} w_x/w &= -\sin\lambda \\ w_y/w &= -\cos\lambda \sin\Phi \\ w_z/w &= \cos\lambda \cos\Phi. \end{aligned} \tag{16}$$

Combining equations (14) - (16), one obtains the time dependence of the flux seen by the neutron monitor,

$$n_1^{s}(\underset{\sim}{w},t) = -\delta_{\parallel} n_0\left[\frac{\omega_{1x}(t)}{\omega_0}\sin\lambda + \frac{\omega_{1y}(t)}{\omega_0}\cos\lambda \sin(2\pi f_e t + \Phi_0)\right]. \tag{17}$$

Consider the observed scintillations in the two important limits, $\lambda \to \pi/2$ (polar detector) and $\lambda \to 0$ (equatorial detector). Note that the latitude corresponds to the asymptotic viewing direction, not to the

geographic latitude of the detector. For $\lambda = \frac{\pi}{2}$, from equation (17) one has

$$n_1^s(t) = -\delta_{\parallel} n_0 \frac{\omega_{1x}(t)}{\omega_0} . \qquad \text{(polar detector)} \tag{18}$$

Application of the Wiener-Khinchin theorem then gives

$$\left.\frac{P^n(f)}{n_0^2}\right]_{\text{seen}} = \frac{P^B_{\varphi\varphi}(f)}{B_0^2} (\delta_{\parallel})^2, \qquad \text{(polar detector)} \tag{19}$$

where in the model considered $P^B_{xx} = P^B_{\varphi\varphi}$ for heliocentric spherical polar coordinates r, θ, φ. This is the same result as given in equation (8), since $\mu = 0$ in this model. The Alert Neutron Monitor has an asymptotic viewing cone with λ near 90^o for the particles (0.5 - 10 GeV) which contribute most to the flux (Shea et al., 1965, Shea, 1972). In Fig. IV-3, I give the result of the theory as in equation (19), using $P^B_{\varphi\varphi}$ given by Quenby and Sear (1971) and $\delta_{\parallel} = 0.9\%$ from equation (13). The result of the theory, and the agreement between theory and observation, are similar to those shown in Fig. IV-1. The agreement of equation (19) with observations appears to be slightly better than the agreement with equation (8), indicating that the scintillations at Alert more closely follow $P^B_{\varphi\varphi}$ than $P^B_{\perp}$, as predicted by the improved treatment of geometry in this Section.

Now consider an equatorial detector, $\lambda = 0$. From equation (17), one has

$$n_1^s(t) = -\delta_{\parallel} n_0 \frac{\omega_{1y}(t)}{\omega_0} \sin(2\pi f_e t + \Phi_0). \qquad \text{(equatorial detector)} \tag{20}$$

The function $n_1^s(t)$ is not strictly a stationary random function because

Figure IV-3: Power spectrum of the flux of the Alert Neutron Neutron Monitor. The histograms give the observed power spectrum, as in Fig. II-8, along with 90% confidence intervals. The curve is the result of the theory (equation 19).

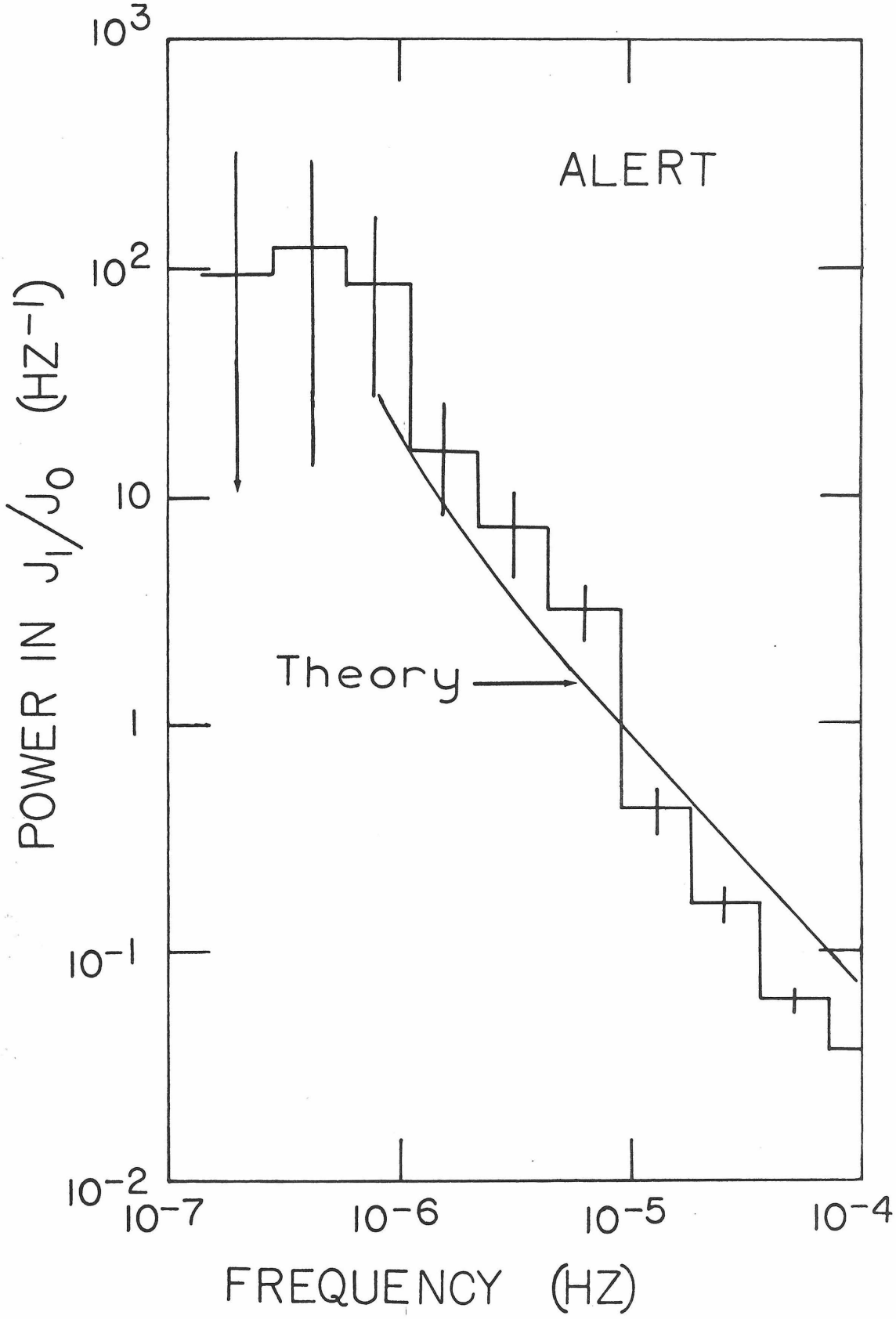
ALERT
Theory
POWER IN J_1/J_0 (HZ^{-1})
FREQUENCY (HZ)
10^3
10^2
10
1
10^{-1}
10^{-2}
10^{-7}
10^{-6}
10^{-5}
10^{-4}

the sine term is deterministic. However, the operations of calculating the correlation function and the power spectrum can be carried out in the usual manner. As discussed in Section II.A, the ergodic hypothesis is used to calculate properties of fluctuations in a random system with only one realization. The correlation function is then given by

$$R^x(\tau) = \langle x(t)\, x(t+\tau)\rangle = \frac{1}{2T}\int_{-T}^{T} x(t'-\tfrac{\tau}{2})\; x(t'+\tfrac{\tau}{2})\; dt', \qquad (21)$$

and the result of the temporal average gives the correlations function if T is large compared with τ and the correlation time τ_c. Using the ergodic hypothesis from equation (21) to calculate the correlation function of $n_1^s(t)$ given by equation (20), after some trigonometric substitutions I obtain

$$R^n(\tau)\Big]_{seen} = \frac{n_0^2(\delta_\parallel)^2}{B_0^2}\left[\cos(2\pi f_e\tau)\underline{\left\{\frac{1}{2T}\int_{-T}^{T} B_{1y}(t'-\tfrac{\tau}{2})\,B_{1y}(t'+\tfrac{\tau}{2})\,dt'\right\}}\right.$$
$$\left. - \frac{1}{2T}\int_{-T}^{T} dt'\,\cos(4\pi f_e t' + 2\Phi_0) B_{1y}(t'-\tfrac{\tau}{2})\,B_{1y}(t'+\tfrac{\tau}{2})\,dt'\right]. \qquad (22)$$

The underlined term is the correlation function of B_{1y} (see equation 21). The last term is negligibly small if $T \gg 1/f_e, \tau_c$ because the terms in B_{1y} are statistically independent of t' and the cosine term oscillates rapidly and integrates to zero. This leaves

$$R^n(\tau)\Big]_{seen} = \cos(2\pi f_e\tau)\,\frac{R^B_{yy}(\tau)}{B_0^2}\,(\delta_\parallel)^2. \quad \text{(equatorial detector)} \qquad (23)$$

Taking the Fourier transform of the correlation function, and using equation (II-4), I obtain the observed power spectrum,

$$\left.\frac{P^n(f)}{n_0^2}\right]_{seen} = \frac{1}{2}\left[\frac{P^B_{yy}(f+f_e)}{B_0^2} + \frac{P^B_{yy}(f-f_e)}{B_0^2}\right] (\delta_{\|})^2. \quad \text{(equatorial detector)} \tag{24}$$

Thus, the effect of the earth's rotation on an "equatorial" neutron monitor is to displace the relevant frequency of the magnetic-field power spectrum from the observing frequency f to $f \pm f_e$. The effect of this displacement is shown in Fig. IV-4, where the dashed curve represents the power spectrum which would be observed by a non-rotating detector and the solid curve gives the power seen by an equatorial neutron monitor. The shape of the magnetic-field spectrum used is similar to that observed for P^B_{rr} in interplanetary space. The earth's rotation effectively cuts off the observed power spectrum for $f < f_e$ and piles those fluctuations into the region near $f = f_e$. Intuitively, this is because the rotation of the asymptotic viewing cones induces a 24-hour periodicity onto scintillations with frequencies smaller than f_e. Higher-frequency scintillations ($f > f_e$) are basically unaffected.

If the magnetic-field fluctuations B_{1x} and B_{1y} are uncorrelated, one can show that the scintillations seen by a neutron monitor with asymptotic latitude λ are given by

$$\left.\frac{P^n(f)}{n_0^2}\right]_{seen} = \sin^2\lambda \left.\frac{P^n(f)}{n_0^2}\right]_{polar} + \cos^2\lambda \left.\frac{P^n(f)}{n_0^2}\right]_{equatorial}, \tag{25}$$

Figure IV-4: Effect of Rotation on an Equatorial Neutron Monitor.

The dashed curve is the power spectrum observed by a (hypothetical) non-rotating neutron monitor, $P^n(f)/n_0^2 = \frac{P_{yy}(f)}{B_0^2}(\delta_{\|})^2$.

The solid-curve is the power spectrum observed by an equatorial neutron monitor, rotating with the earth, under the assumptions of the simplified model in this section (equation 24).

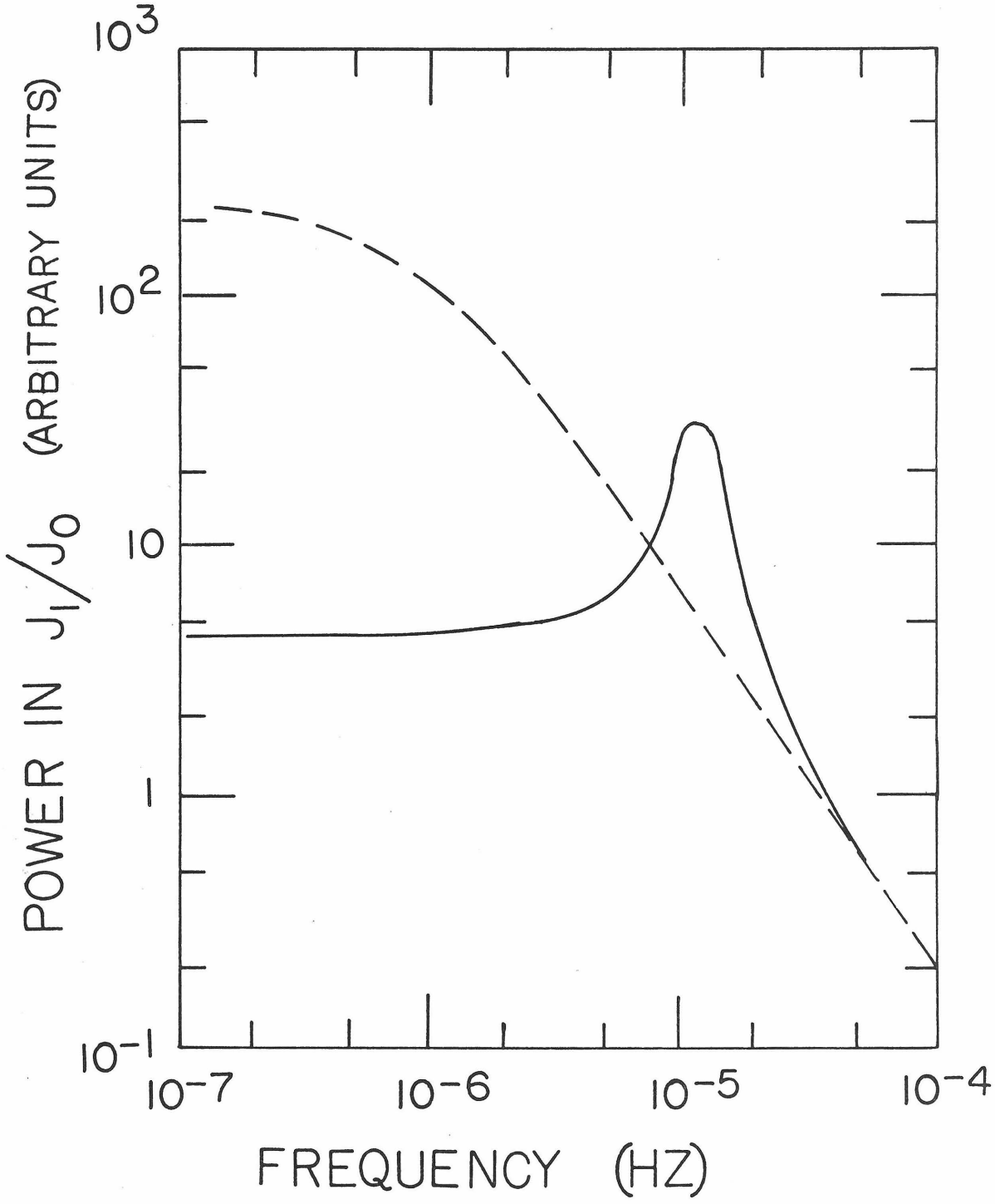
10^3
10^2
10
1
10^{-1}
POWER IN J_1/J_0 (ARBITRARY UNITS)
10^{-7}
10^{-6}
10^{-5}
10^{-4}
FREQUENCY (HZ)

where the "polar" and "equatorial" power spectra are given by equations (19) and (24), respectively.

The Deep River Neutron Monitor has an asymptotic viewing cone which is fairly close to the geomagnetic equator; Shea et. al. (1965) find that protons with energies near 2 GeV have an asymptotic latitude $\lambda \sim -22^{o}$. Since particles near this energy give the dominant contribution to the flux observed at Deep River, from equation (25) one sees that this neutron monitor can be idealized as 14% "polar" and 86% "equatorial".

Letting $P^{B}_{yy} \approx P^{B}_{rr}$, and using the measured magnetic-field power spectra $P^{B}_{rr}(f)$ and $P^{B}_{\varphi\varphi}(f)$ given by Quenby and Sear (1971), I present in Fig. IV-5 the theoretical result from equation (25). Also plotted on Fig. IV-5 is a high-resolution power spectrum of the Deep River Neutron Monitor flux given by Ables (1967). The diurnal anisotropy, which was the item of interest to Ables, appeared on his spectrum as a small and well-resolved spike at precisely one cycle per day. The diurnal and multidiurnal anisotropies are due to spatial gradients in n_0 (rather than temporal fluctuations in n_1) and thus are not relevant to the current discussion of scintillations. The contribution of these anisotropies to the broad-band power spectrum (as in Fig. IV-5) is negligible. The interesting feature in Fig. IV-5 near 10^{-5}Hz appeared merely as a broad and unnoticed enhancement on the log-linear scale of the spectrum presented by Ables (see his Fig. 10). The feature was discovered when Ables' spectrum was replotted on a log-log scale in an attempt to verify whether the predicted enhancement in the neutron-monitor scintillations (as shown in Fig. IV-4 and equation 25) were present in the observed

Figure IV-5: Power spectra of the flux of the Deep River Neutron Monitor. The starred points are the high-resolution spectrum of Ables (1967), with the diurnal anisotropy removed. The vertical (amplitude) normalization of Ables' spectrum is unknown and was adjusted to match my power spectrum (solid histograms with 90% error bars) of Fig. II-9. The solid curve gives the prediction of the model (equation 25) assuming that Deep River's asymptotic latitude is -22^{o}, corresponding to ~2 GeV particles. The appearance of a peak of the proper shape and size near about f ~ 1/day ~ 10^{-5}Hz, plus the general agreement in shape for frequencies 10^{-6}Hz < f < 10^{-4}Hz, are indications of the validity of the model considered.

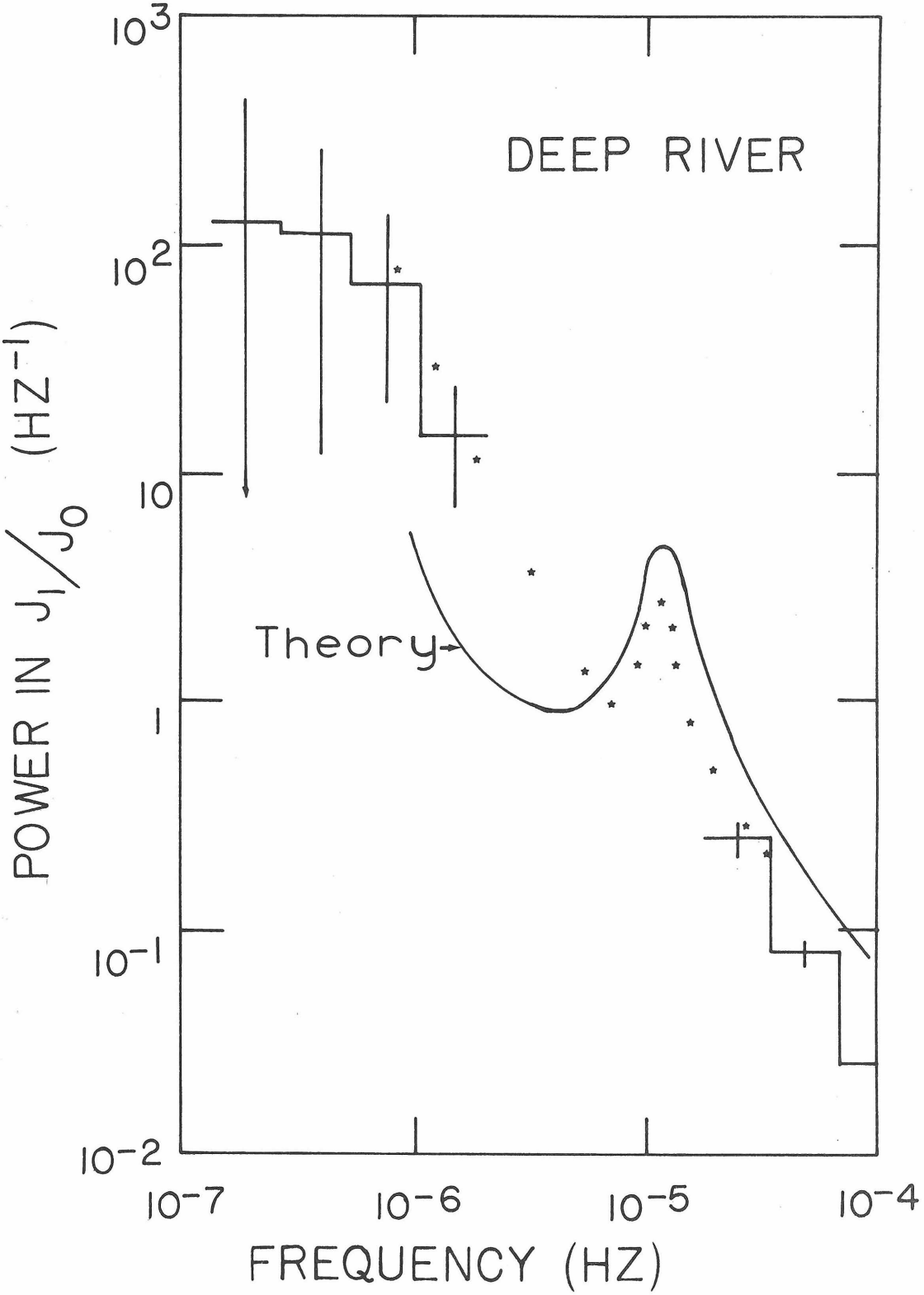
DEEP RIVER
Theory
POWER IN J_1/J_0 (HZ^{-1})
FREQUENCY (HZ)
10^3
10^2
10
1
10^{-1}
10^{-2}
10^{-7}
10^{-6}
10^{-5}
10^{-4}

high-resolution power spectrum.

Although the theory and observations given in Fig. IV-5 are not in precise agreement, the similarity in spectral shape is striking. The effect of the earth's rotation on the observed interplanetary scintillations is obvious in the peak at 10^{-5}Hz. Not only the general shape of the observed power spectrum, but also the amplitude, location, and width of the dominant feature in the spectrum are quantitatively in agreement with the theoretical predictions of the model presented in this Chapter. It is difficult to imagine another model for the scintillation which could duplicate the shape of the peak precisely, as well as explain why it is absent in the spectrum of the Alert Neutron Monitor flux (Fig. IV-3). The detailed agreement of theory with observation as exhibited in Fig. IV-3 and Fig. IV-5 provides strong evidence that the model of interplanetary scintillations presented in this Thesis is the appropriate model to use in discussing cosmic-ray fluctuations at neutron-monitor energies.

Assuming that the model presented here is correct, there is a relation between cosmic-ray scintillations, the cosmic-ray anisotropy, and the power spectrum of the interplanetary magnetic field. Since the model is based on assumptions similar to those used in the derivation of the Fokker-Planck diffusion equation (see Appendix B), the agreement with observations provides a test of the standard theory of cosmic-ray diffusion. Observations of neutron-monitor scintillations may also be valuable in inferring properties of the interplanetary magnetic field from ground-based measurements, and since the level of the magnetic-field power spectrum varies from day to day (Siscoe et al., 1968) it

would be useful to use cosmic-ray scintillations to monitor these variations. A further feature of the model is that the scintillations depend on the magnetic fluctuations actually seen by a particle, so scintillation measurements may be useful in deducing the magnetic power spectrum to be used in calculating diffusion coefficients without encountering the ambiguities inherent in inferring $P_{\perp}^{B}(\underset{\sim}{k})$ from the observed $P_{ij}^{B}(f)$ (see, e.g., Jokipii, 1971, Fisk and Sari, 1973). A definitive check on the validity of the model of interplanetary scintillations presented here requires the use of simultaneous interplanetary data on the magnetic field and the counting rate of a large-area proton detector pointing in a fixed direction in space.

V. INTERPLANETARY SCINTILLATIONS II: GENERAL THEORY

In this Chapter, a more detailed theory of interplanetary scintillations is developed. The analysis of Chapter IV is generalized to include fluctuations with arbitrary wavenumber k and to consider an arbitrary (rather than field-aligned) cosmic-ray anisotropy. These generalizations, while not changing the physical picture nor the final results significantly, necessitate the consideration of a considerably more complex set of equations. It is discovered that the usual quasi-linear theory cannot be used to obtain an equation for the scintillations because it breaks down near the cyclotron resonance ($\underset{\sim}{k}\cdot\underset{\sim}{w} = \omega_0$) due to the strong (non-linear) interaction between cosmic rays and magnetic-field fluctuations. A generalization of the quasi-linear method, involving a non-linear closure approximation based on dimensional analysis, allows the non-linear terms which are essential to the theory near cyclotron resonances to be included in the analysis in a natural way. The resulting equations, which include the non-linear terms in an explicit but approximate way, can be solved exactly to give the cosmic-ray scintillations in terms of particle gradients and magnetic-field fluctuations. A more precise method of including the effects of the non-linear terms is developed from non-linear plasma theory in Appendix C below, but the equations there can only be solved approximately and do not differ significantly from the results obtained in this Chapter.

The general scintillation equations are solved in several important limits: for an omnidirectional detector, for a unidirectional

detector, and for a unidirectional detector in interplanetary space with $k_\perp = 0$. The non-linear interaction determines the width of the resonances which occur, and the power spectra of the cosmic-ray scintillations and the magnetic-field fluctuations are related by a frequency-dependent response function (see Fig. V-1 and V-4). The results of the general theory are applied to particles of neutron-monitor energies ($T \gtrsim 0.5$ GeV), under the assumption that $k_\perp = 0$. The major result (Fig. V-4) is that the low-frequency limit of Chapter IV is approximately valid for neutron monitors even in the resonant regime, for frequencies up to 10^{-4} Hz.

A. The Power Spectrum of Magnetic-Field-Induced Cosmic-Ray Scintillations

As discussed in Chapter I, the motion of fast, charged particles in astrophysical plasmas is dominated by effects of the magnetic field. If production and collisional particle-particle interactions are ignored, Liouville's equation for conservation of particles in phase space is

$$\left[\frac{\partial}{\partial t} + \underset{\sim}{w}\cdot\frac{\partial}{\partial x} + (\underset{\sim}{w}\times\underset{\sim}{\omega})\cdot\frac{\partial}{\partial \underset{\sim}{w}}\right] n(\underset{\sim}{x},\underset{\sim}{w},t) = 0, \tag{1a}$$

where

$$\underset{\sim}{\omega} = \frac{q\underset{\sim}{B}}{\gamma mc}. \tag{1b}$$

Here the particle velocity is $\underset{\sim}{w}$ and the relativistic mass and charge of the particle are γm and q; c is the speed of light, t and $\underset{\sim}{x}$ are time and position, $\underset{\sim}{B}$ is the magnetic field, and $n(\underset{\sim}{x},\underset{\sim}{w},t)$ is the distribution function of cosmic rays in phase space. Equations (1) are relativistically correct. It will be assumed that the magnetic field $\underset{\sim}{B}$ is of the form

$$\underset{\sim}{B} = \underset{\sim}{B}_0+\underset{\sim}{B}_1, \quad \langle\underset{\sim}{B}\rangle = \underset{\sim}{B}_0, \quad \langle\underset{\sim}{B}_1\rangle = 0, \tag{2}$$

where $\langle\underset{\sim}{B}\rangle$ represents the ensemble average as in Chapter II. The average field $\underset{\sim}{B}_0$ is assumed to have scales of variation (in time and space) which are large compared to the scales of variation of $\underset{\sim}{B}_1$, so that to lowest order $\underset{\sim}{B}_0$ can be regarded as constant and $\underset{\sim}{B}_1$ as a stationary, homogeneous random function of time and position. Similarly, defining

$$\underset{\sim}{\omega} = \underset{\sim}{\omega}_0+\underset{\sim}{\omega}_1, \quad \langle\underset{\sim}{\omega}\rangle = \underset{\sim}{\omega}_0, \quad \langle\underset{\sim}{\omega}_1\rangle = 0 \tag{3a}$$

and

$$n = n_0 + n_1, \quad \langle n \rangle = n_0, \quad \langle n_1 \rangle = 0, \tag{3b}$$

where $\underset{\sim}{\omega}_0$ and n_0 denote the average parts of $\underset{\sim}{\omega}$ and n, and inserting equations (3) into (1a), I obtain

$$\left[\frac{\partial}{\partial t} + \underset{\sim}{w}\cdot\frac{\partial}{\partial \underset{\sim}{x}} + \underset{\sim}{w}\times\underset{\sim}{\omega}_0\cdot\frac{\partial}{\partial \underset{\sim}{w}} + \underset{\sim}{w}\times\underset{\sim}{\omega}_1\cdot\frac{\partial}{\partial \underset{\sim}{w}}\right](n_0(\underset{\sim}{x},\underset{\sim}{w},t) + n_1(\underset{\sim}{x},\underset{\sim}{w},t)) = 0\,. \tag{4}$$

The physical interpretation of this model is that fluctuations in $\underset{\sim}{B}$ drive fluctuations in n, so that the cosmic-ray particle distribution function has a fluctuating part, n_1, which depends on $\underset{\sim}{B}_1$ in a manner to be determined.

Taking the ensemble average of (4), and then subtracting the resulting equation from (4), one obtains the two coupled differential equations

$$\left[\frac{\partial}{\partial t} + \underset{\sim}{w}\cdot\frac{\partial}{\partial \underset{\sim}{x}} + (\underset{\sim}{w}\times\underset{\sim}{\omega}_0)\cdot\frac{\partial}{\partial \underset{\sim}{w}}\right]n_0(\underset{\sim}{x},\underset{\sim}{w},t) = -\left\langle(\underset{\sim}{w}\times\underset{\sim}{\omega}_1)\cdot\frac{\partial}{\partial \underset{\sim}{w}}n_1(\underset{\sim}{x},\underset{\sim}{w},t)\right\rangle \tag{5}$$

and

$$\left[\frac{\partial}{\partial t} + \underset{\sim}{w}\cdot\frac{\partial}{\partial \underset{\sim}{x}} + (\underset{\sim}{w}\times\underset{\sim}{\omega}_0)\cdot\frac{\partial}{\partial \underset{\sim}{w}} + \hat{\alpha}\right]n_1(\underset{\sim}{x},\underset{\sim}{w},t) = -(\underset{\sim}{w}\times\underset{\sim}{\omega}_1)\cdot\frac{\partial}{\partial \underset{\sim}{w}}n_0(\underset{\sim}{x},\ \underset{\sim}{w},\ t), \tag{6}$$

where the operator $\hat{\alpha}$ is given by

$$\hat{\alpha}n_1(\underset{\sim}{x},\underset{\sim}{w},t) \equiv (\underset{\sim}{w}\times\underset{\sim}{\omega}_1)\cdot\frac{\partial}{\partial \underset{\sim}{w}}n_1(\underset{\sim}{x},\underset{\sim}{w},t) - \left\langle(\underset{\sim}{w}\times\underset{\sim}{\omega}_1)\cdot\frac{\partial}{\partial \underset{\sim}{w}}n_1(\underset{\sim}{x},\underset{\sim}{w},t)\right\rangle. \tag{7}$$

Equations (5)- (7) are exact.

It is often of interest to investigate the behavior of particles in a weakly stochastic magnetic field, so that

$$\langle \underset{\sim}{B}_1\cdot\underset{\sim}{B}_1\rangle \ll \underset{\sim}{B}_0\cdot\underset{\sim}{B}_0. \tag{8}$$

Although this approximation may be crude for many cases of interest, it appears to be necessary in order to obtain a mathematically tractable system of equations. Since the fluctuations n_1 in the particle

distribution are driven by the magnetic irregularities, it is assumed that

$$\langle n_1^2 \rangle \ll n_0^2, \tag{9}$$

and this assumption must be checked *a posteriori*. Since the relative cosmic-ray scintillations will turn out to be much smaller than the relative magnetic-field fluctuations, (9) is true if (8) is. Under the conditions of equations (8) and (9), several investigators (Hall and Sturruck, 1967, Hall, 1967, Hasselmann and Wibberenz, 1968, Jokipii, 1971) have noted that equations (5) and (6) can be closed by ignoring the term $\hat{\alpha}$ on the left-hand side of equation (6), which is reasonable for weak turbulence because $\hat{\alpha}$ is of higher order in the small parameters $\underset{\sim}{\omega}_1$ and n_1 than the remaining terms. Equation (6) can then be solved by integration along an unperturbed trajectory, and after elimination of an initial-value term the insertion of the solution for $n_1(\underset{\sim}{x},\underset{\sim}{w},t)$ into equation (5) produces a *diffusion* equation for n_0. The diffusion equation has the form

$$\left[\frac{\partial}{\partial t} + \underset{\sim}{w}\cdot\frac{\partial}{\partial \underset{\sim}{x}} + (\underset{\sim}{w}\times\underset{\sim}{\omega}_0)\cdot\frac{\partial}{\partial \underset{\sim}{w}}\right] n_0(\underset{\sim}{x},\underset{\sim}{w},t) = \frac{\partial}{\partial s_i} D_{ij} \frac{\partial}{\partial s_j} n_0(\underset{\sim}{x},\underset{\sim}{w},t), \tag{10}$$

where $s_i = (x_i, w_i)$ and D_{ij} are the diffusion coefficients, which depend on the structure of the magnetic-field irregularities. The derivation of the diffusion coefficients is given in Appendix B, using a new technique which will be discussed in this Section. The diffusion equation has been applied with success to the propagation of cosmic rays in the solar system (for a recent review, see Jokipii, 1971).

It has not been previously noted that, given the average

distribution function n_0, equation (6) can be used to find the form of the fluctuation n_1 and thus the power spectrum of the cosmic-ray fluctuations. I will show how this can be done.

Consider equations (10) and (6), written in the symbolic notation

$$(\frac{dn_0}{dt})_u = - \hat{S}n_0 \tag{11}$$

$$(\frac{dn_1}{dt})_u = - \hat{\alpha}n_1 + \hat{D}n_0. \tag{12}$$

Here $(\frac{d}{dt})_u$ signifies the time derivative evaluated along an unperturbed trajectory (a helix). The terms $\hat{S}$ and $\hat{\alpha}$ represent stochastic scattering operators, and the term $\hat{D}n_0$ is an external "driving" term in equation (12). The non-linear term (involving $\hat{\alpha}$) in equation (12) represents an effective scattering and since the isotropic state is the equilibrium configuration for both n_0 and n_1, it is clear that the effect of the $\hat{\alpha}\ n_1$ term is to provide a "damping" mechanism whereby fluctuations decay with time along the unperturbed trajectory. A method for considering this higher-order term analytically will be discussed in Appendix C, but for the present an approximate method of treating the term will be used. Notice first that

$$<\hat{\alpha}n_1> = 0. \tag{13}$$

This implies that $\hat{\alpha}$ is either non-stochastic or else statistically independent of the fluctuations in n_1. In either case, a reasonable first approximation is to take $\hat{\alpha}$ to be a (non-stochastic) constant, α_0. Since, to lowest order, $n_1 \sim \frac{\omega_1}{\omega_0}n_0$, equation (13) implies that α is of <u>second order</u> in ω_1. From a comparison of equation (11) with equation (12), and from dimensional analysis, it can be seen that $\alpha_0 \sim \frac{|\omega_1|^2}{\omega_0} \sim 1/\tau_s$,

where $|\omega_1|$ is the typical size of a componant of $\underset{\sim}{\omega}_1$ and τ_s is the typical scattering time for particles in the random magnetic field. Therefore, in order to evaluate the equations in closed form, I will make the "non-linear closure approximation",

$$\hat{\alpha} n_1 = \alpha_0 n_1 \tag{14}$$

where α_0 is a positive constant with value given approximately by

$$\alpha_0 \sim \frac{|\omega_1|^2}{\omega_0} \sim 1/\tau_s . \tag{15}$$

The quasi-linear approximation, which ignores the higher-order terms entirely, can then easily be recovered by letting $\alpha_0 \to 0$.

Note that the quasi-linear theory gives an approximate solution of equations (5) and (6), which is correct through order ω_1^2. The current method, in contrast, gives an exact solution of an approximate set of equations, (5) and (6) with $\hat{\alpha} \to \alpha_0$, a constant. The exact non-linear terms are subsumed into the a quasi-phenomenological constant α_0, whose approximate size is given by dimensional analysis. To the extent that the non-linear terms are adequately represented by α_0, the current approach is valid for arbitrary (not just negligibly small) ω_1/ω_0. An analytic method for obtaining the operator $\hat{\alpha}$ correct to terms of order ω_1^2 will be discussed in Appendix C, but the operator nature of $\hat{\alpha}$, even to lowest non-vanishing order, is sufficiently complex that an analytic solution to the equations is impossible. For this reason, the non-linear closure approximation of equation (14) will be used in the present analysis. It will be seen that the term $\hat{\alpha}$ contributes only near cyclotron resonances, for $|\hat{\alpha}|/\underset{\sim}{\omega}_0 \lesssim 1$. Thus, if a more accurate

estimate of $\hat{\alpha}$ as a function of velocity and wavenumber is obtained (as in Appendix C), the results of this Chapter will remain valid if $\hat{\alpha}$ is evaluated at the appropriate cyclotron resonance.

Choose coordinates so that $\underset{\sim}{B}_0 = B_0 \hat{e}_z$, where $\hat{e}_z$ is a unit vector along the z-axis. Then using spherical polar coordinates in velocity space, with the definitions

$$w_x = w \cos\phi \sqrt{1 - \mu^2} \tag{16a}$$

$$w_y = w \sin\phi \sqrt{1 - \mu^2} \tag{16b}$$

$$w_z = w\mu, \tag{16c}$$

I find that

$$(\underset{\sim}{w} x \underset{\sim}{\omega}_0) \cdot \frac{\partial n_1}{\partial \underset{\sim}{w}}(\underset{\sim}{x}, \underset{\sim}{w}, t) = -\omega_0 \frac{\partial n_1}{\partial \phi} . \tag{17}$$

If the scattering of cosmic rays due to magnetic irregularities occurs on a time scale much larger than the cyclotron time, then the motion of the particles will be dominated by the spiral unperturbed (helical) trajectories of particles in a constant magnetic field. Under these circumstances, it is often useful to assume that the distribution function n_0 depends not on the instantaneous position of the particle but rather on the position of the guiding center,

$$x_0 = x - w_y/\omega_0 \tag{18a}$$

$$y_0 = y + w_x/\omega_0 \tag{18b}$$

$$z_0 = z. \tag{18c}$$

This "guiding-center approximation" is made explicitly in the derivation of the diffusion equation (10) discussed above (Hall, 1967,

Hasselmann and Wibberenz, 1968, and Appendix B), and it is implicit in the derivation of the Fokker-Planck coefficients leading to the diffusion equation (Jokipii, 1966). Further, since the cyclotron motion dominates, one assumes that n_0 is independent of the velocity phase, ϕ. Therefore, I take

$$n_0(\underset{\sim}{x},\underset{\sim}{w},t) = n_0(\underset{\sim}{x}_0,w,\mu,t). \tag{19}$$

Upon transforming from coordinates x,y,z,w_x,w_y,w_z to x_0,y_0,z_0,w,μ,ϕ, I obtain

$$(\underset{\sim}{w}\times\underset{\sim}{\omega}_1)\cdot\frac{\partial}{\partial\underset{\sim}{w}}n_0(\underset{\sim}{x}_0,\underset{\sim}{w},t) = \omega_{1x}\left[-\frac{w\mu}{\omega_0}\frac{\partial}{\partial x_0}-\sqrt{1-\mu^2}\sin\phi\frac{\partial}{\partial\mu}\right]n_0 \tag{20}$$

$$+\omega_{1y}\left[-\frac{w\mu}{\omega_0}\frac{\partial}{\partial y_0}+\sqrt{1-\mu^2}\cos\phi\frac{\partial}{\partial\mu}\right]n_0+\omega_{1z}\left[\frac{w\sqrt{1-\mu^2}}{\omega_0}\left\{\sin\phi\frac{\partial}{\partial y_0}+\cos\phi\frac{\partial}{\partial x_0}\right\}\right]n_0.$$

Inserting the results of equations (14), (17), and (20) into (6), and taking the Fourier transform of both sides of the equation, treating $n_0(\underset{\sim}{x}_0,w,\mu,t)$ as a constant because its scales of variation are large compared with those of $\underset{\sim}{\omega}_1$ and n_1, I obtain

$$\left[i(\omega-k_{\parallel}w\mu)-ik_{\perp}w\sqrt{1-\mu^2}\cos(\phi-\beta)+\alpha_0-\omega_0\frac{\partial}{\partial\phi}\right]\tilde{n}_1(\underset{\sim}{k},\underset{\sim}{w},\omega) =$$

$$\left\{\omega_{1x}(\underset{\sim}{k},\omega)\left[\frac{w\mu}{\omega_0}\frac{\partial}{\partial x_0}+\sqrt{1-\mu^2}\sin\phi\frac{\partial}{\partial\mu}\right]\right. \tag{21}$$

$$+\omega_{1y}(\underset{\sim}{k},\omega)\left[\frac{w\mu}{\omega_0}\frac{\partial}{\partial y_0}-\sqrt{1-\mu^2}\cos\phi\frac{\partial}{\partial\mu}\right]+\omega_{1z}\left[\frac{w\sqrt{1-\mu^2}}{\omega_0}\left\{-\sin\phi\frac{\partial}{\partial y_0}\right.\right.$$

$$\left.\left.\left.-\cos\phi\frac{\partial}{\partial x_0}\right\}\right]\right\}n_0(\underset{\sim}{x}_0,w,\mu,t).$$

The wavenumber $\underset{\sim}{k}$ is expressed in cylindrical coordinates ($k_{\parallel}$, $k_{\perp}$, β) about the z-axis, and ω is the frequency. In this equation, all functional dependences are explicitly shown. It can be seen that this equation is a simple first-order linear differential equation in the

azimuthal angle ϕ, with the other variables entering simply as parameters. The solution is given by

$$n_1(\underset{\sim}{k},\underset{\sim}{w},\omega) = e^{-i[u\phi+a\ \sin(\phi-\beta)]}\int_{\phi_0}^{\phi} d\phi' e^{i[u\phi'+a\ \sin(\phi'-\beta)]}\ \frac{RHS(\phi')}{\omega_0} \tag{22}$$

where

$$u = \frac{\omega - k_{||} w\mu - i\alpha_0}{\omega_0} \tag{23}$$

$$a = \frac{k_\perp w\sqrt{1-\mu^2}}{\omega_0}, \tag{24}$$

and RHS denotes the right-hand side of equation (21).

Integrals of the form

$$I\begin{Bmatrix}1\\2\\3\end{Bmatrix} = \int d\phi'\ e^{i[u\phi'+a\ \sin(\phi'-\beta)]}\begin{Bmatrix}1\\ \sin\phi'\\ \cos\phi'\end{Bmatrix} \tag{25}$$

are required on the right side of equation (22). Using the expansion of the exponential function in the form

$$e^{ib\sin\Psi} = \sum_{m=-\infty}^{\infty} J_m(b)e^{im\Psi}, \tag{26}$$

where $J_m(b)$ is the Bessel function of order m and argument b, I obtain the result

$$I\begin{Bmatrix}1\\2\\3\end{Bmatrix} = \frac{1}{i}\sum_{m=-\infty}^{\infty} J_m(a)e^{-im\beta}e^{i(u+m)\phi}\begin{Bmatrix} 1 \\ \frac{1}{2i}\left[\frac{e^{i\phi}}{u+m+1} - \frac{e^{-i\phi}}{u+m-1}\right] \\ \frac{1}{2}\left[\frac{e^{i\phi}}{u+m+1} + \frac{e^{-i\phi}}{u+m-1}\right]\end{Bmatrix}. \tag{27}$$

Equation (22) then becomes

$$\begin{aligned}\tilde{n}_1(\underset{\sim}{k},\underset{\sim}{w},\omega) = {} & \frac{\tilde{\omega}_{1x}(\underset{\sim}{k},\omega)}{\omega_0}\left[I_1\frac{w\mu}{\omega_0}\frac{\partial}{\partial x_0} + I_2\sqrt{1-\mu^2}\frac{\partial}{\partial\mu}\right]n_0 \\ & + \frac{\tilde{\omega}_{1y}(\underset{\sim}{k},\omega)}{\omega_0}\left[I_1\frac{w\mu}{\omega_0}\frac{\partial}{\partial y_0} - I_3\sqrt{1-\mu^2}\frac{\partial}{\partial\mu}\right]n_0\end{aligned} \tag{28}$$

(Continued on next page)

$$+ \frac{\omega_{1z}(\underset{\sim}{k},\omega)}{\omega_0}\left[I_3 \frac{w\sqrt{1-\mu^2}}{\omega_0}\frac{\partial}{\partial x_0} - I_2 \frac{w\sqrt{1-\mu^2}}{\omega_0}\frac{\partial}{\partial y_0}\right] n_0, \qquad \text{(28 cont'd)}$$

where the symbols I_i are given by

$$I_i = e^{-ia\sin(\phi-\beta)} \frac{1}{i} \sum_{m=-\infty}^{\infty} J_m(a) e^{im(\phi-\beta)} \left\{ Q_i(\phi) - \exp\left[-\frac{\alpha_0}{\omega_0}(\phi-\phi_0)\right] Q_i(\phi_0) \right\} \qquad (29a)$$

with

$$Q_1 = \frac{1}{u+m} \qquad (29b)$$

$$Q_2 = \frac{1}{2i}\left[\frac{e^{i\phi}}{u+m+1} - \frac{e^{-i\phi}}{u+m-1}\right] \qquad (29c)$$

$$Q_3 = \frac{1}{2}\left[\frac{e^{i\phi}}{u+m+1} + \frac{e^{-i\phi}}{u+m-1}\right]. \qquad (29d)$$

Equation (28) gives the scintillations $\tilde{n}_1(\underset{\sim}{k},\underset{\sim}{w},\omega)$ in terms of the gradients of the average distribution function $n_0(\underset{\sim}{x},\underset{\sim}{w},t)$ and the magnetic-field fluctuations $\underset{\sim}{\omega}_1(\underset{\sim}{k},\omega)$. The terms involving ϕ_0 are the initial-value terms, which I will now demonstrate to be negligibly small. In all three of the functions I_i of equations (29), the initial-value terms have oscillating factors in ϕ_0 and an over-all multiplicative factor of $\exp\left[-\frac{\alpha_0}{\omega_0}(\phi-\phi_0)\right]$. At the boundaries of the turbulent region the fluctuations vanish, so $\tilde{n}_1(\underset{\sim}{k},\underset{\sim}{w},\omega) = 0$ for all $\underset{\sim}{k}$ and ω. Therefore the boundary corresponds to $\phi = \phi_0$, since from equations (29) $\tilde{n}_1(\underset{\sim}{k},\underset{\sim}{w},\omega) = 0$ for $\phi = \phi_0$. Since the cyclotron motion dominates the motion of the charged particles, the unperturbed trajectories are given by $\phi - \phi_0 = \omega_0 t$ and the exponential $\exp\left[-\frac{\alpha_0}{\omega_0}(\phi-\phi_0)\right]$ is much less than 1 if $\alpha_0 t \sim \frac{\tau}{\tau_s} \gg 1$. Therefore, the initial-value terms are negligible for particles which

have traveled through several scattering lengths. If one restricts the discussion to positions more than several scattering lengths inside the turbulent region, as will be done throughout the discussion of interplanetary scintillations in this work, the terms in ϕ_0 ignorable and equations (29) become

$$I_1 = \left[\right] \left\{ \frac{1}{u+m} \right\} \tag{30a}$$

$$I_2 = \left[e^{-ia\,\sin(\phi-\beta)} \frac{1}{i} \sum_{m=-\infty}^{\infty} J_m(a) e^{im(\phi-\beta)} \right] \left\{ \frac{1}{2i}\left[\frac{e^{i\phi}}{u+m+1} - \frac{e^{-i\phi}}{u+m-1} \right] \right\} \tag{30b}$$

$$I_3 = \left[\right] \left\{ \frac{1}{2}\left[\frac{e^{i\phi}}{u+m+1} + \frac{e^{-i\phi}}{u+m-1} \right] \right\}. \tag{30c}$$

This discussion indicates quantitatively the contribution of the initial-value terms and demonstrates the crucial role played by the non-linear terms (involving $\hat{Q}$) of equation (6) in damping out the initial conditions. This approach is an improvement over those used by previous authors (Hall, 1967, Hasselmann and Wibberenz, 1968), who neglected the non-linear terms and merely <u>postulated</u> that the initial conditions make no contribution. Jokipii (1972) has shown from independent arguments that the initial-value terms do not contribute to the diffusion equation.

Equations (28) and (30) specify the cosmic-ray scintillations, $\tilde{n}_1(\underset{\sim}{k},\underset{\sim}{w},\omega)$, in terms of the magnetic-field fluctuations $\omega_{1i}(\underset{\sim}{k},\omega)$ and the average cosmic-ray distribution function. The four-dimensional Wiener-Khinchin theorem (a generalization of equation II-10) can be written

$$P^n(\underset{\sim}{k},\underset{\sim}{w},\omega)\delta^3(\underset{\sim}{k}-\underset{\sim}{k}')\delta(\omega-\omega') = \left(\frac{1}{2\pi}\right)^4 \langle n_1(\underset{\sim}{k},\underset{\sim}{w},\omega) n_1(\underset{\sim}{k}',\underset{\sim}{w},\omega')^* \rangle. \tag{31}$$

Thus, one obtains the power spectrum of the cosmic-ray scintillations by multiplying equation (28) by its own complex conjugate and taking

the ensemble average. The general result is of the form

$$P^{n}(\underset{\sim}{k},\underset{\sim}{w},\omega) = \frac{P_{ij}^{B}(\underset{\sim}{k},\omega)}{B_0^2} C_{ijk\ell}(\underset{\sim}{k},\underset{\sim}{w},\omega)\left\{\frac{\partial}{\partial s_k} n_0(\underset{\sim}{x},w,\mu)\right\}\left\{\frac{\partial}{\partial s_\ell} n_0(\underset{\sim}{x},w,\mu)\right\} \qquad (32)$$

where P^{n} is the power spectrum of the cosmic-ray scintillations, P_{ij}^{B} is the cross-spectrum of B_i and B_j, $C_{ijk\ell}$ is a tensor depending on factors like $I_1\ I_1^*$, and $\underset{\sim}{S} \equiv (x_0, y_0, \mu)$.

The form of equation (32) is sufficiently complex that restrictions must be made in order to obtain results which are amenable to physical interpretation. These special cases will be considered in the next three sections.

B. Scintillations Seen By a Unidirectional (Narrow-Angle) Detector

Suppose that a detector is sensitive only to a small solid angle. Then the derivation of the previous Section is applicable, and the scintillations are as given by equation (32). However, since particles orbit rapidly about the average magnetic field, consider only the average of the power spectrum over the two azimuthal phase angles, ϕ (in velocity) and β (in wavenumber). That is, consider

$$P^n(k_{||},\ k_\perp, w, \mu, \omega) = \int_0^{2\pi} \frac{d\phi}{2\pi} \int_0^{2\pi} \frac{d\beta}{2\pi}\, P^n(\underset{\sim}{k}, \underset{\sim}{w}, \omega), \text{ or} \tag{33a}$$

$$P^n(k_{||},\ k_\perp, w, \mu, \omega) = \left[\int_0^{2\pi} \frac{d\phi}{2\pi} \int_0^{2\pi} \frac{d\beta}{2\pi} \frac{P_{ij}^B(\underset{\sim}{k}, \omega)}{B_0^2}\, C_{ijk\ell}(\underset{\sim}{k}, \underset{\sim}{w}, \omega)\right]$$

$$\left\{\frac{\partial}{\partial S_k} n_0(\underset{\sim}{x}_0, w, \mu)\right\}\left\{\frac{\partial}{\partial S_\ell} n_0(\underset{\sim}{x}_0, w, \mu)\right\} \quad . \tag{33b}$$

where the last equation follows from (32) since $\frac{\partial n_0}{\partial S_k}$ is independent of of phase.

Averaging over ϕ and β gives increased simplicity at the cost of some information. It is realized that information about the azimuthal angles may be desired in some cases, but the full functional dependence is so complex that a physical interpretation and a quantitative discussion of the results are difficult. For simplicity, therefore, I will consider the average of the scintillations seen over all directions. Since the angular factors are all of order unity, the averaging over angles allows the results to be presented in a mathematically simpler form without much loss of generality.

In order to perform the integrals, one must know the

properties of the magnetic-field fluctuation. For simplicity, I assume that the fluctuations are cylindrically symmetric about the average field direction (see Appendix A, equation A-14), so the power spectrum is given by

$$[P_{ij}^{B}] = \begin{bmatrix} k_z^2 & 0 & -k_x k_z \\ 0 & k_z^2 & -k_y k_z \\ -k_x k_z & -k_y k_z & k_x^2 k_y^2 \end{bmatrix} A'(k_z^2 \equiv k_{\parallel}^2,\ k_x^2 + k_y^2 \equiv k_{\perp}^2, \omega). \quad (34)$$

Then the integrals over ϕ in equation (33b) are of the form

$$\int_0^{2\pi} \frac{d\phi}{2\pi} e^{i(n-n')\phi} = \delta_{n,n'} \quad (35)$$

and similarly for the integrals over β. The Kronecker delta symbols can be used to evaluate one of the two sums in each of the terms like, for example,

$$I_1 I_1^* = \sum_{m=-\infty}^{\infty} \sum_{m'=-\infty}^{\infty} J_m(a) J_{m'}(a) e^{-i(m-m')\beta} e^{i(m-m')\phi} \frac{1}{(u+m)\ (u+m')^*} .$$

The result of the straightforward but tedious calculation of the phase-averaged scintillations from a unidirectional detector is

$$P^n(k_{\parallel}, k_{\perp}, \mu, \omega) = \frac{P_{\perp}^B}{B_0^2} \frac{w^2 \mu^2}{\omega_0^2} C_1\left[\left(\frac{\partial n_0}{\partial x_0}\right)^2\right] + \frac{P_{\perp}^B}{B_0^2}(1-\mu^2) C_2\left[\left(\frac{\partial n_0}{\partial \mu}\right)^2\right] + \frac{P_{\parallel}^B}{B_0^2} \frac{w^2(1-\mu^2)}{\omega_0^2} \frac{C_2}{2}\left[\left(\frac{\partial n_0}{\partial x_0}\right)^2 + \left(\frac{\partial n_0}{\partial y_0}\right)^2\right] \quad (36a)$$

where

$$C_1 = \sum_{m=-\infty}^{\infty} J_m^2(a)\left[\frac{\omega_0^2}{(\omega - k_{\parallel} w\mu + m\omega_0)^2 + \alpha_0^2}\right], \quad (36b)$$

$$C_2 = \sum_{m=-\infty}^{\infty} J_m^2(a) \frac{1}{2}\left[\frac{\omega_0^2}{(\omega - k_{\parallel} w\mu + (m+1)\omega_0)^2 + \alpha_0^2} + \frac{\omega_0^2}{(\omega - k_{\parallel} w\mu + (m-1)\omega_0)^2 + \alpha_0^2}\right]. \quad (36c)$$

Here I have introduced the functions

$$P_{\perp}^{B} \equiv P_{xx}^{B} = P_{yy}^{B} \text{ and } P_{\parallel}^{B} \equiv P_{zz}^{B}.$$

$P_{\parallel}^{B}$ and $P_{\perp}^{B}$ are functions of $k_{\parallel}$, $k_{\perp}$, and ω.

Equations (36) give the power spectrum of cosmic-ray scintillations seen by a narrow-angle detector, in terms of the magnetic-field power spectrum and gradients of the average distribution function. If n_0 depends only on μ and $|\underset{\sim}{k}||\underset{\sim}{w}| \ll \omega_0$, equation (36a) reduces to the previously-derived low-frequency limit of Chapter IV (see equation IV-8). For arbitrary $\underset{\sim}{k}$, equations (36) indicate that the cosmic-ray scintillations depend on the two wavenumber and frequency-dependent "filters" $C_1(\underset{\sim}{k},\omega)$ and $C_2(\underset{\sim}{k},\omega)$. The filters have resonances whenever $\omega - k_{\parallel} w\mu = n\omega_0$, where n is an integer, or at integral harmonics of the cosmic-ray cyclotron frequency. The filters have a Breit-Wigner shape, with the width of the resonances given by α_0 in the non-linear closure approximation.

C. Scintillations Seen by an Omnidirectional Detector

The cosmic-ray fluctuations as a function of $\underset{\sim}{k}, \underset{\sim}{w}$, and ω are given by equations (28) and (30), for a detector pointing in a fixed direction in space. An omnidirectional detector measures the flux $\bar{\tilde{n}}_1(\underset{\sim}{k},w)$ averaged over all directions in velocity space, or over μ and ϕ. Therefore, I define

$$\bar{\tilde{n}}_1(\underset{\sim}{k},w,\omega) = \frac{1}{2}\int_{-1}^{1} d\mu \int_0^{2\pi} \frac{d\phi}{2\pi}\, \tilde{n}_1(\underset{\sim}{k},\underset{\sim}{w},\omega). \tag{37}$$

Expanding the initial exponential

$$e^{-i\, a\, \sin(\phi-\beta)} = \sum_{m=-\infty}^{\infty} J_m(a) e^{-im(\phi-\beta)} \tag{38}$$

in I_1, I_2, and I_3, and performing the integral over ϕ and μ, I obtain an expression for $\bar{\tilde{n}}_1(\underset{\sim}{k},w,\omega)$. The power spectrum of the scintillations is obtained as in equation (31), and after averaging over the phase angle β in wavenumber space, assuming cylindrical symmetry of the magnetic-field fluctuations (equation 34) I get

$$\begin{aligned}
\bar{\bar{P}}^n(k_\parallel, k_\perp, w, \omega) = {} & \frac{P_\perp^B}{B_0^2}\frac{w^2}{\omega_0^2}\left\{\left|\hat{A}_0\ \mu\ \frac{\partial n_0}{\partial x_0}\right|^2 + \left|\hat{A}_0\ \mu\ \frac{\partial n_0}{\partial y_0}\right|^2\right\} \\
& + \frac{P_\perp^B}{B_0^2}\ \frac{1}{2}\left\{\left|\hat{A}_-\sqrt{1-\mu^2}\,\frac{\partial n_0}{\partial \mu}\right|^2 + \left|\hat{A}_+\sqrt{1-\mu^2}\,\frac{\partial n_0}{\partial \mu}\right|^2\right\} \\
& + \frac{P_\parallel^B}{B_0^2}\frac{w^2}{4\omega_0^2}\left\{\left|\hat{A}_+\sqrt{1-\mu^2}\,\frac{\partial n_0}{\partial x_0}\right|^2 + \left|\hat{A}_-\sqrt{1-\mu^2}\,\frac{\partial n_0}{\partial x_0}\right|^2\right. \\
& \left. + \left|\hat{A}_+\sqrt{1-\mu^2}\,\frac{\partial n_0}{\partial y_0}\right|^2 + \left|\hat{A}_-\sqrt{1-\mu^2}\,\frac{\partial n_0}{\partial y_0}\right|^2\right\} .
\end{aligned} \tag{39a}$$

The quantities $\hat{A}_0$, $\hat{A}_+$, and $\hat{A}_-$ are integral operators given by

$$\hat{A}\begin{Bmatrix}+\\0\\-\end{Bmatrix} = \int_{-1}^{1} \frac{d\mu}{2} \sum_{m=-\infty}^{\infty} \frac{J_m(a)J_{m+1}(a)\begin{Bmatrix}+0\\-1\end{Bmatrix}}{u+m} \quad . \tag{39b}$$

where a and u are as in equations (23) and (24).

An important point to notice is that, depending on the form of the magnetic-field power spectrum and the average distribution function, the power observed by unidirectional and omnidirectional detectors may differ substantially. Suppose, for example, that n_0 depends only on pitch-angle μ and that the magnetic fluctuations have $\omega \approx 0$ and $k_\perp \approx 0$. (This is the $k_\perp \to 0$ limit, which will be considered at length in the next Section.) Then $J_m(a) \tilde{=} 0$ except for $J_0(a) \approx 1$, leaving from equations (36) and (39)

$$P^n(k_\parallel,w,\mu) \approx (1-\mu^2)\frac{P_\perp^B(k_\parallel)}{B_0^2}\left(\frac{\partial n_0}{\partial \mu}\right)^2 \frac{\omega_0^2}{(\omega_0 - k_\parallel w\mu)^2+\alpha_0^2} \quad \text{for} \quad \begin{matrix} P_{ij}^B(k_\parallel,k_\perp,\beta,\omega)=P_{ij}^B(k_\parallel) \\ n_0(\underset{\sim}{x}_0,w,\mu)=n_0(w,\mu) \end{matrix} \tag{40a}$$

whereas

$$\overline{\overline{P}}^n(k_\parallel,w) \approx 0. \tag{40b}$$

Therefore, in the $k_\perp \to 0$ limit, scintillations seen by an omnidirectional detector are much smaller than those seen by a narrow-angle detector, as indicated by the observations discussed in Chapter II.

D. The $k_\perp \to 0$ and Diffusion Limits

For purposes of discussion here, I define the $k_\perp \to 0$ limit by the relations

$$\omega \ll \omega_0, \tag{41a}$$

$$k_\perp w \sqrt{1 - \mu^2} \ll \omega_0 \tag{41b}$$

and

$$k_\perp / k_\parallel \ll 1. \tag{41c}$$

The first condition, that the frequency of the fluctuations be smaller than the particle cyclotron frequency, is well satisfied by the electromagnetic waves which interact with cosmic rays in interplanetary and interstellar space. Since this is true, the frequency dependence of the power spectra is ignorable and the waves are quasistatic structures in the plasma rest frame. The second and third conditions, which essentially require $k_\perp \to 0$, involve the assumption that the fluctuations of interest propagate only along the average magnetic-field direction. This assumption is consistent with observations in the solar wind (Belcher, et al., 1969, Belcher and Davis, 1971), which indicate that about half of the magnetic irregularities are transverse Alfvén waves propagating <u>away</u> from the sun <u>along</u> $\underset{\sim}{B}_0$. However, the observations are <u>not</u> precise enough to determine unambiguously that $k_\perp / k_\parallel \ll 1$. This approximation may be viewed as an assumption which introduces tremendous mathematical simplicity and which is not in conflict with observations in the solar system.

In the $k_\perp \to 0$ limit, the power spectrum for a narrow-angle cosmic-ray detector, from equations (36), is

$$P^n(k_\parallel,w,\mu)=\frac{P_\perp^B(k_\parallel)}{B_0^2}\frac{w^2\mu^2}{\omega_0^2}R_1(k_\parallel)\left[\left(\frac{\partial n_0}{\partial x_0}\right)^2+\left(\frac{\partial n_0}{\partial y_0}\right)^2\right]+\frac{P_\perp^B(k_\parallel)}{B_0^2}(1-\mu^2)R_2(k_\parallel)\left(\frac{\partial n_0}{\partial \mu}\right)^2 \qquad (42a)$$

where the dimensionless resonance functions R_1 and R_2 are given by

$$R_1(k_\parallel) = \frac{\omega_0^2}{(k_\parallel w\mu)^2+\alpha_0^2} \qquad (42b)$$

and

$$R_2(k_\parallel) = \frac{1}{2}\left[\frac{\omega_0^2}{(k_\parallel w\mu+\omega_0)^2+\alpha_0^2}+\frac{\omega_0^2}{(k_\parallel w\mu-\omega_0)^2+\alpha_0^2}\right]. \qquad (42c)$$

The corresponding diffusion equation for the average distribution function is (Jokipii, 1966, 1971; also, Appendix B, equation B-8)

$$\frac{\partial n_0}{\partial t}+w\mu\frac{\partial n_0}{\partial z}=\frac{1}{2}\frac{\partial}{\partial \mu}\left\langle\frac{\Delta\mu^2}{\Delta t}\right\rangle\frac{\partial n_0}{\partial \mu}+\frac{1}{2}\frac{\partial}{\partial x_0}\left\langle\frac{\Delta x^2}{\Delta t}\right\rangle\frac{\partial n_0}{\partial x_0}+\frac{1}{2}\frac{\partial}{\partial y_0}\left\langle\frac{\Delta y^2}{\Delta t}\right\rangle\frac{\partial n_0}{\partial y_0}. \qquad (43)$$

It is observed that cosmic rays have a small anisotropy. For this reason, it is appropriate to consider the <u>diffusion limit</u>, in which scattering in pitch-angle is rapid compared to scattering perpendicular to the magnetic field lines, and the distribution function is nearly isotropic. One then expands the distribution function $n_0(\underset{\sim}{x}_0,w,\mu)$ in spherical harmonics, following Jokipii (1968), to get

$$n_0(\underset{\sim}{x}_0,w,\mu) = U(\underset{\sim}{x}_0)+\sum_{i=1}^{\infty} n_i(\underset{\sim}{x}_0)P_i(\mu)\approx U(\underset{\sim}{x}_0)+\mu n_1(\underset{\sim}{x}_0) \qquad (44)$$

where P_i is the i^{th} Legendre polynomial, and assumes that $U_0 \gg n_1 \gg n_2, n_3 \ldots$ U_0 is the omnidirection intensity of cosmic rays. Earl (1973) has investigated the properties of equation (43) and found that this

expansion (equation 44), while not the exact asymptotic expansion, is a good approximation for the Fokker-Planck coefficients appropriate to cosmic-ray diffusion in the solar system. Using the form of equation (44), assuming gradients are of higher order, and taking the first two moments in μ of equation (43), one finds (Jokipii, 1971)

$$\frac{\partial U}{\partial t} = K_{\parallel} \frac{\partial^2 U}{\partial z^2} + K_{\perp} \left[\frac{\partial^2 U}{\partial x_0^2} + \frac{\partial^2 U}{\partial y_0^2}\right] \tag{45}$$

where

$$K_{\parallel} = \frac{2w^2}{9}\left[\int_0^1 \left\langle \frac{(\Delta\mu)^2}{\Delta t}\right\rangle d\mu\right]^{-1} = \frac{2w^2}{9\omega_0^2}\left[\int_0^1 d\mu \; P_{\perp}^{B}\left(k_{\parallel} = \frac{\omega_0}{w\mu}\right)\right]^{-1} \tag{46a}$$

$$K_{\perp} = \frac{1}{2}\int_0^1 \left\langle \frac{(\Delta x)^2}{\Delta t}\right\rangle d\mu = \frac{1}{2}\frac{w}{B_0^2}\left[\int_0^1 d\mu \; P_{\perp}^{B}(k_{\parallel} = 0)\right]. \tag{46b}$$

Here $K_{\parallel}$ and $K_{\perp}$ are the usual spatial diffusion coefficients for cosmic rays in a turbulent magnetic field. The anisotropic amplitude n_1 is given by

$$n_1 = -\frac{3}{w} K_{\parallel} \frac{\partial U}{\partial z}. \tag{47}$$

As discussed above, for simplicity I will consider the scintillations seen by a narrow-angle detector but <u>averaged</u> over all angles in velocity and wavenumber. In the diffusion limit, the <u>pitch-angle average</u> of equations (42) for the power spectrum of cosmic-ray scintillations is

$$P^n(k_{\parallel},w) \equiv \frac{1}{2}\int_0^1 d\mu \; P^n(k_{\parallel},w,\mu) = \frac{P_{\perp}^{B}(k_{\parallel})}{B_0^2}\frac{w^2}{\omega_0^2}\chi_0(k_{\parallel})\left[\left(\frac{\partial U}{\partial x_0}\right)^2 + \left(\frac{\partial U}{\partial y_0}\right)^2\right] + \frac{P_{\perp}^{B}(k_{\parallel})}{B_0^2}\frac{9K_{\parallel}^2}{2w^2}\chi_1(k_{\parallel})\left[\frac{\partial U}{\partial z}\right]^2. \tag{48a}$$

The two resonance integrals χ_0 and χ_1 are defined by

$$\chi_0(k_\parallel) = \int_0^1 d\mu \frac{\omega_0^2 \mu^2}{\alpha_0^2 + (k_\parallel w\mu)^2} \tag{48b}$$

and

$$\chi_1(k_\parallel) = \int_0^1 d\mu \frac{(1-\mu^2)}{2} \left\{ \frac{\omega_0^2}{\alpha_0^2 + (\omega_0 + k_\parallel w\mu)^2} + \frac{\omega_0^2}{\alpha_0^2 + (\omega_0 - k_\parallel w\mu)^2} \right\} . \tag{48c}$$

From equations (48), it can be seen that the amplitude of the scintillations with the "non-resonant" filter χ_0 depends on the <u>transverse</u> gradients of the cosmic-ray distribution function, while the contribution of the part with the "resonant" filter χ_1 depends on the <u>longitudinal</u> gradient. This is similar to the behavior of the diffusion coefficients given in equations (46), since in this limit $K_\parallel$ depends on the magnetic-field power spectrum at the resonant wavenumber $k_\parallel = \omega_0/w$, and $K_\perp$ depends on the magnetic-field power spectrum at zero wavenumber.

Equations (48) give the cosmic-ray scintillations seen by a <u>unidirectional</u> detector, averaged over all directions for simplicity, and valid in the rest frame of the plasma. The functions χ_0 and χ_1 act as filters in wavenumber space. The filters χ_0 and χ_1 are plotted in Fig. V-1 as a function of the two parameters

$$\eta = \frac{k_\parallel w}{\omega_0} \tag{49a}$$

and

$$\varepsilon = \alpha_0/\omega_0 . \tag{49b}$$

The width of the resonant filter χ_1 is determined by the strength of the scattering of the cosmic rays by the random magnetic

Figure V-1: Resonance functions χ_0 and χ_1. The functions are defined in equations (48) and are plotted as functions of η and ϵ (see equations 49). The dashed curve has $\epsilon = 0.1$ and the solid curve $\epsilon = 0.2$. The cyclotron resonance occurs at $\eta \tilde{=} 1$, and χ_1 is peaked there. χ_0 peaks at $\eta = 0$. The height of the resonances varies inversely with ϵ, and $\chi_1(\lambda) \sim \eta^{-1}$ for $\eta \gg 1$.

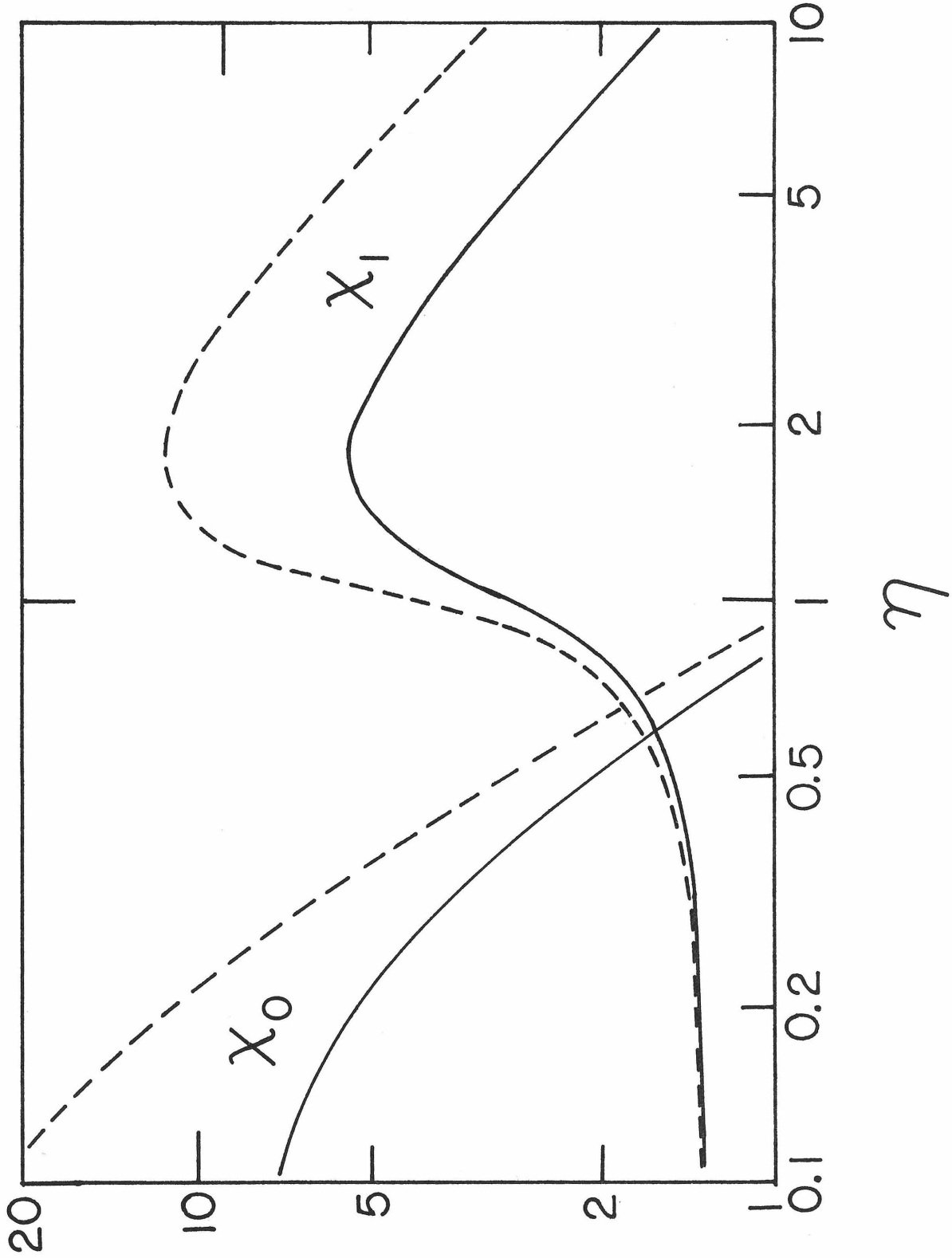
20
10
5
2
1
0.1
0.2
0.5
1
2
5
10
η
χ0
χ1

fields. If the interaction is small, $\alpha_0 \tilde{=} 1/\tau_s$ is small and each particle with velocity near the resonant one spends a large amount of time being driven by the perturbing field. If the interaction is large, however, a typical particle with near-resonant velocity will be scattered to another position in phase space before a large cosmic-ray fluctuation can be induced. Notice that the usual quasi-linear theory, which has $\alpha_0 \to 0$, would produce an infinitely large resonance. Therefore the non-linear terms in equation (6) are <u>crucial</u> in the resonant region. Conversely, the study of high-resolution cosmic-ray power spectra in the regime near resonance can be used as a tool in investigating the non-linear interaction between particles and fields and thus may prove to be a valuable approach in studying turbulence.

It is instructive to consider the results obtained by <u>maintaining</u> the diffusion limit but considering the <u>general</u> scintillation equations (36) for arbitrary $\underset{\sim}{k}$ and ω. The derivation proceeds as above, with equations (36) in place of the simplified expression (equations 42) and with the expressions for the diffusion coefficients as derived in Appendix B rather than equations (46). The general equation for the scintillations seen by a narrow-angle detector (averaged over all directions) is

$$P^n(k_\parallel, k_\perp, w, \omega) \equiv \int_{-1}^{1} \frac{d\mu}{2} P^n(k_\parallel, k_\perp, w, \mu, \omega) = \frac{P_\perp^B}{B_0^2} \frac{w^2}{\omega_0^2} \chi_0' \left[\left(\frac{\partial U}{\partial x_0}\right)^2 + \left(\frac{\partial U}{\partial y_0}\right)^2 \right]$$
$$+ \frac{P_\perp^B}{B_0^2} \frac{9}{2} \frac{K_\parallel^2}{w^2} \chi_1' \left(\frac{\partial U}{\partial z}\right)^2 + \frac{P_\parallel^B}{B_0^2} \frac{w^2}{\omega_0^2} \frac{\chi_1'}{2} \left[\left(\frac{\partial U}{\partial x_0}\right)^2 + \left(\frac{\partial U}{\partial y_0}\right)^2 \right], \tag{50}$$

where the resonant integrals are now given by

$$\chi_0' = \int_0^1 d\mu \sum_{m=-\infty}^{\infty} J_m\left(\frac{k_\perp w\sqrt{1-\mu^2}}{\omega_0}\right)^2 \frac{\mu^2\omega_0^2}{(\omega - k_\parallel w\mu + m\omega_0)^2 + \alpha_0^2} \tag{51a}$$

$$\chi_1' = \int_0^1 \frac{d\mu}{2} \sum_{m=-\infty}^{\infty} J_m\left(\frac{k_\perp w\sqrt{1-\mu^2}}{\omega_0}\right)^2 \left\{ \frac{(1-\mu^2)\omega_0^2}{(\omega - k_\parallel w\mu + (m+1)\omega_0)^2 + \alpha_0^2} + \frac{(1-\mu^2)\omega_0^2}{(\omega - k_\parallel w\mu + (m-1)\omega_0)^2 + \alpha_0^2} \right\}. \tag{51b}$$

The width of the resonances is again determined by α_0, but each integral now has an infinite number of cyclotron resonances, each multiplied by a different Bessel function of the perpendicular wavenumber. Since the resonances occur at different frequencies, the sum over all resonances and Bessel functions will smooth out the shape of the resonant integrals. Therefore, the $k_\perp \to 0$ limit and its resulting resonance integrals as shown in Fig. V-1 probably over-state the importance of the cyclotron resonance for finite $k_\perp/k_\parallel$. A detailed evaluation of this effect requires knowledge of the complete three-dimensional wavenumber spectrum of the magnetic field, and additional observational data are necessary before an investigation of the full structure of equation (50) is warranted.

E. Cosmic-Ray Scintillations in Interplanetary Space

In this section, I apply the results of the previous sections to the propagation of cosmic rays in the solar system. I adopt the usual model of cosmic-ray propagation and scattering (Jokipii, 1971), in which a uniform flux of galactic cosmic rays is incident upon the solar cavity. Cosmic rays are scattered by random magnetic irregularities superimposed upon an average magnetic field which is taken to be an Archimedes spiral (Parker, 1963) with angle

$$\psi = \arctan\left(\frac{r\,\Omega_\odot \sin\theta}{V_w}\right) \tag{52}$$

from a solar radius vector. Here heliocentric spherical polar coordinates are adopted (r,θ,ϕ) and the inclination of the ecliptic is ignored. V_w is the velocity of the solar wind, which is taken to flow radially with constant velocity $V_w \approx 350$ km/sec, and $\Omega_\odot$ is the sun's rotational angular velocity.

For simplicity, I will adopt as a model for cosmic-ray scintillations the $k_\perp \to 0$, diffusion limit of the previous Section. The extension to the more general case is conceptually trivial (though algebraically complex) and can be done if subsequent observations warrant a more precise consideration of the full complexity of the general scintillation equations, (50) and (51). Adopting the results of equations (48), and transforming from coordinates with the z-axis along $\underset{\sim}{B}_0$ to heliocentric coordinates, one obtains

$$P^n(k_\parallel,w) = \frac{P_\perp^B(k_\parallel)}{B_0^2}\left\{\left[\frac{w^2}{\omega_0^2}\chi_0 \sin^2\psi + \frac{9K_\parallel^2}{2w^2}\chi_1\cos^2\psi\right]\left(\frac{\partial U}{\partial r}\right)^2 + \left[\frac{w^2}{\omega_0^2}\chi_0\right]\left(\frac{1}{r}\frac{\partial U}{\partial\theta}\right)^2\right. \tag{53}$$

(Continued on next page)

$$+ \left[\frac{w^2}{\omega_0^2}\chi_0\cos^2\psi + \frac{9K_\parallel^2}{2w^2}\chi_1\sin^2\psi\right]\left(\frac{1}{r\sin\theta}\frac{\partial U}{\partial\Phi}\right)^2\Bigg). \qquad (53\text{ con't})$$

For most models of steady-state cosmic-ray transport near earth,

$$\frac{1}{r}\frac{\partial U}{\partial\theta} \ll \frac{\partial U}{\partial r} \text{ and } \frac{1}{r\sin\theta}\frac{\partial U}{\partial\Phi} \ll \frac{\partial U}{\partial r}, \qquad (54)$$

so the terms involving θ and Φ derivatives in equation (53) will be ignored. The remaining terms in equation (53) provide a resonable model for cosmic-ray scintillations in the solar system provided that

a) the radial gradient of the average cosmic-ray distribution function is dominant, and

b) the magnetic-field fluctuations satisfy $k_\perp/k_\parallel \ll 1$, $k_\perp w/\omega_0 \ll 1$, and $\omega/\omega_0 \ll 1$.

All of the discussion above is applicable in the <u>rest frame of the plasma</u>. Since the scattering centers of the magnetic field are being <u>convected</u> in the radial direction with velocity $V_w \gg \omega/k$, the <u>spatial</u> fluctuations will be convected past a stationary observed who will see <u>temporal</u> fluctuations at a frequency

$$f = k_r V_w/2\pi. \qquad (55)$$

The observed frequency power spectrum will then be (Jokipii, 1971, Appendix I)

$$P^n(f,w)=\left(\frac{1}{2\pi}\right)^3\frac{1}{V_w}\int_{-\infty}^{\infty}dk_\theta\int_{-\infty}^{\infty}dk_\Phi\int_{-\infty}^{\infty}d\omega\,P^n\left(k_r=\frac{2\pi f}{V_w},k_\theta,k_\Phi,\omega\right) \qquad (56)$$

or from equation (53),

$$P^n(f,w) = \frac{9}{2}\frac{K_\parallel^2}{w^2}\left[\chi_1\cos^2\psi + \frac{2}{9}\frac{w^4}{K_\parallel^2\omega_0^2}\chi_0\sin^2\psi\right]\left(\frac{\partial U}{\partial r}\right)^2\frac{P_\perp^B(f)}{B_0^2}. \qquad (57a)$$

In the resonant integrals χ_0 and χ_1, the substitution

$$k_{\parallel} = \frac{2\pi f}{V_w \cos\psi} \tag{57b}$$

must be made. The transformation to the stationary reference frame also changes the average cosmic-ray distribution function, introducing the Compton-Getting anisotropy (Compton and Getting, 1935, Forman, 1970). However, the changes in the power spectrum due to this effect are of order V_w/w and therefore are insignificant for particles with kinetic energy $T \gtrsim 1$ MeV.

As indicated by equations (48) and (49), the resonance integrals χ_0 and χ_1 have maxima ("resonances") at zero wavenumber and at the cyclotron wavenumber $k_{\parallel} \cong \omega_0/w$, respectively. The width of these filter factors depends on the ratio $\epsilon = \alpha_0/\omega_0$, where α_0 is the non-linear closure parameter (equations 14 and 15) and ω_0 is the mean cyclotron frequency of the cosmic-ray particles. There are essentially two estimates of the ratio ϵ given in equation (15). The first,

$$\epsilon_1 \equiv \frac{\alpha_0}{\omega_0} \simeq \frac{|\underset{\sim}{\omega}_1|^2}{\omega_0^2} \simeq \frac{\langle B_{1_\perp}^2 \rangle}{B_0^2}, \tag{58}$$

is based on dimensional arguments and the fact that equation (13) is true. It depends only on the structure of the magnetic fluctuations and is independent of the <u>energy</u> of the cosmic rays. The second estimate,

$$\epsilon_2 \equiv \frac{\alpha_0}{\omega_0} \simeq \frac{1}{\omega_0 \tau_s} \tag{59}$$

is based on the similar structure (equations 11 and 12) of the equations for the fluctuations and for the average distribution function,

and the assumption that the Fokker-Planck coefficients are good for all particles regardless of whether they happen to be near the unperturbed positions in phase space or not. In the interplanetary medium, scattering is dominated by the parallel diffusion coefficient,

$$K_{\parallel} = \frac{1}{3} \lambda w \simeq \frac{1}{3} w^2 \tau_s \qquad (60)$$

where λ is the scattering mean-free path and $\lambda \approx w \tau_s$. From equations (59) and (60), I obtain

$$\epsilon_2 \simeq \frac{w^2}{3K_{\parallel} \omega_0} = \frac{6.7\beta R \times 10^{20} cm^2/sec}{K_{\parallel}} , \qquad (61)$$

where in the latter form $\beta = w/c$, R is the rigidity ($R = \gamma m c^2/q$) in GV, and the average magnetic field strength has been taken as $5\gamma = 5 \times 10^{-5}$ guass. In general, this estimate of ϵ depends on the energy of the particle involved. For protons, the ratio ϵ_2 from equation (61) is plotted as a function of kinetic energy (T) in Fig. V-2. Also indicated is the estimate of ϵ_1 taken from equation (58); both estimates are based on the power spectrum and derived parallel diffusion coefficient given by Jokipii and Coleman (1968). Both estimates should be considered accurate to no better than a factor of two, and this uncertainty is indicated on the figure. Over the energy range of interest for scintillations, 100 MeV $\lesssim$ T $\lesssim$ 10 GeV, the two estimates of ϵ give mutually consistent results. This is an indication that the non-linear closure approximation of equation (14) and the value of α_0 obtained from the estimates are not unreasonable. Another estimate (ϵ_3) will be obtained in Appendix C from a more formal consideration of the non-

Figure V-2: Estimates of the parameter ϵ for cosmic-ray protons. Conditions for propagation of cosmic rays in the interplanetary medium near earth were used, as discussed in the text. The parameter ϵ is plotted as a function of proton kinetic energy, T. The straight line is the estimate ϵ_1 of equation (58), and the curve is the estimate ϵ_2 of equation (61). The uncertainty of a factor of ~2 in the estimates is shown by the error bar.

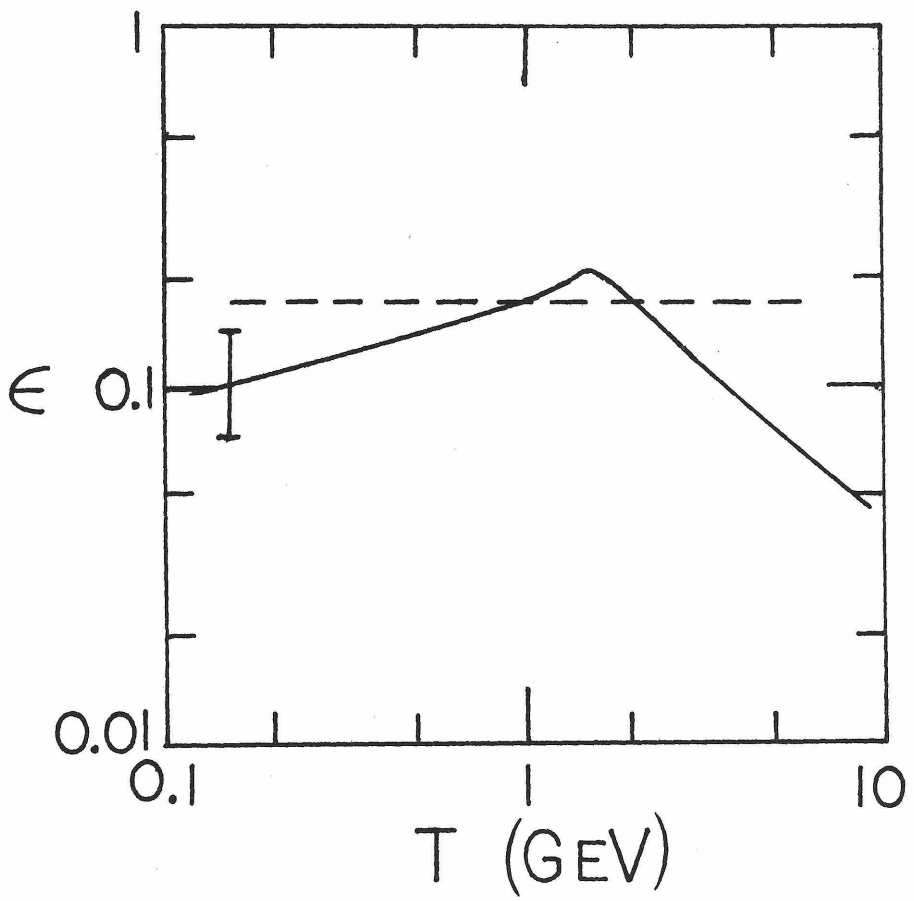
1
ϵ 0.1
0.01
0.1
1
10
T (GEV)

linear terms in equation (6). The value of ε_3 is larger than ε_1 and ε_2 by a factor of ~2 for the frequencies (near resonance) for which the contribution of ε is most important.

The observing frequency f_0 at which the cyclotron resonance will occur for cosmic rays near earth can be obtained from $k_{\parallel} = \omega_0/w$ and equation (57b), giving

$$f_0 = \frac{V_w \cos\psi}{w} \frac{\omega_0}{2\pi}. \qquad (62)$$

The resonant frequency is plotted in Fig. V-3 as a function of kinetic energy for protons in a 5γ magnetic field, with V_w = 350 km/sec and $\cos\psi = 1/\sqrt{2}$. The low-frequency limit corresponds to $f < f_0$ and is indicated on the figure. In this region, the simpler theory of Chapter IV is applicable. The fuller theory of this Chapter is required for $f \gtrsim f_0$.

In order to apply equations (57) to observations, one needs the magnetic-field power spectrum and the cosmic-ray scintillation spectrum for the same period. Coleman (1966) has shown that the two perpendicular magnetic fields $B_{\perp 1} = B_\theta$ and $B_{\perp 2} = B_r \sin\psi + B_\varphi \cos\psi$ are distributed with gaussian probability amplitude and zero mean. However, the power spectra of $B_{\perp 1}$ and $B_{\perp 2}$ are not precisely equal, as assumed in deriving the cylindrically symmetric limit in Appendix A. The asymmetry may be caused by the sector structure of the magnetic field (Wilcox and Ness, 1965). Here I will simply use the cylindrically symmetric results derived above and use as the perpendicular power spectrum the average,

$$P^B_\perp = \frac{1}{2}(P^B_{\perp 1} + P^B_{\perp 2}) = \frac{1}{2}\left[P^B_{\theta\theta} + P^B_{rr}\sin^2\psi + (P^B_{r\varphi} + P^B_{\varphi r})\sin\psi\cos\psi + P^B_{\varphi\varphi}\cos^2\psi\right]. \qquad (63)$$

Figure V-3: Resonant frequency f_0 for cosmic-ray protons near earth. Equation (62) and the parameters V_w = 350 km/sec, $\cos\psi \tilde{=} 0.7$, $B_0 = 5\gamma$ have been used, and f_0 is plotted as a function of the proton's kinetic energy, T. The region in which the low-frequency limit is applicable is the area below the curve, as indicated.

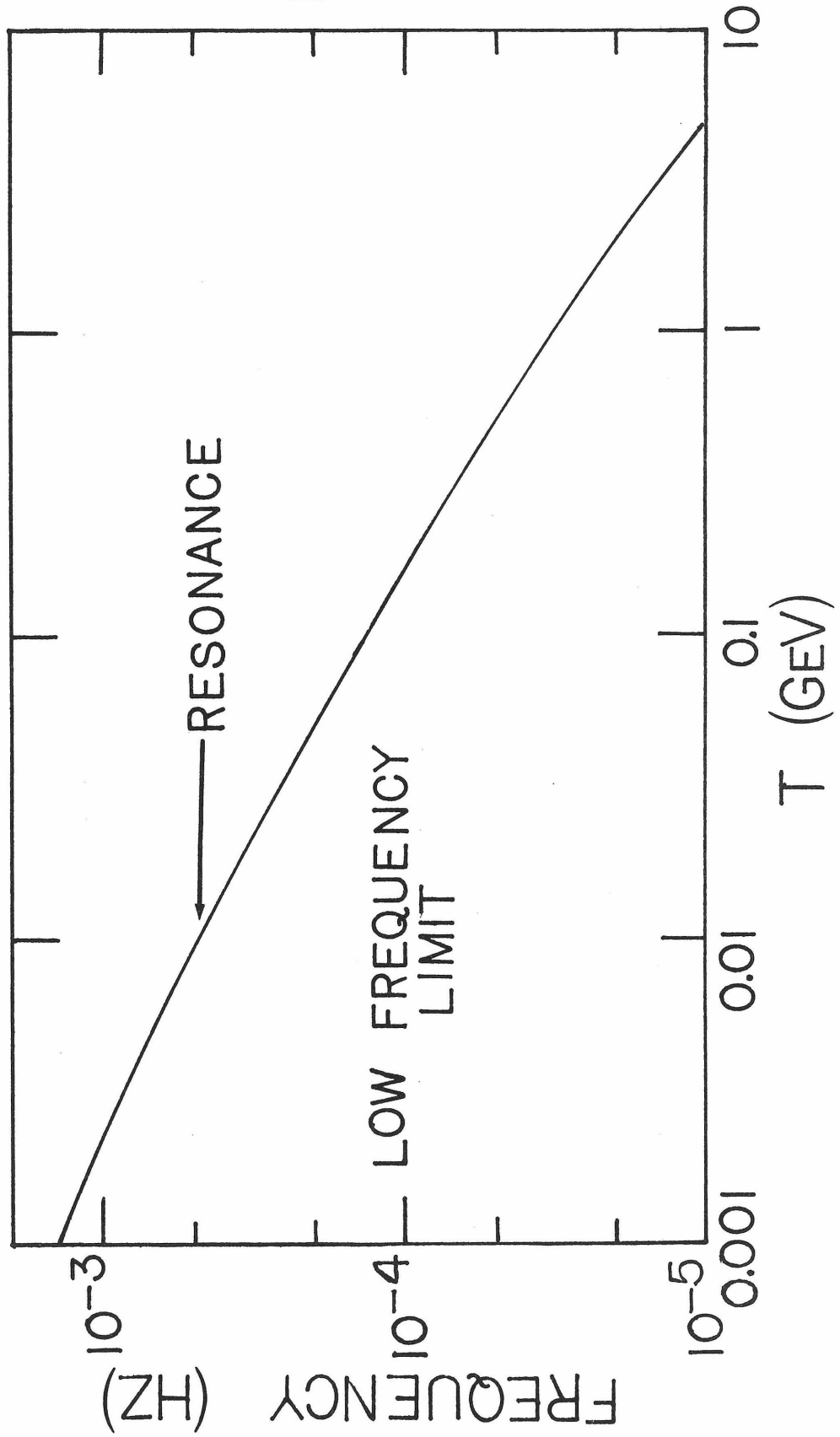
FREQUENCY (HZ)
10^{-3}
10^{-4}
10^{-5}
RESONANCE
LOW FREQUENCY LIMIT
0.001
0.01
0.1
1
10
T (GEV)

The last equality follows from the definition of the field $B_{\perp}{}^2$, and $P^B_{r\varphi}$ and $P^B_{\varphi r}$ are the cross-spectra of B_r and B_φ. Coleman (1966, Table 6) has shown that the coherence squared, $C^2 = |P_{r\varphi}|^2/P_{rr}P_{\varphi\varphi} \approx 0.04$ for frequencies $10^{-5}\text{Hz} \lesssim f \lesssim 10^{-3}\text{Hz}$, so B_r and B_φ are basically uncorrelated over this range of frequencies and to a good approximation one has

$$P^B_{\perp} = \frac{1}{4}\,(2P^B_{\theta\theta} + P^B_{\varphi\varphi} + P^B_{rr}), \tag{64}$$

where $(\sin\psi)^2 \approx (\cos\psi)^2 \approx \frac{1}{2}$ has been used.

F. Scintillations of Low-Energy (1 MeV $\lesssim$ T $\lesssim$ 100 MeV) Cosmic-Ray Protons

In terms of the parameter ϵ_2 as given by equation (61), equation (57a) can be written

$$P^n(f,w)/U^2 = P^j(f,w)/j_0^2 = \frac{2}{L^2}\left(\frac{3K_\parallel}{2w\underline{a}}\right)^2 [\chi_1 \cos^2\psi + 2\epsilon_2^2 \chi_0 \sin^2\psi] \frac{P_\perp^B(f)}{B_0^2}. \quad (65)$$

Here $j = (\gamma mw)^2 n$ is the differential intensity, $P^j(f,w)$ is the power spectrum of the fluctuations in the differential intensity, $\underline{a}$ is one astronomical unit, and L is the radial gradient scale (in A.U.) of the cosmic-ray intensity, defined by

$$\frac{1}{U}\frac{\partial U}{\partial r} = \frac{1}{L\underline{a}} . \quad (66)$$

Since the resonance integrals χ_0 and χ_1 are of order unity, the relative scintillations of cosmic rays in the solar system are proportional to the relative fluctuations of the magnetic field times the amplitude factor

$$\text{Amp} \approx \left(\frac{K_\parallel}{wL\underline{a}}\right)^2 . \quad (67)$$

For ~1 MeV protons, $K \sim 10^{20}$ cm^2/sec and $L \gtrsim 1$, so Amp $\lesssim 10^{-4}$ and the scintillations are much smaller than the magnetic fluctuations. For a typical power spectrum of the interplanetary magnetic field (Quenby and Sear, 1971), $P_\perp^B(f)/B_0^2 \approx 400$ Hz^{-1} near $f \sim 10^{-4}$Hz, so that

$$P^j(f\sim 10^{-4}\text{Hz},\ 1\text{ MeV})/j_0^2 \lesssim 4 \times 10^{-2}\text{Hz}^{-1} \quad (68)$$

is the <u>interplanetary scintillation contribution</u> to the 1 MeV proton power spectrum. However, as shown in Chapter III, detectors inside the

magnetosphere see a componant of scintillations due to the magnetosheath with an amplitude of ~50 Hz^{-1} for ~1 MeV protons at $f \sim 10^{-4}$ Hz. Therefore, near-earth detectors in the low-energy ($T \sim 1$ MeV) range see scintillations which are of magnetospheric rather than interplanetary origin. An interplanetary detector of ~1 MeV protons, due to Poisson noise power (as discussed in Section II.C), would require a counting rate of >50 sec^{-1} to detect scintillations at ~10^{-4} Hz.

In the energy range 10 MeV $\lesssim T \lesssim$ 100 MeV, the cosmic-ray energy spectrum is $j(T) \cong AT$. Rygg and Earl (1971) have shown that such a spectrum indicates a very small cosmic-ray gradient. Observations (Anderson, 1968) also indicate that the radial gradient is small in this energy range. It therefore appears that interplanetary scintillation measurements in the low-energy range (1 MeV < T < 100 MeV) will require an interplanetary instrument with a counting rate of the order of 50 sec^{-1} or more. Data from such an instrument are not currently available.

G. Scintillations of High-Energy ($T \gtrsim 500$ MeV) Cosmic Rays

The modulation equation for galactic cosmic rays near the sun (Jokipii and Parker, 1967, Jokipii, 1971) can be solved approximately for cosmic-ray protons with energies $T \gtrsim 500$ MeV. The result (Gleeson and Axford, 1968, Jokipii and Coleman, 1968) of the calculation, assuming spherical symmetry, can be expressed as

$$\frac{1}{U}\frac{\partial U}{\partial r} = \frac{2+\alpha\Gamma}{3}\frac{V_w}{K_{\parallel}\cos^2\psi} \tag{69}$$

in the same notation as that used in equation (IV-12). From equations (57) and (69), I have

$$P^j(f,w)/j_0^2 = \frac{(2+\alpha\Gamma)^2}{2\cos^2\psi}\left(\frac{V_w}{w}\right)^2 \chi_3 \frac{P_\perp^B(f)}{B_0^2}\,, \tag{70}$$

where

$$\chi_3 = \chi_1 + 2\varepsilon_2^2 \tan^2\psi\, \chi_0\,. \tag{71}$$

Near earth, $2\cos^2\psi \approx \tan^2\psi \approx 1$, and $\Gamma \sim 2.6$ for $T \gtrsim 5$ GeV. This is very similar to the result obtained in the low-frequency limit of Chapter IV, where the numerical factor of $1-\mu^2 \approx \frac{2}{3}$ in equation (IV-8) has been replaced by the frequency-dependent resonance function $\frac{1}{2}\chi_3$ in equation (70).

The small observed (and calculated) cosmic-ray scintillation amplitude for protons at $T \sim 1$ GeV of

$$P^j(f\sim 10^{-4}\text{Hz},\ 1\text{ GeV})/j_0^2 \sim 3 \times 10^{-2}\text{Hz}^{-1} \tag{72}$$

means that a detector with a counting rate of $\sim 100\ \text{sec}^{-1}$ is required in order to observe scintillations near $f \sim 10^{-4}$Hz for $T \sim 1$ GeV protons.

Because of their large counting rate, neutron monitors are ideal detectors to use in searching for interplanetary scintillations. The higher-latitude neutron moniters (such as Alert and Deep River) respond primarily to cosmic rays with energies 0.5 GeV $\lesssim T \lesssim$ 10 GeV. The scintillations seen by the detectors will then be given by equation (70) averaged over the energy of the particles detected, or

$$P^j(f)/j_0{}^2]_{NM} = \frac{\int_{T_0}^{\infty} \left(P^j(f,T)/j_0{}^2\right) j_0(T)\, dT}{\int_{T_0}^{\infty} j_0(T)\, dT} \quad . \tag{73}$$

Therefore,

$$P^j(f)/j_0{}^2]_{NM} = \frac{P_\perp^B(f)}{B_0{}^2}\, Amp(f), \tag{74}$$

where the frequency-dependent amplitude giving the relative cosmic-ray scintillation power spectrum in terms of the relative magnetic-field power spectrum is:

$$Amp(f) = \frac{\int_{T_0}^{\infty} (2+\alpha(T)\Gamma(T))^2 \left(\frac{V_w}{w}\right)^2 \chi_3(f,T)\, j_0(T)\, dT}{\int_{T_0}^{\infty} j_0(T)\, dT} \quad . \tag{75}$$

I have calculated the amplitude factor of equation (75) under the assumptions that

$$\epsilon = \frac{\alpha_0}{\omega_0} = 0.15 \text{ (independent of energy)} \tag{76a}$$

$$T_0 = 0.5 \text{ GeV} \tag{76b}$$

and

$$j_0(T) = (\text{const}) \ (T + 2)^{-2.6} \tag{76c}$$

where T is the energy in GeV. The last expression is my simple analytic approximation for the proton energy spectrum given by Gloeckler and Jokipii (1967). The result of the calculation is shown on Fig. V-4, along with two comparison curves. The straight line is the estimate $\text{Amp} \sim \frac{2}{3} (\delta_{\parallel})^2 \sim \frac{2}{3} (0.9\%)^2$ given by the low-frequency limit of Chapter IV. The dashed curve is the amplitude that would be obtained from equation (75) if all protons detected had the energy 2 GeV. While the cyclotron resonance is evident in the prediction of the level of scintillations seen by neutron monitors, it is clear that the large energy-response window of the detectors smooths out the resonance somewhat. Thus, the simplified theory of Chapter IV (see Fig. IV-1, IV-3, and IV-5) gives a reasonable prediction of the level of neutron-monitor scintillations even in the resonant regime, or for frequencies up to $f \sim 10^{-4}$Hz.

The interesting question of the resonance width α_0 and the possibility of exploring non-linear plasma interactions with cosmic rays will be discussed in Appendix C. It is evident from Fig. V-4, however, that tests of various theories above the size of α_0 will be difficult to perform with neutron monitors due to the "smearing out" of the resonance by particles of different energies. A relatively narrow-energy-band ($\Delta T < T$) detector with a counting rate $\sim 100 \text{ sec}^{-1}$ will be required to investigate the non-linear effects, assuming that the $k_{\perp} \to 0$, diffusion limit is applicable. If $k_{\perp} \sim k_{\parallel}$, the various resonance

Figure V-4: Amplitude Amp(f) of equation (75). The amplitude gives the ratio of the relative scintillations of the cosmic-ray flux to the relative magnetic-field fluctuations. The solid curve is the result of equation (75), appropriate for high-latitude neutron monitors. The dashed curve is the amplitude ratio for a hypothetical detector with narrow energy bandwidth centered at T = 2 GeV. The dashed line is the result of the low-frequency model of Chapter IV. Note that the more general theory of equation (75) differs from the estimate of Chapter IV by less than a factor of 2 over the entire range of frequencies $f \lesssim 10^{-4}$ Hz.

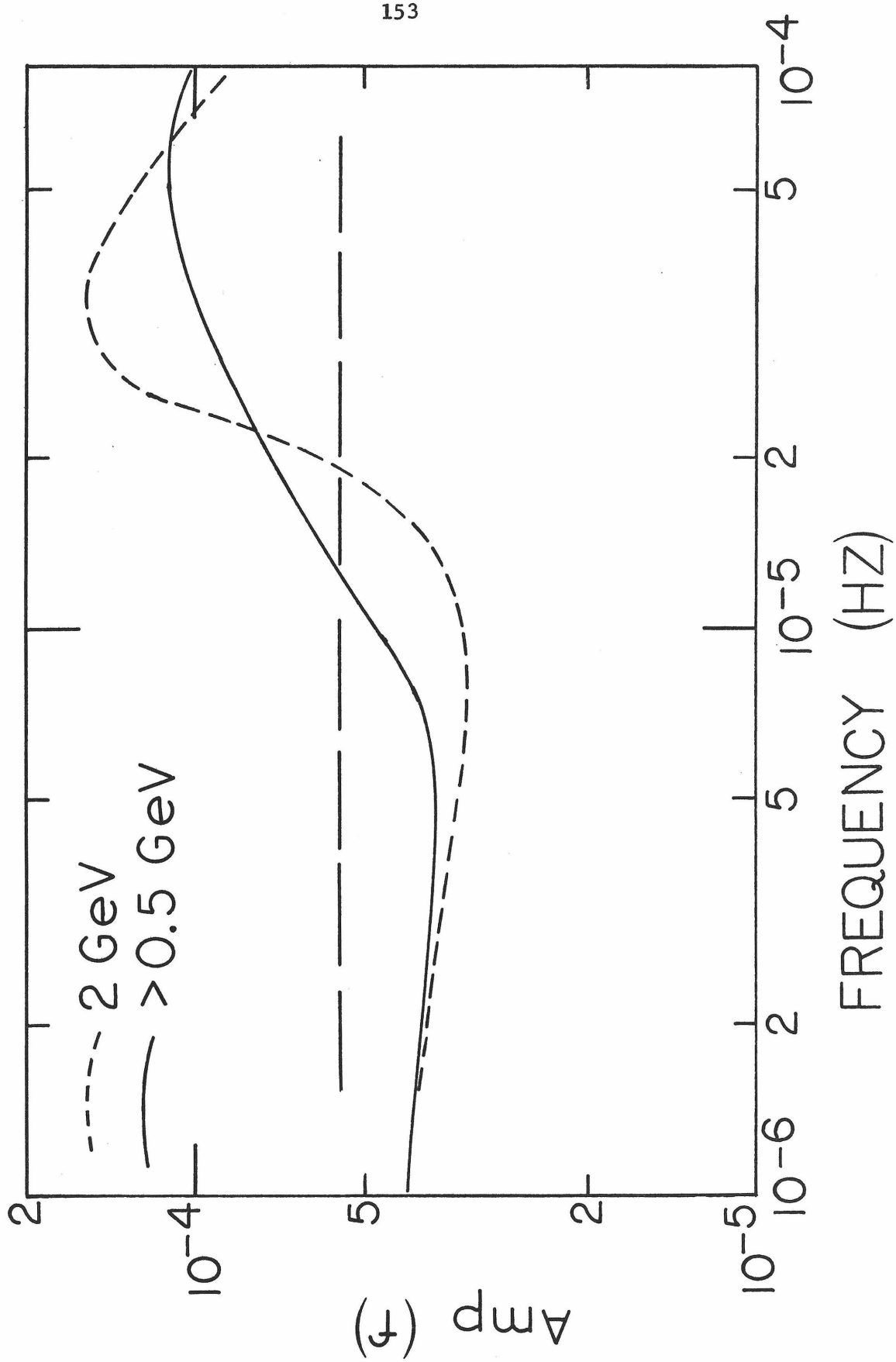
Amp (T)
FREQUENCY (HZ)
2 GeV
>0.5 GeV
2
10⁻⁴
5
2
10⁻⁵
10⁻⁶
2
5
10⁻⁵
2
5
10⁻⁴

terms (for $k_{\parallel} = n \frac{\omega_0}{w\mu}$) will tend to produce overlapping effects and thus each resonance will be less pronounced than the single resonance given by the $k_{\perp} \rightarrow 0$, T = 2 GeV case shown in Fig. V-4.

Please note that a summary of results and a discussion of the implications that can be drawn from this research are included in Chapter I above.

APPENDIX A

AXISYMMETRIC POWER SPECTRUM

In this Appendix, I consider the conditions that axial symmetry and a divergence-free magnetic field require of the magnetic-field power spectrum. Symmetry conditions and the assumed stationarity of the random field will also be used to find the most general form of the power spectrum which is consistent with a priori knowledge of the magnetic field.

First, consider the tensor properties of the magnetic-field power spectrum. The power spectrum is defined as

$$P_{ij}(\underset{\sim}{k},\omega) = \int d^3\underset{\sim}{r}\, dt\, e^{i(\omega t - \underset{\sim}{k}\cdot\underset{\sim}{r})} \langle B_i(\underset{\sim}{r}_0,t_0) B_j(\underset{\sim}{r}_0+\underset{\sim}{r},t_0+t)\rangle . \qquad (1)$$

It is a second-rank tensor, and by assumption the tensor depends only on the two vectors $\underset{\sim}{k}$ and $\underset{\sim}{e}$ and the scalar ω. Therefore, the tensor must be of the form

$$\begin{aligned} P_{ij}(\underset{\sim}{k},\omega;\underset{\sim}{e}) = {} & A\,\delta_{ij} + Bk_ik_j + Ce_ie_j + D(k_ie_j + k_je_i) \\ & + E(\epsilon_{ik\ell}k_j + \epsilon_{jk\ell}k_i)\,k_k e_\ell + F(\epsilon_{ik\ell}e_j + \epsilon_{jk\ell}e_i)k_k e_\ell \\ & + G(k_ie_j - k_je_i) + H\epsilon_{ijk}k_k + I\epsilon_{ijk}e_k \\ & + J(\epsilon_{ik\ell}k_j - \epsilon_{jk\ell}k_i)k_k e_\ell \\ & + K(\epsilon_{ik\ell}e_j - \epsilon_{jk\ell}e_i)k_k e_\ell . \end{aligned} \qquad (2)$$

In equation (2), all the capital letters A through K are functions of

the three rotational invariants k^2, $\underset{\sim}{k}\cdot\underset{\sim}{e}$, and ω, and the terms A through F are even in interchange of i and j while the terms G through K are odd under that interchange.

I now wish to apply constraints to the coefficients in (2) to obtain some relations between them. First is the divergence condition,

$$\underset{\sim}{\nabla}\cdot\underset{\sim}{B} = 0, \tag{3}$$

which when Fourier-analyzed yields trivially

$$k_i P_{ij} = P_{ij} k_j = 0 \quad \text{CONDITION I.} \tag{4}$$

Since $\underset{\sim}{B}$ is a stationary random function,

$$\langle B_i(\underset{\sim}{r}_0,t_0)B_j(\underset{\sim}{r}_0+\underset{\sim}{r},t_0+t)\rangle = \langle B_i(\underset{\sim}{r}_0-\underset{\sim}{r},t_0-t)B_j(\underset{\sim}{r}_0,t)\rangle, \tag{5}$$

which combined with (1) yields the stationarity condition,

$$P_{ij}(\underset{\sim}{k},\omega) = P_{ji}(-\underset{\sim}{k},-\omega) \quad \text{CONDITION II.} \tag{6}$$

A third property of the magnetic field is that it is real, so that $\langle B_i B_j\rangle^* = \langle B_i B_j\rangle$, from which follows the reality condition,

$$[P_{ij}(\underset{\sim}{k},\omega)]^* = P_{ji}(\underset{\sim}{k},\omega) \quad \text{CONDITION III.} \tag{7}$$

The final two conditions deal with symmetry. The wavenumber $\underset{\sim}{k}$, being the Fourier transform of $\underset{\sim}{r}$, is a polar vector. The vector $\underset{\sim}{e}$ may be either a polar vector (corresponding, for instance, to a direction in space) or a pseudovector (corresponding, for instance, to the average direction of the magnetic field). Electromagnetic phenomena both conserve parity (i.e., posses inversion symmetry) and have time-reversal

invariance. Thus one has the parity condition

$$P_{ij}(\underset{\sim}{k},\omega,\underset{\sim}{e}_V) = P_{ij}(-\underset{\sim}{k},\omega,-\underset{\sim}{e}_V)$$

or CONDITION IV (8)

$$P_{ij}(\underset{\sim}{k},\omega,\underset{\sim}{e}_A) = P_{ij}(-\underset{\sim}{k},\omega,\underset{\sim}{e}_A)$$

and the time-reversal condition,

$$P_{ij}(\underset{\sim}{k},\omega,\underset{\sim}{e}_V) = P_{ij}(\underset{\sim}{k},-\omega,\underset{\sim}{e}_V)$$

or CONDITION V. (9)

$$P_{ij}(\underset{\sim}{k},\omega,\underset{\sim}{e}_A) = P_{ij}(\underset{\sim}{k},-\omega,-\underset{\sim}{e}_A)$$

In equation (7) and (8), the notations $\underset{\sim}{e}_V$ and $\underset{\sim}{e}_A$ indicate that $\underset{\sim}{e}$ is either a polar vector or an axial vector, and use has been made of the relations

$$\hat{P}\,\underset{\sim}{e}_V = -\underset{\sim}{e}_V, \quad \hat{P}\,\underset{\sim}{e}_A = \underset{\sim}{e}_A$$

$$\hat{T}\,\underset{\sim}{e}_V = \underset{\sim}{e}_V, \quad \hat{T}\,\underset{\sim}{e}_A = -\underset{\sim}{e}_A \qquad (10)$$

where $\hat{P}$ represents the inversion operator and $\hat{T}$ the time reversal operator. The symmetries under time-reversal are appropriate for a polar vector ($\underset{\sim}{e}_V$) pointing along a direction in space (i.e., away from the sun) and for an axial vector ($\underset{\sim}{e}_A$) with a rotational character generated by a cross product between a directional vector and a velocity vector (i.e., a magnetic field or vortex).

The implications for the coefficients that each of these conditions imply are indicated in Table A-1 and Table A-2, for $\underset{\sim}{e}$ being a polar vector and an axial vector, respectively. There are four

conditions used, C-II, C-III, C-IV, and C-V, and under each condition is listed the relevant product. The entries tell whether the coefficients are even or odd in the products listed. Using the auxiliary condition that only $\underset{\sim}{k}\cdot\underset{\sim}{e}$ can enter, from the rotation tensor symmetry, I have five conditions which <u>overdetermine</u> the four componants $(\underset{\sim}{k},\underset{\sim}{e},\omega,i)$ of the symmetry of each coefficients. Those coefficients with contradictory symmetry requirements must be zero. The final column gives the symmetry factor for each coefficient; when these factors are separated out from the capital-letter coefficients, the remaining part of each coefficient is real and even in $\underset{\sim}{k}\cdot\underset{\sim}{e}$ and ω.

Finally, I apply the final (divergence) condition of equation (4) to the forms of (1) restricted by the data in Tables A-1 and A-2. For the <u>polar vector</u> case, $k_i P_{ij} = 0$ yields

$$\begin{aligned}&[A + Bk^2 + D'(\underset{\sim}{k}\cdot\underset{\sim}{e})^2]k_j + [C\ \underset{\sim}{k}\cdot\underset{\sim}{e}+D'k^2\underset{\sim}{k}\cdot\underset{\sim}{e}]e_j \\ &\quad i[G'k^2]e_j - i[G'\underset{\sim}{k}\cdot\underset{\sim}{e}]k_j = 0,\end{aligned} \tag{11}$$

where the symmetry factors of Table A-1 have been explicitly included. Equation (11) is really four equalities, since the real and imaginary parts and the two vectors $\underset{\sim}{k}$ and $\underset{\sim}{e}$ are independent. The imaginary part eliminates the G' term, and using the two real equalities to eliminate B and D', I obtain

$$[P_{ij}(\underset{\sim}{k})] = \begin{pmatrix} (k_y^2+k_z^2)A+k_z^2A' & -k_xk_yA & -k_xk_z(A+A') \\ -k_xk_yA & (k_x^2+k_z^2)A+k_z^2A' & -k_yk_z(A+A') \\ -k_xk_z(A+A') & -k_yk_z(A+A') & (k_x^2+k_y^2)(A+A') \end{pmatrix}. \tag{12}$$

[polar vector case]

Amplitude	C-II	C-III	C-IV	C-V	Symmetry Factor
Product:	$(k)(\omega)$	$(i)(k)(\omega)$	$(k)(e)$	(ω)	
A	+	+	+	+	1
B	+	+	+	+	1
C	+	+	+	+	1
D	-	-	+	+	$\underset{\sim}{k}\cdot\underset{\sim}{e}$
E	+	+	-	+	0
F	-	-	-	+	0
G	+	-	+	+	i
H	+	-	-	+	0
I	-	+	-	+	0
J	-	+	-	+	0
K	+	-	-	+	0

Table A-1: Polar Vector Case

Amplitude	C-II	C-III	C-IV	C-V	Symmetry Factor
Product:	$(k)(\omega)$	$(i)(k)(\omega)$	(k)	$(\omega)(e)$	
A	+	+	+	+	1
B	+	+	+	+	1
C	+	+	+	+	1
D	-	-	-	-	$\underset{\sim}{k}\cdot\underset{\sim}{e}$
E	+	+	+	-	0
F	-	-	-	+	0
G	+	-	-	-	0
H	+	-	-	+	$i\omega\ \underset{\sim}{k}\cdot\underset{\sim}{e}$
I	-	+	+	-	$i\omega$
J	-	+	+	-	$i\omega$
K	+	-	-	+	$i\omega\ \underset{\sim}{k}\cdot\underset{\sim}{e}$

Table A-2: Axial Vector Case

In this equation, the axis of symmetry is chosen to be along the z direction and the arbitrary real functions A and $A' = C/k^2$ depend only on $k_\perp^2 = (k_x^2+k_y^2)$, $k_\parallel^2 = k_z^2$, and ω^2.

If the summetry is <u>spherical</u>, (i.e., the turbulence is <u>isotropic</u>), then G' = 0 and G is a function only of $|\underset{\sim}{k}|$. In this case,

$$P_{ij}(\underset{\sim}{k}) = A(|\underset{\sim}{k}|)(k^2\delta_i\delta_j - k_ik_j). \quad \text{(spherical symmetry)} \qquad (13)$$

I define the term <u>cylindrical symmetry</u> (about the z-axis) to mean that $P_{xx}(\underset{\sim}{k}) = P_{yy}(\underset{\sim}{k})$ for all $\underset{\sim}{k}$, which requires A = 0 via inspection in (12), leaving

$$P_{ij}(\underset{\sim}{k}) = A'(k_z^2, k_\perp^2 = k_x^2+k_y^2) \begin{pmatrix} k_z^2 & 0 & -k_xk_z \\ 0 & k_z^2 & -k_yk_z \\ -k_xk_z & -k_yk_z & k_\perp^2 \end{pmatrix} . \qquad (14)$$

(cylindrical symmetry)

The isotropic result was previously derived by Batchelor (1960), and the general result in the polar vector case was derived by Owens and Jokipii (1972) under the assumption that the power spectrum P_{ij} is symmetric under interchange of i and j.

If a <u>pseudovector</u>, such as the average magnetic field direction, is the vector describing the symmetry axis, one must use the results of Table A-2. From equations (1) and (4), with the symmetry factors of Table A-2 demonstrated explicitly, I obtain

$$[A+Bk^2+D(\underset{\sim}{k}\cdot\underset{\sim}{e})^2]k_j + [C\underset{\sim}{k}\cdot\underset{\sim}{e}+D'k^2\underset{\sim}{k}\cdot\underset{\sim}{e}]e_j$$
$$+i\,[-\omega I' - k^2J' - (k\cdot e)^2K'](\underset{\sim}{k}\times\underset{\sim}{e})_j = 0. \qquad (15)$$

Using these equations to eliminate B and D' (as above) and I', I obtain

$$(P_{ij})_{\text{axial vector}} = (P_{ij})_{\text{polar vector}} + i\omega \underset{\sim}{k}\cdot\underset{\sim}{e}\ \epsilon_{ijk} k_k H'$$

$$+ i\omega J' \left[-k^2\ \epsilon_{ijk}\ e_k + (\epsilon_{ik\ell} k_\ell - \epsilon_{jk\ell} k_i) k_k\ e_\ell\right] \qquad (16)$$

$$+ i\omega \underset{\sim}{k}\cdot\underset{\sim}{e} K' \left[-\underset{\sim}{k}\cdot\underset{\sim}{e}\ e_{ijk} + (\epsilon_{ik\ell} e_j - \epsilon_{jk\ell}\ e_i) k_k\ e_\ell\right],$$

where H', J', and K' are real functions of k^2, $(\underset{\sim}{k}\cdot\underset{\sim}{e})^2$, and ω^2.

It is instructive to compare the two results, given in equations (12) and (16), for true vector and pseudovector as the axis-defining vector. The polar vector result has two arbitrary functions in the power spectrum, a "spherically symmetric" function and a "cylindrically symmetric" function. The power spectrum is real and symmetric, and the result is the same as that which was obtained in the Appendix of Chapter III by a set of assumptions ignoring the pseudovector nature of the magnetic field. The pseudovector case allows the same two vector-like functions but permits as well three additional functions. The additional terms are imaginary, antisymmetric, and odd in frequency.

APPENDIX B

COSMIC-RAY DIFFUSION EQUATION

The solution to the general scintillation problem, presented in Chapter V, utilizes tools which can easily be applied to the derivation of the diffusion equation for cosmic rays in a stochastic magnetic field. Although this problem has previously been solved in various limits by the calculation of Fokker-Planck coefficients (Jokipii, 1966, Hasselmann and Wibberenz, 1968) and by a somewhat similar use of Liouville's equation (Hall, 1967, Hasselmann and Wibberenz, 1968), the present method is simpler and more straightforward.

Consider equation (V-5) from the text. Using the fact that $(\frac{\partial}{\partial \underset{\sim}{w}})\ (\underset{\sim}{w} x \underset{\sim}{\omega}_1) = 0$ and taking the Fourier transforms of $\underset{\sim}{\omega}_1$ and n_1, I have

$$\left[\frac{\partial}{\partial t} + \underset{\sim}{w}\cdot\frac{\partial}{\partial \underset{\sim}{x}} + (\underset{\sim}{w} x \underset{\sim}{\omega}_0)\cdot\frac{\partial}{\partial \underset{\sim}{w}}\right] n_0 = -\frac{1}{\omega_0}\frac{\partial}{\partial \underset{\sim}{w}}\cdot\left[\underset{\sim}{w} x \int \frac{d^3k\,d\omega}{(2\pi)^4}\int \frac{d^3k'\,d\omega'}{(2\pi)^4}\right. \tag{1}$$

$$\left.\langle \tilde{\underset{\sim}{\omega}}_1(\underset{\sim}{k},\omega)\ \tilde{n}_1(\underset{\sim}{k}',\omega')\rangle\right].$$

The solution for $\tilde{n}_1(\underset{\sim}{k},\omega)$ is given, in the general case, by equations (V-28) and (V-30). The fluctuating amplitude $\tilde{n}_1(\underset{\sim}{k},\omega)$ has terms of the form

$$\frac{1}{u + n} = \frac{1}{-\frac{k_{\parallel} w\mu}{\omega_0} + n - i\frac{\alpha_0}{\omega_0}} \tag{2}$$

in it, where $\varepsilon = \alpha_0/\omega_0 \lll 1$. When an integral over $k_{\parallel}$ is to be performed, the Plamelj formula yields

$$\frac{1}{u + n} \to \pi i \frac{\omega_0}{w|\mu|}\,\delta\left(k_{\parallel} - \frac{n\omega_0}{w\mu}\right). \tag{3}$$

Since ϵ is finite instead of arbitrarily small, the exact expression for equation (3) involves terms which differ from the $k_{\parallel} = n\omega_0/w\mu$ delta function by $\Delta k_{\parallel} \approx (\frac{\alpha_0}{\omega_0}) k_{\parallel}$; for $\epsilon \ll 1$ as required in the expansion, this makes no difference in the calculated diffusion coefficients unless the magnetic-field power spectrum has sharp peaks with width $\Delta k_B \lesssim \Delta k_{\parallel}$. The discussion here is the first to quantitatively discuss the criteria necessary for replacing equation (2) by (3) in the Liouville approach; the quasilinear limit $\alpha_0 \to 0$ was considered in previous derivations.

Equation (1) is linear in $\tilde{\underset{\sim}{\omega}}_1(\underset{\sim}{k},\omega)$, and from equation (V-28) one sees that $\tilde{n}_1(\underset{\sim}{k}',\omega')$ is linear in $\tilde{\underset{\sim}{\omega}}_1(\underset{\sim}{k}',\omega')$, so the terms on the right side of equation (1) involve

$$\langle \tilde{\omega}_{1i}(\underset{\sim}{k},\omega)\, \tilde{\omega}_{1j}(\underset{\sim}{k}',\omega') \rangle = (2\pi)^4\, \delta(\underset{\sim}{k}-\underset{\sim}{k}')\, \delta(\omega-\omega') P^{\omega}_{ij}(\underset{\sim}{k},\omega). \tag{4}$$

Here the Wiener-Khinchin theorem (equation II-10 generalized to four dimensions) has been used. The initial imaginary exponential term of I_1, I_2 and I_3 (equations V-30) can be expanded in a Bessel series,

$$e^{-ia \sin(\varphi-\beta)} = \sum_{m'=-\infty}^{\infty} e^{-im'(\varphi-\beta)} J_{m'}(a), \tag{5}$$

so that the equation for $\tilde{n}_1(\underset{\sim}{k},\omega)$ (see equations V-28 and V-30) becomes

$$\begin{aligned}\tilde{n}_1(\underset{\sim}{k},\omega) = \Big[\frac{1}{i}\Big] \sum_{m',m=-\infty}^{\infty} & J_m(a) J_{m'}(a) e^{i(m-m')(\varphi-\beta)} \Bigg(\frac{\tilde{\omega}_{1x}}{\omega_0} \Big[\frac{w\mu}{\omega_0} \frac{1}{u+m} \frac{\partial}{\partial x_0} \\ & + \frac{1}{2i}\Big(\frac{e^{i\varphi}}{u+m+1} - \frac{e^{-i\varphi}}{u+m-1}\Big) \sqrt{1-\mu^2}\, \frac{\partial}{\partial \mu}\Big] + \frac{\tilde{\omega}_{1y}}{\omega_0} \Big[\frac{w\mu}{\omega_0} \frac{1}{u+m} \frac{\partial}{\partial y_0} \\ & - \frac{1}{2}\Big(\frac{e^{i\varphi}}{u+m+1} + \frac{e^{-i\varphi}}{u+m-1}\Big) \sqrt{1-\mu^2}\, \frac{\partial}{\partial \mu}\Big] \\ & + \frac{\tilde{\omega}_{1z}}{\omega_0} \Big[\frac{1}{2} \frac{w\sqrt{1-\mu^2}}{\omega_0} \Big(\frac{e^{i\varphi}}{u+m+1} + \frac{e^{-i\varphi}}{u+m-1}\Big) \frac{\partial}{\partial x_0} - \frac{1}{2i} \frac{w\sqrt{1-\mu^2}}{\omega_0} \Big(\frac{e^{i\varphi}}{u+m+1} - \frac{e^{-i\varphi}}{u+m-1}\Big) \frac{\partial}{\partial y_0}\Big] \Bigg) n_0 .\end{aligned} \tag{6}$$

For concreteness, I assume that the magnetic-field fluctuations are cylindrically symmetric (equation A-14). Also, I assume (as in Chapter V) that $n_0(\underset{\sim}{x}_0, \underset{\sim}{w}, t)$ is a function of $\underset{\sim}{x}_0, w, \mu, t$, and not of the phase angle φ. I average equation (1) over φ and obtain

$$\left(\frac{\partial}{\partial t} + w\mu \frac{\partial}{\partial z}\right) n_0 = -\frac{\partial}{\partial s_k}\Bigg[\underbrace{\int_0^{2\pi}\frac{d\varphi}{2\pi}\int_0^{2\pi}\frac{d\beta}{2\pi}\int_0^{\infty}\frac{dk_\perp k_\perp}{2}\int_{-\infty}^{\infty} dk_\parallel C'_{ijk\ell} P^B_{ij}(\underset{\sim}{k},\omega)}_{D_{k\ell}}\Bigg]\frac{\partial n_0}{\partial s_\ell}, \qquad (7)$$

where the coefficients $C'_{ijk\ell}$ are determined from equations (1), (3), (4) and (6). The variables are $[s_i] = (x_0, y_0, \mu)$, and $D_{k\ell}$ are the diffusion coefficients.

The integrations indicated in equation (7) are straightforward. The φ and β integrals are of the form

$$\int_0^{2\pi}\frac{d\varphi}{2\pi} e^{in\varphi} = \delta_{n,0}$$

where $\delta_{i,j}$ is the Kronecker delta symbol.

The details of the calculation will not be presented here. The general result is

$$\frac{\partial n_0}{\partial t} + w\mu \frac{\partial n_0}{\partial z} = \frac{1}{2}\frac{\partial}{\partial \mu}\frac{\langle \Delta\mu^2\rangle}{\Delta t}\frac{\partial n_0}{\partial \mu} + \frac{1}{2}\frac{\partial}{\partial x_0}\frac{\langle \Delta x_\perp^2\rangle}{\Delta t}\frac{\partial n_0}{\partial x_0} + \frac{1}{2}\frac{\partial}{\partial y_0}\frac{\langle \Delta x_\perp^2\rangle}{\Delta t}\frac{\partial n_0}{\partial y_0}, \qquad (8)$$

where the "Fokker-Planck" diffusion coefficients are given by

$$\frac{\langle \Delta\mu^2\rangle}{\Delta t} = \frac{1}{2}\frac{1-\mu^2}{w|\mu|}\frac{q^2}{\gamma^2 m^2 c^2}\int_0^{\infty} k_\perp\, dk_\perp \sum_{m=-\infty}^{\infty} J_m^2\left(\frac{k_\perp w\sqrt{1-\mu^2}}{\omega_0}\right)$$
$$\left\{ P^B(k_\perp, k_\parallel = \frac{(m+1)\omega_0}{w\mu}) + P^B(k_\perp, k_\parallel = \frac{(m-1)\omega_0}{w\mu}) \right\} \qquad (9)$$

and

$$\frac{\langle \Delta x_\perp^2 \rangle}{\Delta t} = w|\mu| \int_0^\infty k_\perp \, dk_\perp \sum_{m=-\infty}^{\infty} J_m^2 \left(\frac{k_\perp w\sqrt{1-\mu^2}}{\omega_0}\right) \frac{P_\perp^B(k_\perp, k_\parallel = \frac{m\omega_0}{w\mu})}{B_0^2}$$

$$+ \frac{1}{4} w \frac{1-\mu^2}{|\mu|} \int_0^\infty k_\perp \, dk_\perp \sum_{m=-\infty}^{\infty} J_m^2 \left(\frac{k_\perp w\sqrt{1-\mu^2}}{\omega_0}\right) \left\{ \frac{P_\perp^B(k_\perp, k_\parallel = \frac{(m+1)\omega_0}{w\mu})}{B_0^2} \right. \tag{10}$$

$$\left. + \frac{P_{zz}^B(k_\perp, k_\parallel = \frac{(m-1)\omega_0}{w\mu})}{B_0^2} \right\} .$$

Here $P_\perp^B = P_{xx}^B = P_{yy}^B$. In the limit $k_\perp \to 0$, the Fokker-Planck coefficients become

$$\langle \frac{\Delta\mu^2}{\Delta t} \rangle = \frac{1-\mu^2}{w|\mu|} \frac{q^2}{\gamma^2 m^2 c^2} P_\perp^B(k_\parallel = \frac{\omega_0}{w\mu}) = \frac{1-\mu^2}{w|\mu|} \omega_0^2 \frac{P_\perp^B(k_\parallel = \frac{\omega_0}{w\mu})}{B_0^2} \tag{11}$$

$$\langle \frac{\Delta x_\perp^2}{\Delta t} \rangle = w|\mu| \frac{P_\perp^B(k_\parallel = 0)}{B_0^2} \tag{12}$$

as given by Jokipii (1971) (noting $P_{zz} = 0$ in this limit).

APPENDIX C

RESONANCE WIDTH FROM NON-LINEAR PLASMA THEORY

In this Appendix, I present an analytic method for calculating the width of the cyclotron resonance, α_0 in the notation of Chapter V, correct through order $(\omega_1/\omega_0)^2$. This analytic method leads to an explicit equation for the non-linear operator $\hat{\alpha}$ (equation 6), and the equation is solved approximately, assuming that the ensemble-average part of the non-linear terms dominates. The result is a wavenumber-dependent resonance width $\epsilon_3(k) = \frac{\langle\hat{\alpha}\rangle}{\omega_0}$ which has a peak near the cyclotron resonance ($k_{\|} w\mu = \omega_0$) and falls off for non-resonant k's. The analysis indicates that the estimates ϵ_1 and ϵ_2 (equations V-58 and V-61) are a factor of ~2 too low near the resonance.

For simplicity, I assume that the fluctuations in the magnetic field and the cosmic rays are characterized as wavenumber fluctuations propagating along the average magnetic field direction (i.e., the $k_{\perp} \to 0$ limit as in Section V.D). Further, I assume that $n_0(\underset{\sim}{x},\underset{\sim}{w},t)$ depends only on pitch-angle, or $n_0 = n_0(\mu)$, as in Chapter IV. Then the <u>exact</u> expression for the perturbed cosmic-ray distribution function, equation (V-6), can be Fourier-transformed to yield

$$\left[-ikw\mu - \omega_0 \frac{\partial}{\partial\varphi}\right] \tilde{n}_1(k) = -w_i\, \epsilon_{ij\ell}\, \tilde{\omega}_{1j}(k)\, \frac{\partial n_0}{\partial w_\ell}$$
$$-w_i\, \epsilon_{ij\ell} \int_{-\infty}^{\infty} \frac{dk'}{2\pi}\, \tilde{\omega}^*_{1j}(k'-k)\, \frac{\partial \tilde{n}_1(k')}{\partial w_\ell} + w_i \epsilon_{ij\ell}\, \delta(k) \left\langle \underset{\sim}{\omega}_{1j} \frac{\partial n_1}{\partial w_\ell} \right\rangle . \qquad (1)$$

Here the notation of Section V.A is used, with $k = k_{\|}$. For wave-

numbers $k \neq 0$, the last term does not contribute and thus will be ignored.

Rudakov and Tsytovich (1971) have considered an analogous problem of the non-linear contribution to the diffusion equation for a plasma with a random electric field. Following their suggestion, I introduce on both sides of equation (1) an effective collision-frequency term

$$\hat{\nu}_k \, \tilde{n}_1(k,\underset{\sim}{w}),$$

where $\hat{\nu}_k$ is a function of k and operates on the velocity dependence of $\tilde{n}_1$ in a manner determined below. The resulting expression, for $k \neq 0$, is

$$\begin{aligned}[-ikw\mu - \omega_0 \frac{\partial}{\partial\varphi} + \hat{\nu}_k] \, \tilde{n}_1(k,\underset{\sim}{w}) &= -w_i \, \epsilon_{ij\ell} \tilde{\omega}_{1j}(k) \frac{\partial n_0}{\partial w_\ell} \\ &+ \hat{\nu}_k \, \tilde{n}_1(k,\underset{\sim}{w}) - w_i \, \epsilon_{ij\ell} \int_{-\infty}^{\infty} \frac{dk'}{2\pi} \, \tilde{\omega}^*_{1j}(k'-k) \frac{\partial \tilde{n}_1(k')}{\partial w_\ell} .\end{aligned} \tag{2}$$

One <u>formally</u> defines the inverse operator $\hat{g}_k$ by

$$\hat{g}_k[-ikw\mu - \omega_0 \frac{\partial}{\partial\varphi} + \hat{\nu}_k] \, \tilde{n}_1(k,\underset{\sim}{w}) = \tilde{n}_1(k,\underset{\sim}{w}), \tag{3}$$

so that the formal solution to equation (2) is

$$\begin{aligned}\tilde{n}_1(k,\underset{\sim}{w}) = \hat{g}_k \, [&-w_i \, \epsilon_{ij\ell} \, \tilde{\omega}_{1j}(k) \frac{\partial n_0}{\partial w_\ell} + \hat{\nu}_k \, \tilde{n}_1(k,\underset{\sim}{w}) \\ &-w_i \, \epsilon_{ij\ell} \int_{-\infty}^{\infty} \frac{dk'}{2\pi} \, \omega_{1j}{}^* (k'-k) \frac{\partial \tilde{n}_1(k')}{\partial w_\ell}] .\end{aligned} \tag{4}$$

The plan is to solve equation (2) by inserting the formal solution of equation (4) into the right-hand side of equation (2) and then choosing the form of the arbitrary operator to eliminate the

$\tilde{n}_1$-dependence of the terms on the right-hand side of the equation. Using the solution (4) for $\tilde{n}_1$ in the last term of equation (2), I get

$$\underset{①}{[-ikw\mu} - \underset{①}{\omega_0 \frac{\partial}{\partial\varphi}} + \underset{③}{\hat{\nu}_k}] \tilde{n}_1(k,\underset{\sim}{w}) = \underset{①}{-w_i\, \epsilon_{ij\ell}\, \tilde{\omega}_{1j}(k)\, \frac{\partial n_0}{\partial w_\ell}}$$

$$+ \underset{③}{\hat{\nu}_k\, \tilde{n}_1(k,w)} - w_i\, \epsilon_{ij\ell} \int_{-\infty}^{\infty} \frac{dk'}{2\pi} \tilde{\omega}^*_{1j}(k-k') \frac{\partial}{\partial w_\ell} \tag{5}$$

$$\left\{ \hat{g}_{k'} [\underset{②}{-w_i \epsilon_{ij\ell} \tilde{\omega}_{1j}(k') \frac{\partial n_0}{\partial w_\ell}} + \underset{④}{\hat{\nu}_{k'} \tilde{n}_1(k',\underset{\sim}{w})} + \underset{③}{w_{i'} \epsilon_{i'j'\ell'} \int_{-\infty}^{\infty} \frac{dk''}{2\pi} \tilde{\omega}_{1j'}(k'-k'') \frac{\partial \tilde{n}_1(k'')}{\partial w_{\ell'}}}] \right\} .$$

As shown by dimensional analysis in Section V.A, $\tilde{n}_1$ is of order 1 and $\hat{\alpha}$ (hence $\hat{\nu}_k$) is of order 2 in the small perturbation ω_1. Away from the cyclotron resonance, $\hat{g}_k$ is of order 0 in the smallness parameter. In the various terms of equation (5), the circled numbers represent the order in ω_1. I now <u>choose</u> $\hat{\nu}_k$ so that the highest-order terms involving $\tilde{n}_1(k,\underset{\sim}{w})$ on the right side cancel, or

$$\hat{\nu}_k \tilde{n}_1(k,\underset{\sim}{w}) = \frac{\partial}{\partial w_\ell} w_i \epsilon_{ij\ell} \int_{-\infty}^{\infty} \frac{dk''}{2\pi} \int_{-\infty}^{\infty} \frac{dk'}{2\pi} \tilde{\omega}^*_{1j}(k-k')\, \tilde{\omega}_{1j'}(k'-k'')\, \hat{g}_{k'}$$

$$\cdot\, w_{i'}\, \epsilon_{i'j'\ell'}\, \frac{\partial \tilde{n}_1(k'')}{\partial w_{\ell'}} . \tag{6}$$

With this definition, keeping only the lowest-order terms on each side of equation (5), one has

$$[-ikw\mu - \omega_0 \frac{\partial}{\partial\varphi} + \hat{\nu}_k]\tilde{n}_1(k,\underset{\sim}{w}) = + \tilde{\omega}_{1x}(k) \sqrt{1-\mu^2}\, \sin\varphi\, \frac{\partial n_0}{\partial \mu}$$

$$- \tilde{\omega}_{1y}(k) \sqrt{1-\mu^2}\, \cos\varphi\, \frac{\partial n_0}{\partial \mu} \tag{7}$$

in the notation of Section V.A.

Equations (6) and (7) give a self-consistent set of equations for the perturbed distribution function $\tilde{n}_1$ and the resonance width $\hat{\nu}_k$ in terms of the magnetic-field fluctuations $\tilde{\omega}_1$ and the pitch-angle derivative of the average distribution function. The equations are correct to lowest non-vanishing order in ω_1. The non-linear "damping" or "scattering" term $\hat{\nu}_k$ is the lowest-order non-vanishing part of the exact operator $\hat{\alpha}$ of equation (V-6). The damping operator is non-local, since it relates fields and particles with different wavenumbers, and it is stochastic.

Since the operator enters into the deterministic "particle propagator" $\hat{g}_k$, it is often <u>assumed</u> (Rudakov and Tsytovich, 1971, Thomson and Benford, 1972a, 1972b) that the dominant contribution comes from the <u>ensemble-averaged</u> part of $\hat{\nu}_k$. That is, one assumes that in equation (7) the term $\hat{\nu}_k \tilde{n}_1$ can be replaced by $\langle \hat{\nu}_k \rangle \tilde{n}_1$. This is merely an assumption, and it does not appear possible to check the validity of the assumption on theoretical or even <u>a posteriori</u> grounds. If only the ensemble average $\langle \hat{\nu}_k \rangle$ is important in equation (7), then the particle propagator $\hat{g}_k$ is non-stochastic also. Using this fact, the Wiener-Khinchin theorem, and taking the ensemble average of the operator $\hat{\nu}_k$ as given in equation (6), I obtain

$$\langle \hat{\nu}_k \rangle \tilde{n}_1(k,\underset{\sim}{w}) = \frac{\partial}{\partial w_\ell}\left[w_i \epsilon_{ij\ell} \omega_0^2 \left\{ \int_{-\infty}^{\infty} \frac{dk'}{2\pi} \frac{P^B_{jj'}(k'-k)}{B_0^2} \hat{g}_{k'} \right\} w_{i'} \epsilon_{i'j'\ell'}\right] \frac{\partial}{\partial w_{\ell'}} \tilde{n}_1(k,\underset{\sim}{w}). \quad (8)$$

Equation (8) shows that the introduction of an effective collision operator $\hat{\nu}_k$ leads to a diffusion term in velocity space for the Fourier componants of the perturbed particle distribution. The

"diffusion coefficients" for $\tilde{n}_1$ are enclosed in brackets in equation (8). In the $k_\perp \to 0$ limit considered here, the assumption of axial symmetry of the magnetic field about the average direction implies (see Appendix A) that the only non-zero componants of $P^B_{ij}(k)$ are $P^B_{xx}(k)=P^B_{yy}(k)\equiv P^B_\perp(k)$. Also, as shown in Chapter V and Appendix B, for $\langle\hat{\nu}_k\rangle \ll \omega_0$ the particle propagator $\hat{g}_k$ becomes a sum of delta functions at the cyclotron frequencies, or

$$\hat{g}_k \equiv \left[-ikw\mu - \omega_0 \frac{\partial}{\partial\varphi} + \langle\hat{\nu}_k\rangle\right]^{-1} \to \frac{\pi}{2}\left[\delta(kw\mu+\omega_0) + \delta(kw\mu-\omega_0)\right], \qquad (9)$$

to lowest order in ω_1. Applying these results to equation (8), I obtain an expression for the scattering term,

$$\langle\hat{\nu}_k,\rangle\tilde{n}_1(k,\underset{\sim}{w}) = \frac{\partial}{\partial\mu}(1-\mu^2)A_k \frac{\partial\tilde{n}_1(k,\underset{\sim}{w})}{\partial\mu} + \frac{\partial}{\partial\varphi}\frac{\mu^2}{1-\mu^2}A_k \frac{\partial n_1(k,\underset{\sim}{w})}{\partial\varphi}\ , \qquad (10)$$

where

$$A_k = \frac{1}{2}\frac{\omega_0^2}{w|\mu|}\left[\frac{P^B_\perp(k-\frac{\omega_0}{w\mu})}{B_0^2} + \frac{P^B_\perp(k+\frac{\omega_0}{w\mu})}{B_0^2}\right]\ . \qquad (11)$$

In the $k_\perp = 0$ limit, the result of the analysis in this Appendix is expressed in equation (7), with $\hat{\nu}_k \to \langle\hat{\nu}_k\rangle$, and equations (10) and (11). Given the magnetic-field power spectrum and the average distribution function, the result is a partial differential equation in the two velocity coordinates μ and φ, with wavenumber entering as a parameter.

Because of the complexity of the partial differential equation for $\tilde{n}_1$ given by the analysis above, I will solve the equations approximately by considering only the dominant terms. If $\langle\hat{\nu}_k\rangle \ll \omega_0$, $\langle\hat{\nu}_k\rangle$ can be treated as a small perturbing constant in

equation (7), and the resulting equation can be solved for $\tilde{n}_1$. This is the approach used in Section V.A. For non-resonant k, or k farther than $\langle\hat{\nu}_k\rangle/w$ from $\pm\omega_0/w\mu$, it can be seen from the results of that discussion (e.g., let $k_\perp = 0$ in equation V-28) that

$$\frac{\partial\tilde{n}_1}{\partial\mu} \sim \frac{\partial\tilde{n}_1}{\partial\varphi} \sim \tilde{n}_1. \qquad \text{(non-resonant k)}$$

Thus, from equation (10), one has

$$\langle\hat{\nu}_k\rangle \approx A_k. \qquad \text{(non-resonant k)} \tag{12}$$

Near a resonance, for example $kw\mu \approx \omega_0$, the dominant terms in the equation for $\tilde{n}_1$ are of the form

$$\tilde{n}_1 \approx \frac{\tilde{\omega}_{1x}(k)}{\omega_0}\sqrt{1-\mu^2}\; e^{i\varphi}\left\{\frac{\omega_0}{-kw\mu+\omega_0-i\langle\hat{\nu}_k\rangle}\right\}\frac{\partial n_0}{\partial\mu}$$

so that the dominant contribution to the pitch-angle derivative $\partial\tilde{n}_1/\partial\mu$ comes from the term in parentheses, to give

$$\frac{\partial\tilde{n}_1}{\partial\mu} \approx \left(\frac{kw}{-kw\mu+\omega_0-i\langle\hat{\nu}_k\rangle}\right)\tilde{n}_1 \sim \frac{\omega_0}{\langle\hat{\nu}_k\rangle}\tilde{n}_1. \qquad \text{(resonant k)}$$

From this relation and equation (10), it follows that

$$\langle\hat{\nu}_k\rangle \approx \frac{\omega_0^{\,2}}{\langle\nu_k\rangle^2}A_k,$$

or

$$\langle\hat{\nu}_k\rangle \approx [\omega_0^{\,2}A_k]^{1/3}. \qquad \text{(resonant k)} \tag{13}$$

As in Chapter V, I define the smallness parameter ϵ by

$$\epsilon_3 \equiv \langle \hat{\nu}_k \rangle / \omega_0 . \tag{14}$$

An expression for ϵ_3 which is valid for both resonant (equation 13) and non-resonant (equation 12) k is

$$\epsilon_3 = \frac{\epsilon_0}{2} \left[\frac{\epsilon_0^2 (k^2 + \frac{\omega_0^2}{w^2\mu^2})}{(k - \frac{\omega_0}{w\mu})^2 + \epsilon_0^2 \frac{\omega_0^2}{w^2\mu^2}} + \frac{\epsilon_0^2 (k^2 + \frac{\omega_0^2}{w^2\mu^2})}{(k + \frac{\omega_0}{w\mu})^2 + \epsilon_0^2 \frac{\omega_0^2}{w^2\mu^2}} \right] \tag{15}$$

where

$$\epsilon_0 \equiv \left(\frac{A_k}{\omega_0} \right)^{1/3} = \left[\frac{1}{2} \frac{\omega_0}{w|\mu|} \frac{P_\perp^B (k - \frac{\omega_0}{w\mu}) + P_\perp (k + \frac{\omega_0}{w\mu})}{B_0^2} \right]^{1/3} . \tag{16}$$

Equations (15) and (16) give the value of the resonance width $\epsilon_3 \equiv \langle \hat{\nu}_k \rangle / \omega_0$ obtained by an approximate solution to equations (7) and (10). Better approximations for the resonance width may be obtained from a more rigorous solution of these equations, but the present method is adequate to indicate the structure of the result. The point is that ϵ_3 is a function of wavenumber k. It will be shown below that $\epsilon_3(k)$ is peaked near the resonant wavenumber, first because near resonance (equation 13) the width goes as $A_k^{1/3}$, where A_k is a small quantity, and also because A_k itself has a maximum near resonant k since the magnetic-field power spectrum has a maximum at zero wavenumber (see equation 11). Since a broader resonance width tends to smear out the effect of the cyclotron resonance, it is of interest to interpret this result physically.

The "smoothing out" of the cyclotron resonance in the cosmic-ray scintillations power spectrum can be understood in terms of the scattering of cosmic rays in a turbulent magnetic field. The cosmic-ray

scintillations are caused by particles being guided along the magnetic-field lines which are fluctuating. For cosmic rays near resonance, the interaction is intensified and the particles have a large increment of fluctuation induced for each increment of time spent in the near-resonant region of phase space. However, particles in the resonant region of phase space are scattered rapidly, so that their "collision frequency" $\langle \hat{\nu}_k \rangle$ is large. Non-resonant particles have scintillations which build up more slowly, but the typical non-resonant particle spends more time moving in phase with the magnetic fluctuation before being scattered away. Near-resonant particles have fluctuations growing at a faster rate, but due to scattering each near-resonant particle spends a shorter time being accelerated by a given magnetic-field irregularity. Thus, there are two competing effects which are acting: the strength of the interaction, and the time a typical particle spends being acted upon before scattering to another region of space.

Consider now cosmic-ray scintillations in interplanetary space, as discussed in Section V.E. The fluctuations, which are static structures in the plasma's frame of reference, are being convected past a stationary observer by the solar wind. The wavenumber fluctuations then become temporal fluctuations with frequency given by

$$f = (V_w \cos\psi/2\pi)k \qquad (17)$$

in the notation of Chapter V. The only change which the results in this Appendix imply to the results of Chapter V is that the resonance integrals χ_0 and χ_1 (equations V-48b and V-48c) have a frequency-dependent resonance width $\langle \hat{\nu} \rangle$ given by equations (15) and (16), with k

replaced by f as in equation (17).

In order to demonstrate the effect of the new estimate ϵ_3 of the resonance width on the theoretical cosmic-ray scintillations power spectrum, I give in Fig. C-1 the resonance width $\epsilon_3(f)$ as a function of frequency, calculated from equations (15) and (16). The parameters used are for 2 GeV protons near earth, with the magnetic-field power spectrum $P_{\perp}^{B}(f) = P_{\theta\theta}^{B}(f)$ given by Jokipii and Coleman (1968). Also shown is the estimate $\epsilon_2 = 0.15$ taken from Fig. V-2. It can be seen that $\epsilon_3(f)$ has a sharp maximum at the convected cyclotron-resonant frequency (f_0). This maximum will tend to decrease the effect of the resonant interaction over that estimated using ϵ_2 as in Chapter V. This effect is shown in Fig. C-2, where the resonance function

$$R_2(k) = \frac{1}{2}\left[\frac{\omega_0^2}{(kw+\omega_0)^2+\alpha_0^2} + \frac{\omega_0^2}{(kw-\omega_0)^2+\alpha_0^2}\right] \qquad (18)$$

corresponding to equation (V-42c) for particles with the pitch-angle $\mu = 1$ is plotted. The two estimates of the resonance width α_0 given by $\alpha_0 = \epsilon_2\omega_0 = 0.15\omega_0$ and $\alpha_0' = \epsilon_3(f)\omega_0$ were used, as indicated, and the values of $\epsilon_3(f)$ were taken from Fig. C-1. The height of the resonance peak using ϵ_3 is about $\frac{1}{4}$ that obtained using $\epsilon_2 = 0.15$.

In general, from equation (18), $R_2 \propto \epsilon^{-2}$ near resonance. As can be seen in Fig. V-1, the important resonance integral χ_1 has an amplitude of enhancement near resonance which is approximately proportional to ϵ^{-1}. In Fig. C-3, I give the resonance width ϵ_3 <u>on resonance</u> ($f = f_0 \equiv \omega_0 V_w \cos\psi/2\pi w$), calculated from equations (11) and (13), as a function of energy for protons near earth. Also plotted is

Figure C-1: Resonance width $\varepsilon_3(f)$ for 2 GeV protons. The width $\varepsilon_3(f)$ calculated from equations (15) and (16) is plotted as a function of frequency for ~2 GeV protons near earth. The resonant frequency $f_0=2.1 \times 10^{-5}$Hz. The estimate $\varepsilon_2 = 0.15$, taken from Fig. V-2, is shown as the dashed line. Note that $\varepsilon_3(f)$ has a sharp peak at $f = f_0$ and exceeds ε_2 near the resonance.

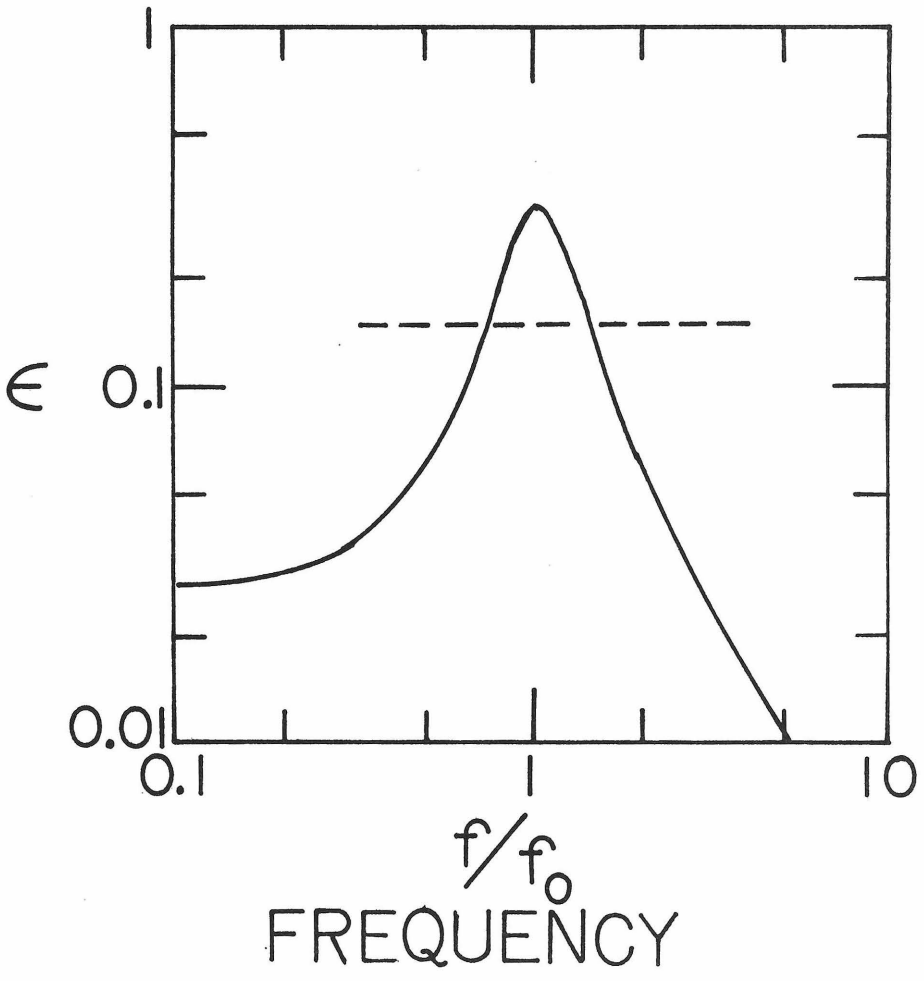
1
ϵ
0.1
0.01
0.1
1
10
f/f0
FREQUENCY

Figure C-2: The resonance function $R_2(k)$. $R_2(k)$, as given by equation (18), is plotted as a function of $\eta = kw/\omega_0$. The solid curve uses $\alpha_0 = \varepsilon_1\omega_0 = 0.15\omega_0$. The dashed curve uses $\alpha_0' = \varepsilon_3\omega_0$, where $\varepsilon_3(f)$ is taken from Fig. C-1.

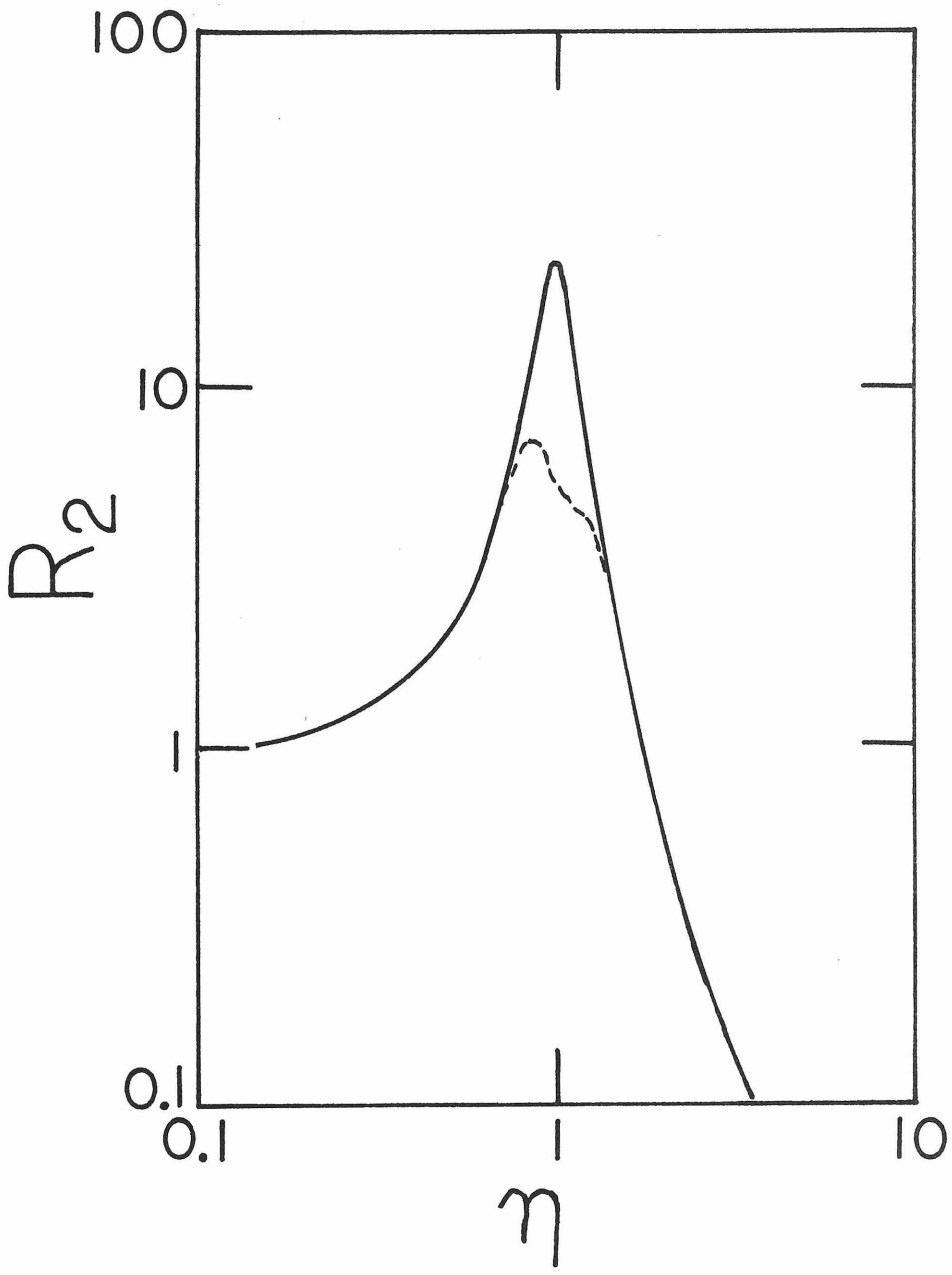
100
10
1
0.1
R_2
0.1
1
10
η

Figure C-3: Resonance width $\varepsilon_3(f)$ on resonance. The width $\varepsilon_3(f)$ at the resonant frequency $f = f_0$ is plotted in the upper curve as a function of proton energy for typical conditions near earth. The lower curve is the estimate $\varepsilon_2(T)$ from Fig. V-2. Note that $\varepsilon_3(f) \gtrsim 2\varepsilon_2$.

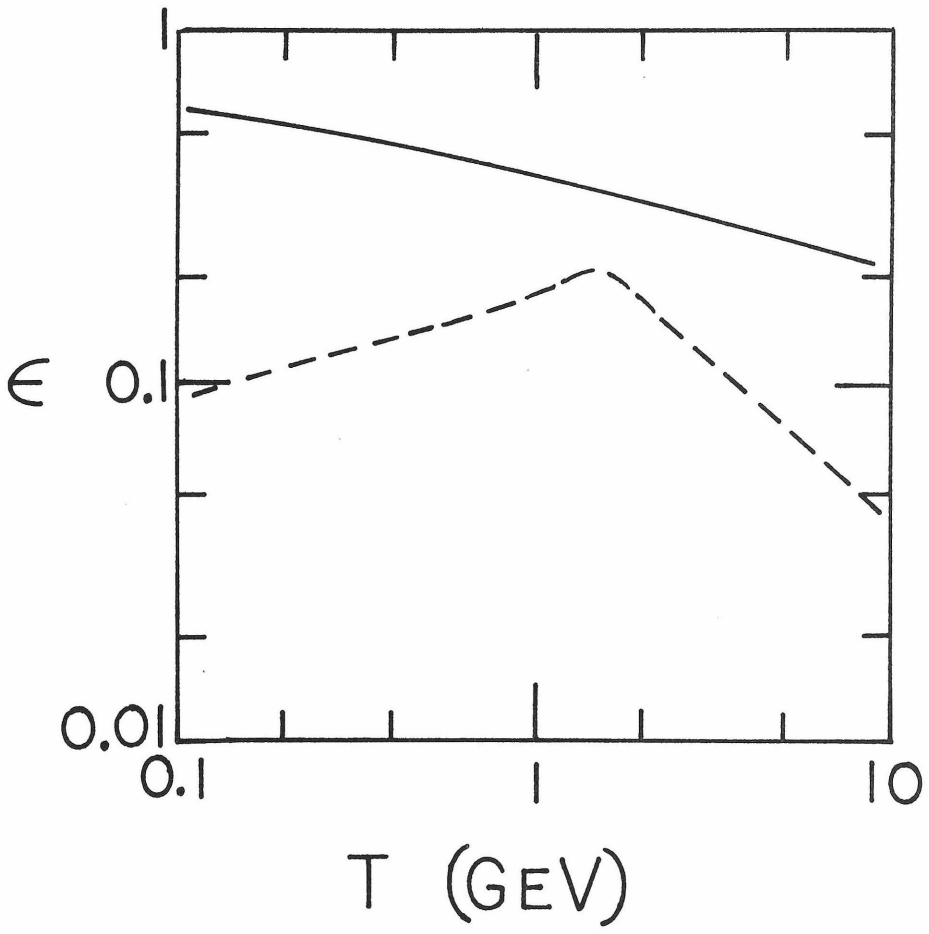
1
ϵ 0.1
0.01
0.1
1
10
T (GEV)

the estimate ϵ_2 used in Chapter V. Since ϵ_3 (on resonance) $\gtrsim 2\epsilon_2$ for the particles (0.5 GeV $\lesssim$ T $\lesssim$ 10 GeV) which contribute most to high-latitude neutron-monitor fluxes, the proportionality of χ_1 to ϵ^{-1} indicates that the resonance width obtained in this Appendix will lead to a peak enhancement near the cyclotron resonance which is smaller by a factor of ~2 than the results obtained in Chapter V. In Fig. V-4, for example, the solid curve (corresponding to the amplitude ratio Amp(f) between the relative neutron-monitor scintillations and the relative interplanetary magnetic-field fluctuations) has the cyclotron peak higher than "background" ($f \lesssim 10^{-5}$Hz) by a factor of ~3. The discussion here indicates that a more precise estimate of this excursion is about a factor of $1\frac{1}{2}$, placing the theory of Chapter V within 50% of the result of the simplified low-frequency limit (Chapter IV) for <u>all</u> frequencies $f \lesssim 10^{-4}$Hz.

The investigation in this Appendix indicates that the non-linear terms in the equation for $\tilde{n}_1$ can, under a reasonable set of assumptions, be taken into account to lowest non-vanishing order by introducing an effective collision-frequency term into equation (1). The resulting equations (7) and (10) can be solved approximately to obtain an estimate of the value of $\langle\hat{\nu}_k\rangle$. This non-linear term then becomes the resonance width α_0 in the notation of Chapter V, and the entire analysis of Chapter V proceeds as before. The only change is that $\langle\hat{\nu}_k\rangle$ is a function of frequency which has a maximum precisely at the cyclotron resonance. The maximum of the resonance width at the cyclotron frequency tends to cancel the effect of the cyclotron resonance, leading to a somewhat smoother power spectrum near resonance than

indicated in Chapter V. As the non-linear terms are considered in greater detail, the result becomes nearer to the simple low-frequency limit of Chapter IV. Thus, for neutron monitors and other detectors which respond to a wide band of energies near 1 GeV, a quantitative consideration of the non-linear particle-wave interactions near the cyclotron resonance indicates that the simple low-frequency limit of Chapter IV gives predictions which are accurate to within 50% for all frequencies up to and even somewhat above 10^{-4}Hz. The fact that the observations (see Fig. IV-3 and IV-5) are in agreement with the low-frequency limit's prediction for frequencies up to 10^{-4}Hz gives evidence that the method discussed here for including the non-linear terms in the scintillation equations is basically correct.

REFERENCES

J. G. Ables, "Persistent and Transient Anisotropies of the Cosmic Radiation", Ph.D. Thesis, Oklahoma State University, Stillwater, Oklahoma, (1967).

H. R. Anderson, "The Radial Gradient of Cosmic Radiation Measured by Mariners 2 and 4", Journal of Geophysical Research, 73, 2897, (1968).

V. K. Balasubrahmanyar, G. H. Ludwig, F. B. McDonald and R. A. R. Palmeira, "Results from the Imp 1 GM Counter Telescope Experiment", Journal of Geophysical Research, 70, 2005, (1965).

G. K. Batchelor, "The Theory of Axisymmetric Turbulence", Proceedings, Royal Society of London, A, 186, 480, (1946).

G. K. Batchelor, The Theory of Homogeneous Turbulence, Cambridge University Press, Cambridge, Mass., (1960).

J. W. Belcher and L. Davis, Jr., "Large-Amplitude Alfvén Waves in the Interplanetary Medium, 2", Journal of Geophysical Research, 76, 3534, (1971).

J. W. Belcher, L. Davis, Jr., and E. J. Smith, "Large-Amplitude Alfvén Waves in the Interplanetary Medium: Mariner 5", Journal of Geophysical Research, 74, 2302, (1969).

J. S. Bendat and A. G. Piersol, Measurement and Analysis of Random Data, John Wiley and Sons, New York, (1966).

R. B. Blackman and J. W. Tukey, The Measurement of Power Spectra, Dover Publications, Inc., New York, (1958).

G. Booth, "I.Q.S.Y. Stations" in Annals of the International Quiet Sun Year, VII, M.I.T. Press, Cambridge, Mass., (1970).

P. J. Coleman, Jr., "Variations in the Interplanetary Magnetic Field: Mariner 2, Observed Properties", Journal of Geophysical Research, 71, 5509, (1966).

P. J. Coleman, Jr., "Turbulence, Viscosity, and Dissipation in the Solar-Wind Plasma", Astrophysical Journal, 153, 371, (1968).

A. H. Compton and I. A. Getting, "An Apparent Effect of Galactic Rotation on the Intensity of Cosmic Rays", Physical Review, 47, 817, (1935).

M. S. Dhanju and V. A. Sarabhai, "Short-Period Variations of Cosmic-Ray Intensity", Physical Review Letters, 19, 252, (1967).

M. S. Dhanju and V. A. Sarabhai, "Short-Period Fluctuations of Cosmic Ray Intensity at Geomagnetic Equator and their Solar Terrestrial Relationship", Journal of Geophysical Research, 75, 1795, (1970).

J. E. Earl, "Diffusion of Charged Particles in a Random Magnetic Field", Astrophysical Journal, 180, 227, (1973).

L. C. Evans, "Magnetospheric Access of Solar Particles and the Configuration of the Distant Geomagnetic Field", Ph.D. Thesis, California Institute of Technology, Pasadena, California, (1972).

L. A. Fisk and J. W. Sari, Journal of Geophysical Research, to be published, (1973).

M. A. Forman, "The Compton-Getting Effect for Cosmic-Ray Particles and Photons and the Lorentz-Invariance of Distribution Functions", Planetary Space Science, 18, 25, (1970).

V. L. Ginzberg, "Origin of Cosmic Rays. I. Introduction. Metagalactic Models", Comments on Astrophysics and Space Physics, 1, 1, (1969).

V. L. Ginzberg, "Origin of Cosmic Rays. II. The Halo Problem. Galactic Models", Comments on Astrophysics and Space Physics, 2, 43, (1970).

V. L. Ginzberg and S. I. Syrovatskii, The Origin of Cosmic Rays, Pergamon Press, New York, (1964).

L. J. Gleeson and W. I. Axford, "Solar Modulation of Galactic Cosmic Rays", Astrophysical Journal, 154, 1011, (1968).

L. J. Gleeson, S. M. Krimigis and W. I. Axford, "Low-Energy Cosmic Rays Near Earth", Journal of Geophysical Research, 76, 2228, (1971).

G. Gloeckler and J. R. Jokipii, "Solar Modulation and Energy Density of Galactic Cosmic Rays", Astrophysical Journal (Letters), 148, L41, (1967).

D. E. Hall, "A Test-Particle Analysis of Plasma Turbulence in Astrophysics", Ph.D. Thesis, Stanford University, (1967).

D. E. Hall and P. A. Sturrock, "Diffusion, Scattering and Acceleration of Particles by Stochastic Electromagnetic Fields", Physics of Fluids, 12, 2620, (1967).

K. Hasselmann and G. Wibberenz, "Scattering of Charged Particles by Random Electromagnetic Fields", Zeitschrift für Geophysik, 34, 353, (1968).

R. E. Holtzer, M. G. McLeod and E. J. Smith, "Preliminary Results from the OGO I Search Coil Magnetometer; Boundary Positions and Magnetic Noise Spectra", Journal of Geophysical Research, 71, 1827, (1966).

J. R. Jokipii, "Cosmic-Ray Propagation, I. Charged Particles in a Random Magnetic Field", Astrophysical Journal, 146, 480, (1966).

J. R. Jokipii, "Addendum and Erratum to Cosmic-Ray Propagation I", Astrophysical Journal, 152, 671, (1968).

J. R. Jokipii, "Stochastic Variations of Cosmic Rays in the Solar System", Astrophysical Journal, 156, 1107, (1969).

J. R. Jokipii, "On the 'Thin Screen' Model of Interplanetary Scintillations", Astrophysical Journal, 161, 1147, (1970).

J. R. Jokipii, "Propagation of Cosmic Rays in the Solar Wind", Review of Geophysical and Space Physics, 9, 27, (1971).

J. R. Jokipii, "Fokker-Planck Equations for Charged-Particle Transport in Random Fields", Astrophysical Journal, 172, 319, (1972).

J. R. Jokipii and P. J. Coleman, Jr., "Cosmic-Ray Diffusion Tensor and Its Variation Observed with Mariner 4", Journal of Geophysical Research, 73, 5495, (1968).

J. R. Jokipii and E. N. Parker, "Energy Changes of Cosmic Rays in the Solar System", Planetary Space Science, 15, 1375, (1967).

F. B. McDonald, T. L. Cline and G. M. Simnett, "Multifarious Temporal Variations of Low-Energy Relativistic Cosmic-Ray Electrons", Journal of Geophysical Research, 77, 2213, (1972).

A. J. Owens and J. R. Jokipii, "Cosmic-Ray Scintillations I. Inside the Magnetosphere", Journal of Geophysical Research, 77, 6639, (1972).

A. J. Owens and J. R. Jokipii, "Interplanetary Scintillations of Cosmic Rays", Astrophysical Journal (Letters), 181, L147, (1973).

E. N. Parker, Interplanetary Dynamical Processes, Interscience Publishers, New York, (1963).

J. J. Quenby and J. F. Sear, "Interplanetary Magnetic Field Fluctuation Measurements and the Long Term Modulation", 12th International Conference on Cosmic Rays, Hobart, Tasmania, Aug. 1971, Paper MOD-64.

B. Rossi, Cosmic Rays, McGraw-Hill, Inc., New York, (1964).

L. I. Rudakov and V. N. Tsytovich, "The Theory of Plasma Turbulence for Strong Wave-Particle Interaction", Plasma Physics, 13, 213, (1971).

T. A. Rygg and J. A. Earl, "Balloon Measurements of Cosmic Ray Protons and Helium Over Half a Solar Cycle 1965-1969", Journal of Geophysical Research, 76, 7445, (1971).

E. E. Salpeter, "Interplanetary Scintillations, I. Theory", Astrophysical Journal, 147, 433, (1967).

M. A. Shea, Private Communication, (1972).

M. A. Shea, D. F. Smart and K. G. McCracken, "A Study of Vertically Incident Cosmic-Ray Trajectories Using Sixth-Degree Simulations of the Geomagnetic Field", Environmental Research Papers, No. 141, Air Force Cambridge Research Laboratories, Bedford, Mass., (1965).

G. L. Siscoe and J. R. Jokipii, Private Communication, (1966).

G. L. Siscoe, L. Davis, Jr., P. J. Coleman, Jr., E. J. Smith and D. L. Jones, "Power Spectra and Discontinuities of the Interplanetary Magnetic Field: Mariner 4", Journal of Geophysical Research, 73, 61, (1968).

J. R. Steljes, "Cosmic Ray NM-64 Neutron Monitor Data XIV", AECL-3560, Atomic Energy of Canada, Ltd., Chalk River, Ontario, (1970).

S. I. Syrovatskii, "Cosmic Rays of Ultra-High Energy", Comments on Astrophysics and Space Physics, 3, 155, (1971).

H. Theil, Principles of Econometrics, John Wiley and Sons, Inc., New York, (1971).

J. J. Thomson and G. Benford, "Turbulent Diffusion in Phase Space", Physical Review Letters, 28, 590, (1972a).

J. J. Thomson and G. Benford, "Probabilistic Model of Plasma Turbulence", University of California - Irvine, Department of Physics, Technical Report No. 72-4, to be published, (1972b).

J. M. Wilcox and N. F. Ness, "Quasi-Stationary Corotating Structure in the Interplanetary Medium", Journal of Geophysical Research, 70, 5793, (1965).

D. J. Williams, "Solar Proton Observations, 1-10 MeV", in Proceedings of the Seminar on Interplanetary Physics Using Cosmic Rays, A. I. Ioffe Physical Technical Institute, Leningrad, USSR, (1969).

A. M. Yaglom, An Introduction to the Theory of Stationary Random Functions, Prentice-Hall, Inc., Englewood Cliffs, New Jersey, (1962).